IOP | Institute of Physics
Semiconductor Physics Group

IOP Institute of Physics
Cymru | Wales

CARDIFF UNIVERSITY
PRIFYSGOL CAERDYDD

SIOE 2021

Semiconductor and Integrated Optoelectronics Conference

30th March – 1st April 2021

Programme and Abstracts

CARDIFF UNIVERSITY
PRIFYSGOL CAERDYDD

Conference Guidance

SIOE Programme and overview

This is the first time we have run SIOE online and we are using a few platforms to provide an interactive conference. We have provided some guidance on each of these below which you can refer to throughout the conference and we will also be on hand to provide support: Conference@cardiff.ac.uk

Zoom

SIOE will be run as Zoom meeting to allow an interactive conference. The conference can be accessed through this link:cardiff.zoom.us/j/81134166635?pwd=MFFrQ01YelkrVmtuZzR1ak1oYzRxdz09;
Meeting ID: 811 3416 6635; Password: 382433. You will also find this link in the joining instructions. We ask that you keep your microphones muted during all talks. Please save questions for the designated Q&A sections. When asking questions, please do this in the chat or by using the "Raise hand" function. If you're not able to ask a question following a talk, there will be an opportunity to meet with speakers and other delegates during break times and at the end of each day in the SIOE Spatial space (see below).

Spatial

All of the breaktimes, poster sessions and the careers session will take place in the SIOE Spatial space: https://spatial.chat/s/sioe2021 The space allows delegates to speak and see each other when stood next to each other in the virtual space and there are designated areas for the break times and poster sessions. You will find full guidance on this at the end of this programme and a facilitator will be on hand in the Spatial virtual foyer area to support you.

Panel questions

During the panel session which will explore the integration of Electronics and Photonics (Session 8 in the programme), delegates will be assigned to break out rooms in Zoom and Mural (see Mural notes below). **We ask that you please consider the questions listed in session 8 of the programme below in advance of the session**. This will help to make the most of the discussion time in break out rooms.

Mural

Mural provides an interactive platform that enables you to write responses to the questions provided for discussion during the panel session (see above). During this session, delegates will be assigned to break out rooms in Zoom where they will be provided with a link to their corresponding Mural break out room. Break out room facilitators will explain how to use Mural at the start of the session, and you will find further Mural guidance at the end of this programme.

Recording on YouTube

Unless delegates have requested that a session is not recorded, all sessions will be recorded and posted on our unlisted SIOE YouTube playlist at the end of each session:
https://www.youtube.com/playlist?list=PL7nlru2b7N6Cy49jv1iI7j4Y_eQMoJEa7

The videos will remain accessible for two months from the last day of the conference and will then be deleted.

Welcome Message

SIOE 2021

Croeso i SIOE

It gives me great pleasure to welcome you to the 34th SIOE conference.

This is the first online SIOE conference and we have made efforts to replicate as much of a traditional conference as possible. To this end we are taking risks with live presentations and are making sure delegates can interact during breaks and poster sessions in the SIOE Spatial space: https://spatial.chat/s/sioe2021

We have an exciting programme that demonstrates the continuing evolution of Semiconductor Integrated OptoElectronics. On Tuesday afternoon we begin with sessions focussed more on a materials perspective or with materials as a driver. This is followed by a poster session, allowing you to interact and talk with poster presenters, other delegates and to make new connections. We finish Tuesday with a careers session (also taking place in the SIOE Spatial space), where delegates will have an opportunity to speak with a representative of the CS Cluster about CS careers and view current job opportunities.

On Wednesday morning we begin with a session on New Approaches for Datacom / Telecom Wavelength Lasers, followed by a session on Lasers and Laser Systems. In the afternoon we welcome Professor Weng Chow from Sandia Labs in the US to deliver an invited talk summarising recent work on Quantum Dot laser modelling and design. This is followed by a session on Compound Semiconductor Devices on Silicon. We finish the day with a panel session exploring the integration of Electronics and Photonics and we are very pleased to welcome our invited panel members:

- Dr Amy Liu from IQE
- Dr Haisheng Rong from Intel
- Prof. Kevin Williams from Eindhoven University of Technology
- Prof. Tao Wang from Sheffield University
- Dr Aaron Zilkie from Rockley Photonics.

Following brief presentations from panel members and an opportunity to ask them questions, delegates will join breakout rooms and consider the questions detailed in the panel session section of the programme before all delegates come back together for a summary session and further discussion.

On Thursday morning we begin with a session on Detectors and Related Materials, followed by a session on Modulators and Modulation. For the last part of the conference, there is a second poster session, before we welcome Professor Asa Haglund from Chalmers University of Technology, Göteborg to deliver an invited talk on very short wavelength VCSELs and light emitters. We conclude the conference with a prize giving session (there are cash prizes) and a final opportunity to network and connect with new colleagues in the SIOE Spatial space after taking in all the conference presentations.

The SIOE 2021 Organising Committee have been instrumental in assessing abstracts, putting together the programme and booklet, as well as in making the necessary arrangements for the conference. Committee members are Dr Nicolás Abadía, Dr Daryl Beggs, Dr Sara-Jayne Gillgrass (associate

member), Dr Manoj Kesaria, Dr Qiang Li, Dr Sang Soon Oh, Dr Sam Shutts, Dr Juan Pereiro Viterbo (associate member). The committee were assisted by Kate James, Grace Mullally and James Atkinson. The Organising Committee wish to thank the following sponsors who have provided generous contributions for prizes: IOP Wales, IOP Semiconductor Physics Group, The Compound Semiconductor Centre (CSC) Ltd.

Prof. Peter Smowton, School of Physics and Astronomy, Cardiff University

Programme

Tuesday 30th March

Welcome Address and Guidance 12.30 – 12.40 (Zoom)

Session 1: Materials Development I 12.40– 14.10 (Zoom)

Break 14.10 – 14.30

Session 2: Materials and Device Development II 14.30 – 15.45 (Zoom)

Break 15.45 – 16.00

Session 3: Poster Session I 16.00 – 17.15 (Spatial)

Careers Session 17.15 – 18.15 (Spatial)

Wednesday 31st March

Session 4: New Approaches for Datacom / Telecom Wavelength Lasers 9.00 – 10.30 (Zoom)

Break 10.30 – 11.00

Session 5: Lasers and Laser systems 11.00 – 12.45 (Zoom)

Lunch 12.45 – 13.30

Session 6: Invited Speaker: Prof. Weng Chow 13.30 – 14.00 (Zoom)

Break 14.00 – 14.10

Session 7: Compound Semiconductor Devices On Silicon 14.10 – 15.40 (Zoom)

Break 15.40 – 16.00

Session 8: Panel Session 16.00 – 17.45

Panel instructions and brief Q&A 16.00-16.40 (Zoom)

Break out discussions 16.40-17.15 (Mural)

Summary session 17.15-17.45 (Zoom)

Thursday 1st April

Session 9: Detectors and Related Materials 9.15 – 10:15 (Zoom)

Break 10:15 – 10:30

Session 10: Modulators and Modulation 10.30 – 11.30 (Zoom)

Session 11: Poster Session II 11.30 – 12.30 (Spatial)

Session 12: Guest Speaker: Prof. Asa Haglund 12.30 – 13.00 (Zoom)

Conference Closing Address and Prize Giving 13.00 – 13.15 (Zoom)

End of conference

Programme, Tuesday 30th March

Welcome Address
Zoom 12.30 – 12.40

Session 1: Materials Development I
Zoom 12.40 – 14.10

12.40 A21_26 **Growth of site-controlled InAs/GaAs quantum dot arrays for integration into photonic devices**

C Ovenden[1], A Trapalis[1], D.J Hallett[2], P.K Patil[3], E Clarke[3], M.S Skolnick[2], I Farrer[1,3] and J Heffernan[1]

[1] Department of Electronic and Electrical Engineering, University of Sheffield, Sheffield, S1 3JD, UK; [2] Department of Physics and Astronomy, University of Sheffield, Sheffield, S3 7RH, UK;[3] EPSRC National Epitaxy Facility, University of Sheffield, Sheffield, S1 3JD, UK.

12.55 A21_55 **Insight on Indium droplet driven nucleation of InAs Nanowires on Graphite**

E Anyebe[1], Q Zhuang[3] M Kesaria[2,1]

[1]School of Engineering, Cardiff University, Cardiff, CF24 3AA, UK; [2]School of Physics, Cardiff University, Cardiff, CF24 3AA, UK; [2]Department of Physics, Lancaster University, LA1 4YW.

13.10 A21_50 **Temperature-Dependent Characterisation of GaN Nanonetwork on Silicon**

H Finch[1], Manoj Kersia[2], Sorcha Hulme[1], Vinod R. Dhanak[3], Ivona Z. Mitrovic[1] and Ian Sandall[1]

[1]Department of Electrical Engineering and Electronics, University of Liverpool, UK; [2]School of Physics and Astronomy, University of Cardiff, UK; [3]Department of Physics and Stephenson Institute for Renewable Energy, University of Liverpool, UK

13.25 A21_42 **Nanorippled MoS2 Ultra-thin Films enable Broadband and Tunable Light Harvesting**

M Gardella[a], M Bhatnagar [a], M.C Giordano[a], D Chowdhury[a], C Mennucci[a], A Mazzanti[b], G Della Valle[b], C Martella[c], P Tummala[c], A Lamperti[c], A Molle[c] and F Buatier de Mongeot[a]

[(a)] Dipartimento di Fisica, Università di Genova, Via Dodecaneso 33, 16146 Genova, Italy; [(b)] Dipartimento di Fisica and IFN-CNR, Politecnico di Milano, Piazza Leonardo da Vinci, 32 - 20133 Milano, Italy [(c)] CNR-IMM Unit of Agrate Brianza, via C. Olivetti 2, Agrate Brianza, I-20864, Italy

13.40 A21_16 **Self-assembled InAs/InP quantum dots via droplet epitaxy in MOVPE at the telecom C-band**

E. M Sala[1, 2],Y. I. Na[2], M Godsland[2], A Trapalis[1,2] and J Heffernan[1,2]

[1]EPSRC National Epitaxy Facility, The University of Sheffield, Broad Lane, S3 7HQ Sheffield, United Kingdom,[2] Department of Electronic and Electrical Engineering, The University of Sheffield, Broad Lane, S3 7HQ Sheffield, United Kingdom

13.55 A21_71 **1550 nm InAs quantum dots on InP and GaAs substrates grown by MOCVD**

B Ratiu, O Abouzaid, P.M Smowton and Q Li

School of Physics and Astronomy, Cardiff University, CF24 3AA, UK

Break 14.10 - 14.30

Session 2: Materials Development II
Zoom; 14.30 – 15.45

14.30 A21_03 **InGaAs/AlAs Asymmetric Spacers RTDs for THz Imaging Applications**
A AlQurashi and M Missous
Department of Electrical and Electronic Engineering, the University of Manchester, United Kingdom

14.45 A21_53 **Uni-polar carrier transport in InGaN quantum well systems: From alloy fluctuations to quantum corrected drift-diffusion calculations**
M. O'Donovan[1,2], P. Farrell[3], T. Streckenbach[3], D. Chaudhuri[1], T. Koprucki[3] and S. Schulz[1]
[1] Tyndall National Institute, University College Cork, Cork, T12 R5CP, Ireland, [2] Department of Physics, University College Cork, Cork T12 NY60, Ireland, [3]Weierstrass Institute (WIAS), Mohrenstr. 39, 10117 Berlin, Germany

15.00 A21_19 **Temperature dependent JV analysis of GaAsBi p-i-n diod**
R. D Richards, F Harun, M.R.M Nawawi, Y Liu, T.B.O Rockett and J.P.R David.
Department of Electronic and Electrical Engineering, University of Sheffield, UK

15.15 A21_65 **3D mapping of nanoscale physical properties of VCSEL devices**
A Niblett[1], M Mucientes[1], S Shutts[2], L Forcieri[1], S Jarvis[1], I Eddie[3], W Meredith[4], M Haji[5], P Smowton[2], and O.V Kolosov[1]
[1]Physics Department and Materials Science Institute, Lancaster University, LA1 4YB, UK, [2]School of Physics and Astronomy, Cardiff University, Cardiff, CF24 3AA, UK, [3]CST Global Ltd, Glasgow, UK, [4]Compound Semiconductor Centre, Cardiff, UK, [5]Time and Frequency Metrology, National Physical Laboratory, Teddington, UK

15.30 A21_05 **Colloidal Quantum Dots Visible Light Communication Mediated by Ligand-assisted Interface Modulation**
Shijie Zhan[1], Hao Wang[1], Xiangbin Fan[1], Nikos Bamiedakis[1], Richard Penty[1], Ian White1, Jong Min Kim[1], Bo Hou[1,2]
[1] University of Cambridge, Department of Engineering, 9 JJ Thomson Ave, Cambridge CB3 0FF, UK, [2]Cardiff University, Department of Physics and Astronomy, The Parade, Cardiff CF24 3AA, UK

Break 15.45 – 16.00

Session 3: Posters I
Spatial; 16:00 – 17.15

A21_61 **Modelling bistability in 1D array of coupled micro-ring resonators**
G Alharbi and S. S Oh
School of Physics and Astronomy, Cardiff University, Cardiff, CF24 3AA, United Kingdom

A21_13 **Analytical model for cantilever optimization towards photoacoustic energy harvesting enhancements with capacitive transduction**
W Trzpil [1], N Maurin[1], D Ayache, R Rousseau [1], A Vicet[1] and M Bahriz [1].
[1]IES, Univ. Montpellier, CNRS, F-34000 Montpellier, France

A21_33 **Efficient optical modulator based on D-shaped photonic crystal fiber**
N.Y.M Dawood[1,2], B.M Younis[1,3], N F.F Areed[2], M.F.O Hameed[3,4,5] and S. S. A. Obayya

[1]Electronics and Communications Department, Misr Higher Institute for Engineering and Technology (MET), Mansoura, Egypt, [2]Electronics and Communications Department, Faculty of Engineering, Mansoura University, Mansoura 35516, Egypt, [3]Centre for Photonics and Smart Materials, Zewail City of Science and Technology, October Gardens, 6th of October City, Giza 12578, Egypt, [4]Nanotechnology and Nanoelectronics Engineering Program, Zewail City of Science and Technology, October Gardens, 6th of October City, Giza 12578, Egypt, [5]Mathematics and Engineering Physics Department, Faculty of Engineering, Mansoura University, Mansoura 35516, Egypt

A21_35 **Dual-Arm Horn Nano-Antenna for Wireless Communications**

M Elsaid [1,2], K.R Mahmoud[3], M Hussein[1,2,4], M.F.O. Hameed[1, 5, 6*], S.S.A. Obayya[1]

[1]Centre for Photonics and Smart Materials, Zewail City of Science and Technology, October Gardens, 6th of October City, Giza, 12578 Egypt, [2] Department of Physics, Faculty of Science, Ain Shams University, Abbassia 11566, Cairo, Egypt, [3]Electronics, Communications, and Computers Department, Faculty of Engineering, Helwan University, Cairo, Egypt, [4]Light Technology Institute, Karlsruhe Institute of Technology, Engesserstrasse 13, 76131 Karlsruhe, Germany, [5]Nanotechnology and Nanoelectronics Engineering Program, Zewail City of Science and Technology, October Gardens, 6th of October City, Giza, 12578 Egypt, [6]Mathematics and Engineering Physics Department, Faculty of Engineering, Mansoura University, Mansoura, Egypt

A21_36 **Highly Sensitive 1D Photonic crystal Hemoglobin Biosensor**

M.S.S Ibrahim[1], M Tarek[1], S.S.A. Obayya[2], M.F.O. Hameed[2, 3,4]

[1]Physics Department, Faculty of Science, El-Arish University, El-Arish, Egypt, [2]Centre for Photonics and Smart Materials, Zewail City of Science and Technology, Zewail City of Science and Technology, October Gardens, 6th of October City, Giza, 12578, Egypt, [3]Nanotechnology and Nanoelectronics Engineering Program, Zewail City of Science and Technology, October Gardens, 6th of October City, Giza, 12578, Egypt, [4]Mathematics and Engineering Physics Department, Faculty of Engineering, Mansoura University, Mansoura, Egypt

A21_31 **Highly Efficient Perovskite Solar Cell**

A Khaled[1], M Hussein[1,2,3], B.M.A Rahman[4], K.T.V Grattan[4], M.F. O Hameed[1,5,6] and S.S.A Obayya[1]

[1] Centre for Photonics and Smart Materials, Zewail City of Science and Technology, October Gardens, 6t[h] of October City, Giza, 12578, Egypt,[2] Department of Physics, Faculty of Science, Ain Shams University, Abbassia 11566, Cairo Egypt, [3]Light Technology Institute, Karlsruhe Institute of Technology, Engesserstrasse 13, 76131 Karlsruhe, Germany, [4]Department of Electrical and Electronic Engineering, City, University of London, London EC 1 V 0HB, United Kingdom, [5] Nanotechnology and Nanoelectronics Engineering Program, Zewail City of Science and Technology, October Gardens, 6[th] of October City, Giza, 12578, Egypt, [6]Mathematics and Engineering Physics Department, Faculty of Engineering, Mansoura University, Mansoura 35516, Egypt

A21_04 **Intermittent Dynamics Switching in Discrete-mode Semiconductor Lasers with Lon External Cavity Optical Feedback**

Z Zhong[1], DaChang[1], W Jin[1], M.W Lee[2], J Tang[1] and YHong[1]

[1] *School of Computer Science and Electronic Engineering, Bangor University, Wales, LL57 1UT, UK, [2] Laboratoire de Physique des Lasers CNRS UMR 7538, Universit´e Paris 13, Sorbonne Paris Cit´e, 93430 Villetaneuse, France.*

A21_10 **Mode selection in L40 photonic crystal cavities via spatial pumping**

L Wang [1], Y Wang[2], H Francis[2], R Lu [1], M Xia [1], F Liu [1], Xi Lin [1], MHopkinson[2] and C Jin[1]

College of information Science and Electronic Engineering, Zhejiang University, China [2] Department of Electronic and Electrical Engineering, University of Sheffield., UK

A21_66 **Gain measurement of Vertical Cavity Surface Emitting Lasers using Segmented Contact Technique**

C Hentschel[1], C.P Allford[1], S-J Gillgrass[1], Z Li[1], J Nabialek[1], W Meredith[2], I Davies[3], S Shutts[1] and P.M Smowton[1]

[1]EPSRC Future Compound Semiconductor Manufacturing Hub, School of Physics and Astronomy, Cardiff University, Cardiff, UK; [2]Compound Semiconductor Centre, UK; [3]IQE plc, Cardiff, UK.

A21_70 **Large-scale metamaterial thermal emitters for infrared heating application**

Y Gong and S.S Oh

School of Physics and Astronomy, Cardiff University, Cardiff, CF24 3AA, United Kingdom.

A21_59 Improved performance of 1.3 µm quantum dot by direct Si doping

H Deng[1], M Tang[1], P Smowton[2], C Jin[3], A Seeds[1], H Liu[1]

[1]Department of Electronic and Electrical Engineering, University College London, London, WC1E 7JE, UK, [2]School of Physics and Astronomy, Cardiff University, Cardiff, CF10 3AT, U.K.

A21_02 Self-Catalyzed AlGaAs Nanowires and AlGaAs/GaAs Nanowire-Quantum Dots on Si Substrates

G Boras,[†,||] X Yu,[†,||] H.A Fonseka,[‡] G Davis,[§] A.V Velichko,[§] J.A Gott,[‡] H Zeng,[†] S Wu,[⁑] P Parkinson,[⌞] X Xu,[⁑] D Mowbray,[§] A.M Sanchez[‡] and H Liu[†]

[†]Department of Electronic and Electrical Engineering, University College London, London WC1E 7JE, United Kingdom, [‡]Department of Physics, University of Warwick, Coventry CV4 7AL, United Kingdom, [§]Department of Physics and Astronomy, University of Sheffield S3 7RH, United Kingdom, [⁑]Institute of Physics, Chinese Academy of Science, Beijing 100190, China, [⌞]Department of Physics and Astronomy and the Photon Science Institute, University of Manchester, Manchester M13 9PL, United Kingdom

A21_29 Cross-shaped-silicon nanowires for highly efficient solar cell

R. El-Bashar,[1,2] M Hussein,[1,3,4] S. F Hegazy,[1.2] Y Badr,[2] S.S.A Obayya [1,*] M.F.O. Hameed,[1,5,6]

[1]Centre for Photonics and Smart Materials, Zewail City of Science and Technology, October Gardens, 6th of October City, Giza 12578, Egypt, [2]National Institute of Laser Enhanced Sciences (NILES), Cairo University, Giza 12613, Egypt, [3]Department of Physics, Faculty of Science, Ain Shams University, Abbassia 11566, Cairo, Egypt, [4]Light Technology Institute, Karlsruhe Institute of Technology, Engesserstrasse 13, 76131 Karlsruhe, Germany, [5]Nanotechnology and Nanoelectronics Engineering Program, Zewail City of Science and Technology, October Gardens, 6th of October City, Giza 12578, Egypt, [6]Mathematics and Engineering Physics Department, Faculty of Engineering, Mansoura University, Mansoura 35516, Egypt

A21_30 Enhanced light trapping in thin film solar cell

M.A Elrabiaey [1], M Hussein[1,2,3], M.F.O Hameed [1,4,5*], and S.S.A Obayya [1]

[1] Centre for Photonics and Smart Materials, Zewail City of Science and Technology, October Gardens, 6t[h] of October City, Giza 12578, Egypt, [2]Department of Physics, Faculty of Science, Ain Shams University, Abbassia 11566, Cairo, Egypt, [3]Light Technology Institute, Karlsruhe Institute of Technology, Engesserstrasse 13, 76131 Karlsruhe, Germany, [4]Nanotechnology and Nanoelectronics Engineering Program, University of Science and Technology, Zewail City of Science and Technology, Giza 12578, Egypt, [5]Mathematics and Engineering Physics Department, Faculty of Engineering, Mansoura University, Mansoura 35516, Egypt,

A21_49 Design and Analysis of GaAs-based Asymmetric SPAcer-layer Tunnel (ASPAT) Diodes for Microwave/mm-wave detection

A Salhi[a], A Hadfield[a], S.G Muttlak[a], J Sextona, M.J Kelly[b], and M Missous[a]

[a]School of Electrical and Electronic Engineering, University of Manchester, Manchester M13 9PL, U.K, [b]Department of Engineering, University of Cambridge, Cambridge CB1 1EG, U.K.

A21_41 Large Optical Bandwidth InGaAs/InAlAs/GaAs metamorphic-PIN Photodiode Suitable for over 20Gb/s Optical Communication Systems

S.G Muttlak[1], A Salhi[1], M Sadeghi[2], K Ian[3] and M Missous[1]

[1]School of Electrical and Electronic Engineering, University of Manchester, UK, [2]Advanced Hall Sensors Ltd, Manchester, UK, [3]Integrated Compound Semiconductors, Manchester, UK

A21_32 Efficient Nanowire Solar Cell with Surface Texturing

G.Y Abdelatif, [1,2] M.F.O Hameed, [1,3,4] M Hussein, [1,5,6] S.S.A Obayya, [1]

[1]Centre for Photonics and Smart Materials, Zewail City of Science and Technology, October Gardens, 6t[h] of October City, Giza, 12578, Egypt.[2] Department of Electronic and Communication Engineering, MISR Higher Institute for Engineering and Technology, Mansoura Ring Road, Mansoura, 35516, Egypt. [3] Nanotechnology and Nanoelectronics Engineering Program, Zewail City of Science and Technology, October Gardens, 6[th] of October City, Giza, 12578, Egypt. [4]Mathematics and Engineering Physics Department, Faculty of Engineering, Mansoura University, Mansoura 35516, Egypt.[5] Department of Physics, Faculty of Science, Ain Shams University, Abbassia 11566, Cairo Egypt. [6]Light Technology Institute, Karlsruhe Institute of Technology, Engesserstrasse 13, 76131 Karlsruhe, Germany

A21_72 **Characterisation and Design of InP QD Material for Passively Mode-locked Lasers**

R Alharbi[1,2], Z Li[1], C Allford[1], S Shutts[1], A Forrest[3,] A Krysa[4], M.A Cataluna[3], P.M Smowton[1]

[1]EPSRC Future Compound Semiconductor Manufacturing Hub, School of Physics and Astronomy, Cardiff University, Cardiff, UK, [2]Department of Physics, King Abdulaziz University, Jeddah 21551, Saudi Arabia, [3]Institute of Photonics and Quantum Sciences, School of Engineering and Physical Sciences, Heriot-Watt University, Edinburgh, EH14 4AS, United Kingdom, [4]EPSRC National Centre for III-V Technologies, University of Sheffield, Sheffield, S1 3JD

Careers Session

Spatial; 17:15 – 18.15

CS Cluster careers overview

Current job opportunities

Programme, Wednesday 31st March

Session 4: New Approaches for Datacom / Telecom Wavelength Lasers

Zoom; 09:00 – 10:30

09.00 A21_63 **Single Mode Nanolaser Monolithically Grown on On-axis Si substrate**

M Tang[1,*], T Zhou[2], S Chen[1], Z Zhang[2], H Liu[1]

[1] Department of Electronic and Electrical Engineering, University College London, London, WC1E 7JE, United Kingdom, [2] School of Science and Engineering, The Chinese University of Hong Kong, Shenzhen, Guangdong, 518172, P.R. China

09.15 A21_27 **Low-threshold strain-compensated InGaAs/(In,Al)GaAs multi-quantum well nanowire lasers emitting near 1.3 µm**

P Schmiedeke[1], A Thurn[1], M Döblinger[2], S Matich[1], J. J Finley[1] and G Koblmüller[1]

[1]Walter Schottky Institut and Physics Department, Technical University of Munich, Garching, Germany [2]Department of Chemistry, Ludwig-Maximilians-Universität München, Munich, Germany

09.30 A21_64 **Low Threshold Type-II GaInAs/GaAsSb "W"-Lasers Operating in the 1.2-1.3µm Wavelength Range**

D.A Duffy[1], I. P Marko[1], C Fuchs[2], T.D Eales[1], J Lehr[2], W Stolz[2] and S.J Sweeney[1]

[1] Advanced Technology Institute and Department of Physics, University of Surrey, Guildford, GU2 7XH, United Kingdom, [2] Materials Sciences Center and Department of Physics, Philipps-Universität Marburg, Renthof 5, 35032, Marburg, Germany

09.45 A21_07 **All-MBE grown InAs/GaAs quantum dot lasers with thin Ge buffer layer on Si substrates**

J Yang[1,5,], Z Liu[1,5], P Jurczak[1,*], M Tang[1,*], K Li[1], S Pan[1], A Sanchez[2], R Beanland[2], J-C Zhang[3], H Wang[3], F Liu[3], Z Li[4], S Shutts[4], P Smowton[4], Si Chen[1], A Seeds[1], H Liu[1,*]

[1]Department of Electronic and Electrical Engineering, University College London, Torrington Place, London, WC1E 7JE, UK, [2]Department of Physics, University of Warwick, CV4 7AL Coventry, UK, [3]Key Laboratory of Semiconductor Materials Science, Institute of Semiconductors, Chinese Academy of Sciences, Beijing 100083, P. R. China, [4]Department of Physics and Astronomy, Cardiff University, Queens Building, The Parade, Cardiff CF24 3AA, UK

10.00 A21_57 **GaSb/GaAs quantum-ring VCSELs operating at telecoms wavelengths**

P.D Hodgson,[1] T.J Wilson,[1] A.J Robson,[1,2] Q.D Zhuang,[1] S McDougall,[3] K Kennedy,[4,5] S Kumar[4] and M Hayne[1,2]

[1]Department of Physics, Lancaster University, Lancaster LA1 4YB, UK, [2]Lancaster Material Analysis, Department of Physics, Lancaster University, Lancaster LA1 4YB, UK, [3]CST Global Ltd, 4 Stanley Blvd, Hamilton International Technology. Park., Glasgow G72 0BN, UK, [4]EPSRC National Centre for III-V Technologies, University of Sheffield, Sheffield, S3 7HQ, UK, [5]Nanofabrication Core Lab, King Abdullah University of Science and Technology (KAUST), Thuwal 23955-6900, Saudi Arabia

10.15 A21_17 **Performance of dilute bismide and dilute nitride multiple quantum well lasers at 1.55m**

Z.C.M Davidson[1], J.M Rorison[1], and C.A Broderick[2,3]

[1]Department of Electrical and Electronic Engineering, University of Bristol, Bristol BS8 1UB, U.K [2].Tyndall National Institute, University College Cork, Lee Maltings, Dyke Parade, Cork T12 R5CP, Ireland,[3] Department of Physics, University College Cork, Cork T12 YN60, Ireland

Break 10.30 – 11.00

Session 5: Lasers & Laser Systems
Zoom; 11:00 – 12:45

11.00 A21_01 **Improved lateral brightness in 940-nm high-power broad-area diode lasers using enhanced self-aligned structure**

M. Elattar, O. Brox, P. Della Casa, A. Maaßdorf, D. Martin, H. Wenzel, A. Knigge, and P. Crump
Ferdinand-Braun-Institut, Leibniz-Institut für Höchstfrequenztechnik, Gustav-Kirchhoff-Str. 4, 12489 Berlin, Germany

11.15 A21_47 **High pulsed power output in the eye-safe wavelength range from a double-asymmetric-structure laser diode with a bulk active layer**

L. Hallman[(a)], B.S. Ryvkin[(a,b)], E.A.Avrutin[(c)], J.T. Kostamovaara[(a)]
[(a)]Dept of Electrical and Information Engineering, University of Oulu, Finland; [(b)]A.F.Ioffe Physico-Technical Institute, St.Petersburg, Russia; [(c)]Dept of Electronic Engineering, University of York, UK,

11.30 A21_68 **Master-Oscillator Power-Amplifier system emitting at 626 nm: Increasing the laser power for future 9Be+ cooling applications**

G Blume, A Koyucuoglu, M Drees, J Pohl, D Feise, A Sahm, and K Paschke
Ferdinand-Braun-Institut gGmbH, Leibniz-Institut für Höchstfrequenztechnik (FBH), Gustav-Kirchoff-Str. 4, 12489 Berlin, Germany

11.45 A21_18 **Experimental Implementation of Ultrafast Photonic Recurrent Neural Networks using Reservoir Computing and Semiconductor Lasers**

J Bueno, J Robertson, M Hejda, and A Hurtado
Institute of Photonics, Dept. of Physics, University of Strathclyde, Technology and Innovation Centre, Glasgow, UK

12.00 A21_58 **Ultrafast non-equilibrium dynamics in GaAs-based nanowire lasers**

A Thurn[1], J Bissinger[1], S Meinecke[2], P Schmiedeke[1], S.S Oh[3], W.W Chow[4], K Lüdge[2], G Koblmüller[1]and J.J Finley[1]
[1]Walter Schottky Institut, Technische Universität München, Am Coulombwall 4, 85748 Garching, Germany, [2]Institut für Theoretische Physik, Technische Universität Berlin, Hardenbergstraße 36, 10623 Berlin, Germany, [3]School of Physics and Astronomy, Cardiff University, Cardiff CF24 3AA, UK, [4]Sandia National Laboratories, Albuquerque, New Mexico 87185-1086, USA.

12.15 A21_51 **Study of the randomness of the dynamics in a laser diode subject to optical feedback with stimulated Brillouin scattering**

L. J Quintero-Rodríguez[1], I.E Zaldívar-Huerta[1], Y Hong[2], C Masoller[3] and M.W Lee[4]
[1]Departamento de Electrónica, Instituto Nacional de Astrofísica, Óptica y Electrónica, Puebla 72000, Mexico, [2]School of Computer Science and Electronic Engineering, Bangor University, Wales, LL57 1UT, UK, [3]Departament de Física, Universitat Politècnica de Catalunya, St. Nebridi 22, 08222, Terrassa, Barcelona, Spain, [4]Laboratoire de Physique des Lasers CNRS - UMR7538, Université Sorbonne Paris Nord, 93430 Villetaneuse, France

12.30 A21_12 **Image Edge Detection with Spiking VCSEL Neurons**

J Robertson, [1] Y Zhang, [1,2] M Hejda, [1] J Alanis, [1] J Bueno, [1] S Xiang, [2] and A Hurtado[1]
[1]Institute of Photonics, Dept. of Physics, University of Strathclyde, Technology and Innovation Centre, Glasgow, UK; [2]State Key Laboratory of Integrated Service Networks, Xidian University, Xi'an 710071, China.

Lunch 12:45 – 13:30

Session 6: Invited Speaker
Zoom; 13:30 – 14:00

13.30 Invited p-doping in quantum dot lasers
W.W Chow[1], Zeyu Zhang[2], J Duan[3] and F Grillot[3]
[1]Sandia National Laboratories, Albuquerque, New Mexico, USA [2]Justin Norman and John E. Bowers, Materials and Electrical and Computer Engineering Departments, University of California, Santa Barbara, California USA [3]Telecom Paris, Institut Polytechnique de Paris, France

Break 14.00 – 14.10

Session 7: Compound Semiconductor Devices on Silicon
Zoom; 14.10 – 15.40

14.10 A21_22 APB annihilation of III-V materials monolithically grown on on-axis silicon (001)
K Li[1], J Yang[1], Y Lu[1], M Tang[1], P Jurczak[1], Z Liu[1], X Yu[1], J-S Park[1], HDeng[1], H Jia[1], M Dang[1], A M. Sanchez[2], R Beanland[2], W Li[3], X Han[3], J-C Zhang[4], H Wang[4], F Liu[4], S Chen[1], A Seeds[1], P Smowton[5] and H Liu[1]
[1] Department of Electronic and Electrical Engineering, University College London, London, WC1E 7JE, United Kingdom,[2] Department of Physics, University of Warwick, Coventry, CV4 7AL, United Kingdom , [3]Institute of the Microstructure and Properties of Advanced Materials, Beijing University of Technology, 100124, Beijing, China, [4] Key Laboratory of Semiconductor Materials Science, Institute of Semiconductors, Chinese Academy of Sciences, Beijing 100083, China,[5] Department of Physics and Astronomy, Cardiff University, Queens Building, The Parade, Cardiff, CF24 3AA, United Kingdom

14.25 A21_15 Linewidth enhancement factor measurement by using phase modulation method for epitaxial quantum dot laser on silicon
S Ding [1], B Dong [1], H Huang [1], J.E Bowers [2], and F Grillot [1, 3]
[1]LTCI, Télécom Paris, Institut Polytechnique de Paris, 91120 Palaiseau, France, [2]Institute for Energy Efficiency, University of California, Santa Barbara, California 93106, USA, [3]Center for High Technology Materials, The University of New-Mexico, Albuquerque, NM 87106, USA

14.40 A21_60 Carrier Transport in Quantum Dot Laser on Silicon: impact of traps and p-type modulation doping on laser performance
M Gioannini, M Saldutti, A Tibaldi and F Cappelluti
Departement of Electronics and Telecommunication, Politecnico di Torino, Italy

14.55 A21_40 Stable 25.5 GHz mode-locked quantum dot lasers operating up to 120 °C
S Pan[1], J Huang[2], L. Ponnampalam[1], Z Zhou[1], K Balakier[1], M Tang[1], Z Cao[2]Z Liu[1], A Seeds[1], H Liu[1], and S Chen[1]
[1]Departement of Electronic and Electrical Engineering, University College London, London WC1E 7JE, United Kingdom; [2]Department of Electronic and Electrical Engineering, Eindhoven University of Technology, Eindhoven 5612AZ, Netherland;

15.10 A21_39 Investigation of edge coupling between quantum dot laser-to silicon
A Uzun[1], F Atar[1], J Justice[1], P Ossieur[2], R Loi[3], I Krestnikov[4], B Corbett[1]
[1]Tyndall National Institute, University College Cork, Ireland, [2]imec-IDLab and Ghent University, Ghent, Belgium, [3]X-Celeprint Ltd, Lee Maltings, Cork, Ireland, [4]Innolume GmbH, Konrad-Adenauer-Allee 11; 44263 Dortmund, Germany.

15.25 A21_21 **Etched-facets Mid-IR laser on on-axis Silicon substrate for photonic integrated circuits**

L.M Bartolomé, M.R Calvo, M Bahriz, J-B Rodriguez, L Cerutti and E Tournié. *IES, Univ. Montpellier, CNRS, 34000 Montpellier, France*.

Break 15.40 – 16.00

Session 8: Panel Session
16.00 – 17.45

Exploring the integration of Electronics and Photonics

Panel instructions and brief Q&A	Zoom; 16.00 -16.40
Break out discussions	Mural; 16.40 -17.15
Summary session	Zoom; 17.15 -17.45

Biographies of the panel members will be available on the SIOE website ahead of the conference:

www.cardiff.ac.uk/conferences/sioe-conference

We ask delegates to please consider the questions below ahead of the panel session. There will be an opportunity to discuss these further in breakout rooms during the session.

1. What important applications will be enabled by optoelectronic integration? And what level of integration is required for each of these?

2. And what technical and scientific issues need to be resolved to allow these to proceed?

Programme, Thursday 1st April

Session 9: Detectors and Related Materials

Zoom; 9:15 – 10:15

09.15 A21_11 **Colloidal Quantum Dots for Indoor and Concentration Solar Cells Applications**

B Hou

School of Physics and Astronomy, Cardiff University

09.30 A21_14 **Theory of radiative recombination in broken-gap InAs/GaSb superlattices**

C Murphy[1,2], E.P O'Reilly[1,2], and A Broderick[1,2]

[1]Tyndall National Institute, University College Cork, Lee Maltings, Dyke Parade, Cork T12 R5CP, Ireland, [2]Department of Physics, University College Cork, Cork T12 YN60, Ireland

09.45 A21_52 **Mid-wavelength infrared (MWIR) type-II InAs/GaSb superlattice for NOx sensing**

D.O Alshahrani[1], D.C.M Kwan[1], D.L Huffaker[1,2,3], E Anyebe[2], and M Kesaria[1]

[1]School of Physics and Astronomy, Cardiff University, UK; [2]School of Engineering, Cardiff University, UK, Present address: [3]Electrical Engineering Department, The University of Texas at Arlington, USA

10.00 A21_54 **Long-wavelength infrared (LWIR) type-II InAs/GaSb superlattice on GaAs**

D.C.M Kwan[1], D.O Alshahrani[1], D.L Huffaker[1,2,3], E Anyebe[2], and M Kesaria[1]

[1]School of Physics and Astronomy, Cardiff University, UK; [2]School of Engineering, Cardiff University, UK, Present address: [3]Electrical Engineering Department, The University of Texas at Arlington, USA

Break 10:15 – 10:30

Session 10: Modulators and Modulation

Zoom; 10:30 - 11:30

10.30 A21_48 **Novel Design for Electroabsorption Modulator Based on Microstrip Transmission Line Technology**

A Al-Moathin, C Li, L Hou, and J.H Marsh

James Watt School of Engineering, University of Glasgow, Glasgow G12 8QQ, U.K.

10.45 A21_46 **Low-Power Photonic Modulators for Neuromorphic Computing**

J.S Male G Duffett, C.P Reardon, and T.F Krauss

11.00 A21_23 **A direct epitaxial approach to achieve a monolithic on-chip integration of a HEMT and a single micro-LED with a high modulation bandwidth**

Y Cai, J.I.H Haggar, C Zhu, P Feng, J Bai and T Wang

Department of Electronic and Electrical Engineering, University of Sheffield, Sheffield, S1 3JD

11.15 A21_44 **High Modulation Bandwidth of Semipolar (11−22) InGaN/GaN LEDs with Long Wavelength Emission**

J.I.H Haggar, Y Cai, S.S Ghataora, R.M Smith, J Bai and T.Wang

Department of Electronic and Electrical Engineering, University of Sheffield, Sheffield, S1 3JD

Session 11: Poster Session II
Spatial; 11.30 – 12.30

A21_08 Time/Frequency Division Multiplexing for magnetic imaging arrays using Quantum Well Hall Effect Sensors

R Murshudov, C.W Liang, J Sexton, J.W Watson, M Missous

A21_06 Noise reduction using Parallel Arrays of Quantum Well Hall Effect Sensors for picoTesla magnetic fields detection.

A.Lindley

A21_37 Hybrid Plasmonic-Grating TE-Pass Polarizer Based on SOI

O.Y. M. Hiza[1], B.M Younis[2,3], N.F.F. Areed[1], S.S.A Obayya[2] and M.F.O Hameed [2,4,5]

[1]Faculty of Engineering, Electronics and Communications Department, Mansoura University, Mansoura 35516, Egypt.[2]Centre for Photonics and Smart Materials, Zewail City of Science and Technology, October Gardens, 6th of October City, Giza 12578, Egypt. [3]Electronics and Communications Department, Misr Higher Institute for Engineering and Technology (MET), Mansoura 35516, Egypt.[4]Nanotechnology and Nanoelectronics Engineering Program, Zewail City of Science and Technology, October Gardens, 6th of October City, Giza 12578, Egypt. [5]Mathematics and Engineering Physics Department, Faculty of Engineering, Mansoura University, Mansoura 35516, Egypt.

A21_38 Highly Efficient Dual D-shaped PCF Biosensor Highly Efficient Dual D-shaped PCF Biosensor

Y Gamal[1,2], B.M Younis[2,3], S.F Hegazy[1,2], Y Badra[1], M.F.O Hameed[4,5], and S.S.A Obayya[2]

[1] Engineering Application of Laser Department, National Institute of Laser Enhanced Science (NILES), Cairo University, Egypt. [2] Center for Photonics and Smart Materials, Zewail City of Science and Technology, October Gardens, 6th of October City, Giza 12578, Egypt. [3] Electronics and Communications Engineering Department, Misr Higher Institute for Engineering and Technology (MET), Mansoura, Egypt. [4] Nanotechnology and Nanoelectronics Department, Zewail City of Science and Technology, October Gardens, 6th of October City, Giza 12578, Egypt. [5] Mathematical and Engineering Physics Department, Faculty of Engineering, Mansura University, Egypt.

A21_34 Tunable Mode Converter Based on Dual Core Photonic Crystal Fiber

M.M.H Mahmoud[1,2], B.M Younis[3,4], N.F.F Areed[2], M.F.O Hameed [3,5,6] and S.S.A Obayya[2]

[1]Telecom Egypt, voice core planning team, Smart Village, 6th of October City, Giza, Egypt. [2] Electronics and Communications Department, Faculty of Engineering, Mansoura University, Mansoura 35516, Egypt. [3]Centre for Photonics and Smart Materials, Zewail City of Science and Technology, October Gardens, 6th of October City, Giza 12578, Egypt. [4]Electronics and Communications Department, Misr Higher Institute for Engineering and Technology (MET), Mansoura 35516, Egypt.[5]Nanotechnology Engineering Program, Zewail City of Science and Technology, October Gardens, 6th of October City, Giza 12578, Egypt.[6]Mathematics and Engineering Physics Department, Faculty of Engineering, Mansoura University, Mansoura 35516, Egypt.

A21_62 An Extension of the Inverse Fourier Method for Index- Patterned Laser Design

N Boohan[1,2][1,2] and E.P.O'Reilly[1,2]

[1]Tyndall National Institute, lee Maltings, Dyke Parade, Cork, T12 R5CP, Ireland, [2] department of Physics, University of Cork, Cork, T12 YN60, Ireland.

A21_67 Effect of external cavity length on speckle generated by a laser diode under optical feedback

C Evered, Y Fan, K Li, A Roula and N Copner

Wireless & Optoelectronics Research & Innovation Centre, Faculty of Computing, Engineering and Science, University of South Wales, Pontypridd, CF37 1DL, United Kingdom

A21_25 Preferred growth direction of III-V nanowires on differently oriented Si substrates

H Zeng,[†,‖] X Yu,[*,†,‖] H.A Fonseka,[‡] G Boras,[†] P Jurczak,[†] T Wang,[§] A.M Sanchez,[‡] and HLiu[†]
[†]Department of Electronic and Electrical Engineering, University College London, London WC1E 7JE, United Kingdom, [‡]Department of Physics, University of Warwick, Coventry CV4 7AL, United Kingdom, [§]Department of Electronic and Electrical Engineering, University of Sheffield, Sheffield, S1 3JD, United Kingdom.

A21_24 **Monte Carlo simulation of the transport characteristics of Gallium Nitride and compound semiconductor materials.**

M Bai, J Rorsion
Department of Electrical and Electronic Engineering, University of Bristol, Bristol BS8 1UB, U.K.

A21_69 **Performance-Mapping for Characterisation of 150mm VCSEL Wafers in Industry**

J Baker[1], D.G Hayes[1], T Peach[2], S Shutts[1], P.M Smowton[1,2], I Davies[3]
[1]EPSRC funded Future Compound Semiconductor Manufacturing Hub, Cardiff University, UK, [2]Institute for Compound Semiconductors, Cardiff [1]University, UK, [3]IQE plc

A21_43 **Checked Patterned Elemental Distribution in AlGaAs Nanowire Branches via Vapor-Liquid-Solid Growth**

X Yu,[†] G Boras,[†] H.A Fonseka,[‡,‖] D Zhang,[§,‖] H Zeng,[†] A.M Sanchez[‡] and H Liu[†]
[†]Department of Electronic and Electrical Engineering, University College London, London WC1E 7JE, United Kingdom, [‡]Department of Physics, University of Warwick, Coventry CV4 7AL, United Kingdom, [§]SKLSM, Institute of Semiconductors, Chinese Academy of Sciences, P.O. Box 912, Beijing 100083, China

A21_20 **PL modelling of GaAsBi layers to assist with improving material quality in optoelectronic devices**

N.J Bailey, T.B.O Rockett, J.P.R David, R.D Richards
Department of Electronic and Electrical Engineering, University of Sheffield, UK

A21_28 **Highly Efficient Multi-Junctional Nanowires Solar Cell**

A.H.K Mahmoud [1], M.Hussein[1,2,3], M.F.O Hameed[1,4,5] and S.S.A Obayya[1]
[1]Centre for Photonics and Smart Materials, Zewail City of Science and Technology, October Gardens, Giza 12578, Egypt. [2]Department of Physics, Faculty of Science, Ain Shams University, Abbassia 11566, Cairo, Egypt[3]Light Technology Institute, Karlsruhe Institute of Technology, Engesserstrasse 13, 76131 Karlsruhe, Germany[4]Nanotechnology and Nanoelectronics Engineering Program, University of Science and Technology, Zewail City of Science and Technology, Giza 12578, Egypt.[5]Mathematics and Engineering Physics Department, Faculty of Engineering, Mansoura University, Mansoura 35516, Egypt,

A21_31 **Highly Efficient Perovskite Solar Cell**

A Khaled[1], M Hussein[1,2,3], B.M.A Rahman[4], K.T.V Grattan[4], M.F.O Hameed[,5,6] and S.S.A Obayya[1]
[1] Centre for Photonics and Smart Materials, Zewail City of Science and Technology, October Gardens, 6t[h] of October City, Giza, 12578, Egypt.
[2] Department of Physics, Faculty of Science, Ain Shams University, Abbassia 11566, Cairo Egypt. [3]Light Technology Institute, Karlsruhe Institute of Technology, Engesserstrasse 13, 76131 Karlsruhe, Germany. [4]Department of Electrical and Electronic Engineering, City, University of London, London EC 1 V 0HB, United Kingdom [5] Nanotechnology and Nanoelectronics Engineering Program, Zewail City of Science and Technology, October Gardens, 6[th] of October City, Giza, 12578, Egypt. [6]Mathematics and Engineering Physics Department, Faculty of Engineering, Mansoura University, Mansoura 35516, Egypt

A21_09 **The Development of Novel Heterostructure Detector Diodes Through Physical Modelling**.

A Hadfield, A Salhi, J Sexton and M Missous
School of Electrical & Electronic Engineering, The University of Manchester Manchester, M13 9PL, United Kingdom

A21_45 **Broadband Photon Harvesting in Organic Photovoltaic Devices Induced by Nanograting Templates**

D Chowdhury[1], S Mohamed[2], G Manzato[1], C Mennucci[1], R Chittofrati[1], M Hussein[2, 3,4] S.S.A Obayya[2], M.F.O Hameed d[2,5,6], F Buatier de Mongeot[1]

[1]University of Genova, Department of Physics, Genova, 16146, Italy. [2] Centre for Photonics and Smart Materials, Zewail City of Science and Technology, October Gardens, 6th of October City, Giza 12578, Egypt. [3] Department of Physics, Faculty of Science, Ain Shams University, Abbassia 11566, Cairo, Egypt.[4]Light Technology Institute, Karlsruhe Institute of Technology, Engesserstrasse 13, 76131 Karlsruhe, Germany. [5]Nanotechnology and Nanoelectronics Engineering Program, Zewail City of Science and Technology, October Gardens, 6th of October City, Giza, 12578 Egypt. [6]Mathematics and Engineering Physics Department, Faculty of Engineering, Mansoura University, Mansoura, Egypt

A21_56 **Modelling type-II superlattices for long-wavelength infrared detectors**

P. E. O'Dowd Phanis[1], D. C. M. Kwan[1], D. O. Alshahrani[1], D. L. Huffaker[1,2] *M. Kesaria[1]*

[1]School of Physics and Astronomy, Cardiff University, UK, Present address: [2]Electrical Engineering Department, The University of Texas at Arlington, United States of America

Session 12: Guest Speaker

Zoom; 12.30 – 13.00

12.30 *Invited* **Membrane-based VCSELs and LEDs from the blue to the ultraviolet wavelength regime**

Åsa Haglund

Chalmers University of Technology, Department of Microtechnology and Nanoscience, Gothenburg, Sweden

Conference Closing Address and Prize Giving

Zoom; 13.00 – 13.15

We will be awarding prizes at SIOE this year and will announce these during the prize giving ceremony. The prizes that will be awarded are:

- IOP Semiconductor Physics Group SIOE Merit awards for oral presentations
- CSC SIOE best oral presentation
- IOP Wales SIOE poster prizes

We will provide an overview of the voting process at the start of the conference and notify delegates how and when to vote at the end of sessions.

Conference Close

Abstracts

Session 1: Materials Development I

A21_26 Growth of site-controlled InAs/GaAs quantum dot arrays for integration into photonic devices

C. Ovenden [1], A. Trapalis[1], D. J. Hallett[2], P. K. Patil[3], E. Clarke[3], M. S. Skolnick[2], I. Farrer[1,3] and J. Heffernan[1]

1. Department of Electronic and Electrical Engineering, University of Sheffield, Sheffield, S1 3JD, UK. 2.Department of Physics and Astronomy, University of Sheffield, Sheffield, S3 7RH, UK. 3. EPSRC National Epitaxy Facility, University of Sheffield, Sheffield, S1 3JD, UK.

Quantum dots (QDs) embedded within photonic devices have been demonstrated to be excellent candidates for quantum information processing, where fundamental experiments have shown their ability to fulfil DiVincenzo's criteria. [1-3] To access exponentially faster computation times, a large number of high-quality quantum bits (qubits) are needed. Site- controlled QD (SCQD) growth is a technique that allows for the engineering of highly scalable qubit systems. The process of deterministically controlling the growth position of the QD often invoves ex-situ fabrication of nanohole arrays. Contaminants and defects introduced during the fabrication process can cause linewidth broadening. [4] This has been mitigated by using thick re-growth buffers that distance the QD from the fabrication interface. [5] However, this is not an option if QDs are going to be integrated into photonic devices, where there is a limited structure height. Therefore, effective surface preparation and low damage etch methods must be employed to achieve high quality QD growth with a thin re-growth buffer. [6]

We demonstrate the growth of low linewidth InAs SCQDs on a thin (30 nm) GaAs re-growth buffer. Nanohole arrays were fabricated using electron beam lithography (EBL) and a low etch rate inductively coupled plasma – reactive ion etching (ICP-RIE) method. In the same step alignment marks, suitable for device fabrication re-alignment procedures, were processed. To maintain the high quality of the QDs, despite only using a thin re-growth buffer, ex-situ wet chemical cleaning and in-situ atomic hydrogen cleaning methods were developed. An atomic force microscope (AFM) image of an un-capped SCQD array is shown (Figure 1) and photoluminescence (PL) emission from regular arrays of SCQDs (Figure 2). Minimum linewidths measured using non-resonant excitation were 26 µeV with a mode of ~ 40 µeV. Using PL imaging best occupancy in the 900 nm to 1000 nm range was ~ 40 % and in AFM 100 % occupancy was achieved. This result demonstrates the high quality growth of SCQDs using a simple growth structure that is compatible with photonic device integration. Additionally, this was achieved using EBL with ICP-RIE, which is a highly scalable nanohole fabrication method.

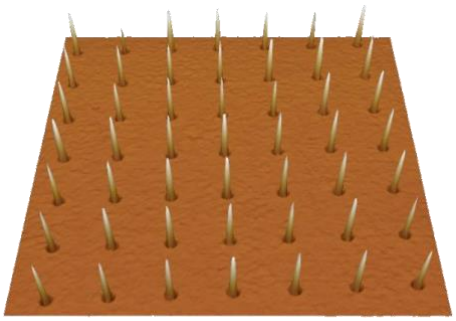

Figure 1. Site-controlled growth of QD arrays demonstrated in AFM.

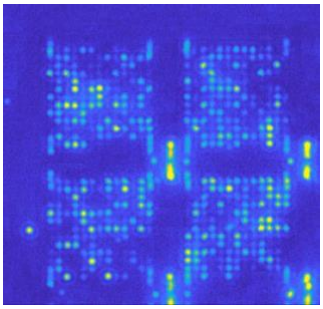

Figure 2. PL emission image from regular arrays of QDs.

1. A. Greilich *et al.*, Nat. Photonics, **5**, 702-708 (2011) 3. P. Lodahl, Quantum Sci. Technol., **3**, 013001 (2017) 5. M. K. Yakes *et al.*, Nano Lett., **13**, 4870-4875 (2013) 2. D. Kim *et al.*, Nat. Phys., **7**, 223-229 (2011).4. J. Herranz *et al.*, Nanotechnology, **26**, 195301 (2015)6. J. Skiba-Szymanska *et al.*, Nanotechnolgy, **22**, 065302 (2011)

A21_55 Insight on Indium droplet driven nucleation of InAs Nanowires on Graphite

Ezekiel Anyebe[1], Q Zhuang[3] Manoj Kesaria[2]

*[1] School of Engineering, Cardiff University, Cardiff, CF24 3AA, UK, [2]School of Physics, Cardiff University, Cardiff, CF24 3AA, UK [2]Department of Physics, Lancaster University, LA1 4YW. *Corresponding email contact: anyebee@cardiff.ac.uk and kesariam@cardiff.ac.uk*

Semiconducting nanowires (NWs) hold enormous potential to become the building block of future photonic and electronic devices due to their unique properties including superior light absorption, enhanced photo-carrier separation and epitaxial growth insensitive to lattice mismatch1. InAs NWs are particularly promising for mid-infrared optoelectronic devices and high-speed electronics due to their narrow direct bandgap, small electron effective mass and high electron mobility2–4. Combined with the scalability and relative aboundance of graphene, the monolithic integration of NWs on graphitic substrates (GS) holds promise for the development of high performance, flexible and cost-effective optoelectronic nanodevices, such as flexible displays, printable electronics, sensors, light emitting diodes and flexible solar cells5,6. For novel flexible devices, III-V optoelectronic devices need to be heterodyne with graphene platform to enable transfer to plastic or flexible metal sheets6. To integrate III-V compound semiconductors onto a different platform, it is essential to mitigate the fundamental limitations posed by intolerance to temperature, sensitivity, power density, capacity and fragility. An investigation of the nucleation mechanism of InAs NWs on graphite via an Indium (In) - droplet assisted technique is presented. Molecular Beam Epitaxy (MBE) growth of InAs NWs was performed on mechanically exfoliated highly oriented pyrolytic graphite (HOPG) sheets transferred onto Si (111) substrates. Prior to the commencement of NWs growth, In droplets were deposited on the GS at a temperature of 220°C and In-flux of 2.2 × 10–7 mbar to facilitate NW nucleation. InAs NWs growth was performed at a temperature of 450−500 °C using As BEP of 9.60 x 10-6 mbar and an Indium growth rate of 0.3 ML/s. To gain detailed insight into the nucleation mechanism, the growth time was varied between 5 and 144 minutes and a reference sample grown for 120 minutes without In droplets predeposition while maintaining same growth condition. FEI XL30 SFEG scanning electron microscope was used to study the surface morphology of as-grown NWs. High-resolution transmission electron microscope (HRTEM) and annular dark field (ADF) scanning TEM images were taken in a JEOL-JEM 2100 and ARM-200F microscopes both working at 200 kV. Focused ion beam (FIB) specimens were prepared using a JIB4500 to investigate the NWs/substrate interface. EDX measurements were carried out with an Oxford Instrument X-MAX 80. It is demonstrated that the uniaxial growth of InAs NWs directly on the GS is driven by the In droplets which etch nanoholes in the GS and promote the formation of InAs seeds underneath the NWs (Figure 1). We highlight that the InAs seed facilitates the vertical directionality of the NWs to enable the growth of InAs NWs exclusively in the [111]/[0001] direction. This study unravels a cost-effective technique for the preferential growth of vertically, well-aligned NWs on graphite with enormous potential for applications in highly efficient and flexible devices.

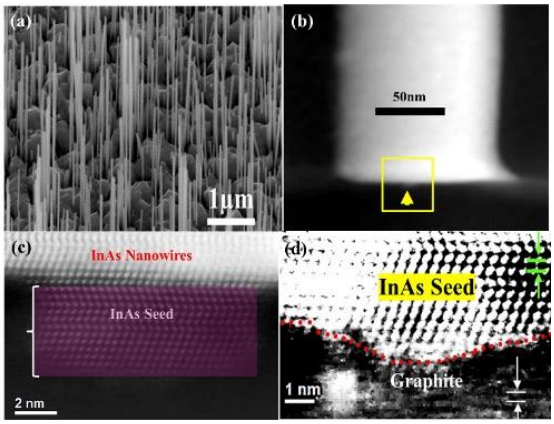

Figure 1: (a) Scanning Electron Micrograph of InAs nanowires; (b) annular dark field (ADF) image depicting a small "seed" underneath the nanowire protruding into the graphitic substrate ; (c) High magnification ADF image showing the InAs seed at the foot of the nanowire; (d) d-spacing of the seed and substrate of 0.35 and 0.34 nm confirms InAs composition of the seed and graphite substrate respectively.

1 W. Wei, X.Y. Bao, C. Soci, Y. Ding, Z.L. Wang, and D. Wang, Nano Lett. 9, 2926 (2009).2 S.-G. Ihn and J.-I. Song., Nanotechnology 18, 355603 (2007).3 E.A. Anyebe and M. Kesaria, Sci. Rep. 9, 1 (2019).4 D. Ren, X. Meng, Z. Rong, M. Cao, A.C. Farrell, S. Somasundaram, K.M. Azizur-Rahman, B.S. Williams, and D.L. Huffaker, Nano Lett. 18, 7901 (2018).5 Y.J. Kim, J.H. Lee, and G.C. Yi, Appl. Phys. Lett. 95, 213101 (2009).6 J.P. Alper, A. Gutes, C. Carraro, and R. Maboudian, Nanoscale 5, 4114 (2013).

A21_50 Temperature-Dependent Characterisation of GaN Nanonetwork on Silicon

Harry Finch[1], Manoj Kersia[2], Sorcha Hulme[1], Vinod R. Dhanak[3], Ivona Z. Mitrovic[1] and Ian Sandall[1]

[1]Department of Electrical Engineering and Electronics, University of Liverpool, UK, [2]School of Physics and Astronomy, University of Cardiff, UK, [3]Department of Physics and Stephenson Institute for Renewable Energy, University of Liverpool, UK

Tunnelling diodes are important electronic devices due to their negative differential resistance (NDR) characteristic, a feature that allows for more efficient power devices and circuit design [1]. The inclusion of gallium nitride (GaN) brings additional benefits; its superior properties, as compared to Si, means GaN-based devices are expected to have stable operation in harsher conditions. Nanowires (NWs) have been grown epitaxially in a direction perpendicular to the substrate at nucleation sites. This results in vertical, one-dimensional structures with a high surface area to volume ratio resulting in a material with reduced defect densities [2] and ideally suited to detector applications. However, the fabrication of devices using NW materials often requires increased complexity. Nanonetwork (NN) devices could offer a solution. GaN NNs have been successfully grown on different substrates [3]–[5] to produce a structure similar to honeycomb with a quasi-planar surface. Metallization of the quasi-planar surface can lead to easier device fabrication compared to NWs while still maintaining enhanced material performance.

In this work, we have investigated the potential of vertical diodes comprising of GaN NNs for use as tunnelling diodes; to the best of authors' knowledge, this is the first time vertical diodes have been demonstrated from this material system. Optimised epitaxial growth of GaN NNs on bare Si (001) and Si (111) has been carried out by varying the substrate temperature, interface layer (SiN), Ga/N flux ratio in order to control the nanowall apex to less than 10 nm and base width to 200 nm. The transmission electron spectroscopy (TEM) and scanning electron microscopy (SEM) images of deposited NN are shown in Figs. 1(a)-(c). The samples were fabricated into vertical diodes by thermal evaporation of Al back contact onto the Si substrate and evaporation of gold onto the GaN layer to create a series of circular diodes with diameters of 0.25, 0.375, 0.5, 1 and 2 mm. The temperature-dependent current-voltage (IV) measurements were taken over the range of 77 K to 275 K, with typical characteristics shown in Fig. 2. At all temperatures, with the exception of 77 K, a clear barrier is observed for the forward current; the onset of this barrier moves to a lower voltage as the temperature is increased. At temperatures below 225 K, a small region of NDR can be seen at voltages after the barrier has been surpassed. To investigate the origin of the barrier (due to Si to SiN or GaN to SiN), an Arrhenius analysis was performed on the onset voltage of the barrier. Figure 3 indicates that two distinct linear regimes exist, suggesting two separate conduction mechanisms are likely to originate from the Si to SiN and GaN to SiN barriers, with change occurring at around 200 K.

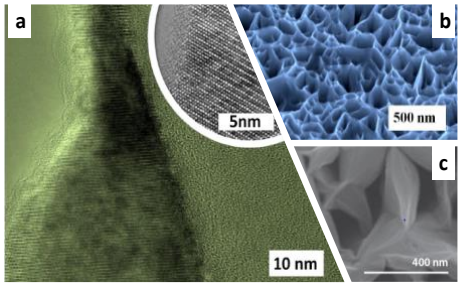

Fig. 1 GaN NN on Si: (a) TEM image; SEM images (b) tilt view (c) top view.

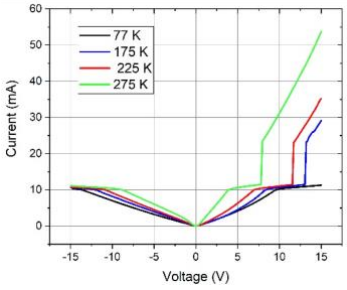

Fig. 2 Temperature dependent IV characteristics of tunnelling diode based on GaN NN on Si.

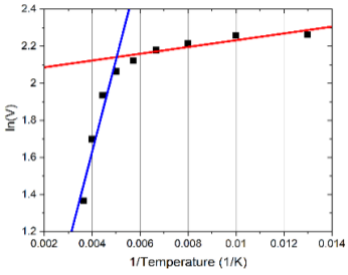

Fig. 3 Arrhenius plot derived from Fig. 2, showing two distinct linear regions

This work provides the first demonstration of vertical diodes based on GaN nanonetworks, with clear tunnelling behaviour being observed as well as evidence of a negative differential resistance at lower temperatures. We have also investigated the spectral response of these devices to evaluate their potential for optoelectronic applications.

Acknowledgement. EPSRC DTP at the University of Liverpool and UGC-UKIERI IND/CONT/G/17-18/18 and F.No.184-1/2018(IC).

[1]S. M. Sadaf *et al.*, *Nano Lett.*, vol. 15, no. 10, pp. 6696–6701 (2015).[2] J. H. Park *et al.*, *J. Nanomater.*, vol. 2014, ID 951360 (2014). [3]M. Kesaria *et al.*, *Cryst. Growth Des.*, vol. 11, no. 11, pp. 4900–4903 (2011). [4]A. Zhong *et al.*, *Nanoscale Res. Lett.*, vol. 7, no. 1, pp. 1–7 (2012).[5] M. Kesaria *et al.*, *Appl. Phys. Lett.*, vol. 99, no. 14, pp. 97–100 (2011)

A21_42 Nanorippled MoS2 Ultra-thin Films enable Broadband and Tunable Light Harvesting

M. Gardella[a], M. Bhatnagar [a], M.C. Giordano[a], D. Chowdhury[a], C. Mennucci[a], A. Mazzanti[b], G. Della Valle[b], C. Martella[c], P. Tummala[c], A. Lamperti[c], A. Molle[c], F. Buatier de Mongeot[a]

(a) Dipartimento di Fisica, Università di Genova, Via Dodecaneso 33, 16146 Genova, Italy
(b) Dipartimento di Fisica and IFN-CNR, Politecnico di Milano, Piazza Leonardo da Vinci, 32 - 20133 Milano, Italy (c) CNR-IMM Unit of Agrate Brianza, via C. Olivetti 2, Agrate Brianza, I-20864, Italy

Transition Metal Dichalcogenides (TMDs) are two-dimensional layered materials that represent a promising candidate for nanophotonics applications thanks to their unique physical properties, like a tunable bandgap and high optical absorption coefficient [1]. However, because of their extremely reduced thickness, innovative strategies for increasing the effective absorption in ultra-thin films are required. To overcome the scalability and reproducibility issues related to the mechanical exfoliation of micrometer scale flakes, large area growth techniques like Chemical Vapour Deposition (CVD) have been recently developed [2].
In our work we moved a step further by growing conformally, via CVD, large area 2D-MoS2 layers on top of nanostructured templates with the aim of increasing optical absorption. We employed Laser Interference Lithography as a cheap and fast lithographic technique to produce a large area (cm2) periodic pattern, from which a silica grating is fabricated. Such substrate is then used as a template for the growth of a conformal MoS2 ultra-thin film. The periodical corrugation introduced by the substrate promotes the excitation of Guided Mode Anomalies (GMA) at the interfaces of the 2D material, confining light into the corrugated MoS2 layer. By tailoring either the grating periodicity or the illumination angle of incidence, the GMA can be tuned from the Near-Ultraviolet to the Near- Infrared. Remarkably, the light absorption enhancement with respect to a flat MoS2 film is not limited to the resonant wavelength of the GMA but is extended to a broadband spectral range due to non- resonant light scattering from the nanogratings [3].
Because of the large area and high throughput achievable, we expect these nanostructured TMDs films to have a strong impact in the field of 2D layered nanophotonics featuring broadband photon harvesting.

[1] D. Jariwala et al. ACS Photonics 2017 [
2] C. Martella et al. Adv. Mater. 2018 [
3] M. Bhatnagar et al. 2020, under review

A21_16 Self-assembled InAs/InP quantum dots via droplet epitaxy in MOVPE at the telecom C-band

E. M. Sala[1,2*], Y. I. Na[2], M. Godsland[2], A. Trapalis[1,2], and J. Heffernan[1,2]
*[1]EPSRC National Epitaxy Facility, The University of Sheffield, Broad Lane, S3 7HQ Sheffield, United Kingdom, [2] Department of Electronic and Electrical Engineering, The University of Sheffield, Broad Lane, S3 7HQ Sheffield, United Kingdom *electronic mail: e.m.sala@sheffield.ac.uk*

We investigate the Droplet Epitaxy (DE) of InAs/InP(001) quantum dots (QDs). DE relies on the self-assembly of group III droplets, which are subsequently crystallized into QDs by the supply of a group V flow, as discovered for the first time by N. Koguchi *et al*. **[1]** in Molecular Beam Epitaxy (MBE). Here, we employ DE in Metal Organic Vapour Phase Epitaxy (MOVPE), the cost effective and large-scale growth technique for semiconductor materials. Among III-V QDs, InAs/InP QDs are to date very attractive for applications in the quantum information technologies, since they are compatible with the low-loss telecom C-band **[2]**. Recently, InAs/InP QDs grown via DE in MOVPE led to the demonstration of the first Quantum Light-Emitting Diode (QLED) operating around 1.55 μm **[2]**. Here, we employ a multi-step growth procedure for Indium droplet crystallization into InAs QDs **[3]**. The growth conditions strongly affect the QD morphology: at crystallization temperatures greater than 500oC, a local material removal takes place in the QD vicinity, leading to QDs positioned in etched pits, as shown in **Fig. 1 (a)**. Controlling the QD morphology and the etching mechanism during growth could lead to a reduction of the fine-structure splitting (FSS) of such QDs, a key parameter for achieving a higher entanglement degree [4].Additional morphological characterizations by transmission electron microscopy (TEM) on buriedQDs reveal their truncated-pyramid shape and local etching, see Fig. 1 (b). Finally, optical investigations by means of low-temperature micro-photoluminescence (LT-PL) show emission ofsingle QDs around 1.55 m, Fig. 1(c), confirming theirgood optical quality at the telecom C-band. This study explores the flexibility of the droplet epitaxy in MOVPE environment for the large-scale fabrication of a broad range of high-quality nanostructures for applications in quantum information technologies at the telecom C-band.

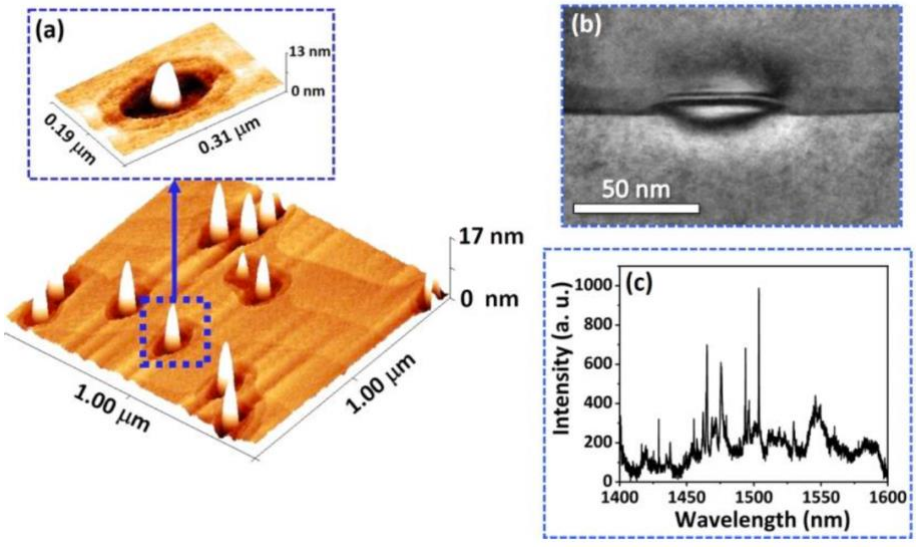

Figure 1 – **(a)** Atomic Force Micrographs (AFM) of free-standing InAs/InP QDs crystallized at 520oC with detail of a single QD placed in an etched pit. **(b)**: TEM micrograph of a single buried InAs/InP QD in an etched pit. **(c)** LT-μPL measurement showing emission from single QDs.

References

[1] N. Koguchi, S. Takahashi and T. Chikyow, Journal of Crystal Growth **111**, 688–692 (1991).
2] T. Müller, J. Skiba-Szymanska, A. B. Krysa, J. Huwer, M. Felle, M. Anderson, R. M. Stevenson, J. Heffernan, D. A. Ritchie, and A. J. Shields, Nature communications **9**, 862 (2018).
[3] E. M. Sala, Y. I. Na, M. Godsland, A. Trapalis, and J. Heffernan, Phys. Status Solidi RRL **2000173**, (2020).
[4] M. Gurioli, Z. Wang, A. Rastelli, T. Kuroda, and S. Sanguinetti, Nature Materials **18**, 799–810 (2019).

A21_71 1550 nm InAs quantum dots on InP and GaAs substrates grown by MOCVD

Bogdan Ratiu, Oumaima Abouzaid, Peter M. Smowton, Qiang Li*

*School of Physics and Astronomy, Cardiff University, CF24 3AA, UK *Email: LiQ44@cardiff.ac.uk*

Quantum dots (QDs) offer many advantages compared to the more established quantum well approach, including lower threshold current, lower temperature dependence, reduced sensitivity to defects and fast gain dynamics [1]. While QD lasers have been demonstrated to be a reliable technology for 1.3 µm emission [2,3], developing high-performance 1.55 µm QD lasers has proven to be more challenging due to issues such as dot uniformity, the formation of quantum dashes and lack of effective DBR for InP structures [1,4]. Nevertheless, the prospect of the lowest attenuation in fibre optics remains very desirable and 1550 nm is an inherently eye- safe wavelength regime for novel 3D imaging and sensing applications. To date, most studies in this area were done with MBE [1,4] whereas MOCVD provides better economic feasibility for large scale production. Achieving this would enable a range of applications in the field of telecommunications, especially in silicon photonics by providing an epitaxially integrated 1550 nm light source.

In this work, we present our findings on the growth of InAs QDs on InP. The growth conditions of the QD layer were studied and correlated to the morphology and optical properties of the dots. We have varied the growth temperature, annealing temperature and annealing duration to optimize the emission of the QDs. Ground state emission around 1550 nm at room temperature with a dot density of 2.8 ×1010 cm-2 and good uniformity has been achieved. An AFM scan of the uncapped layer shows the slightly elongated dots. An increase in PL integrated intensity from a triple layer QD stack has been also observed.

We have grown QDs on both InP substrates and metamorphic InP buffers on GaAs substrates. The InP buffer is grown using a two-temperature process, optimised to reduce the surface roughness. We have investigated the impact of the increased surface roughness and defect density on the morphological and emission properties of the QDs grown on GaAs substrates. Further investigation is being done on encapsulating QDs in a quaternary compound such as InAlGaAs towards practical laser applications.

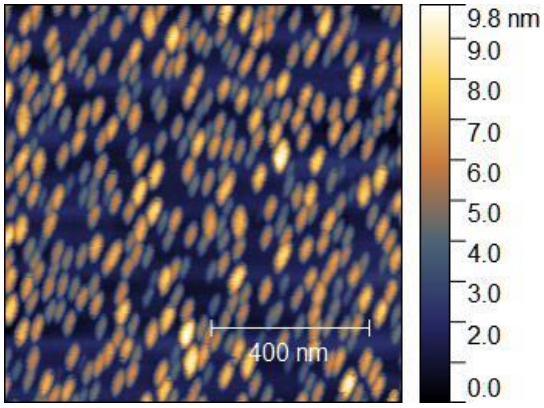

Fig. 1. Uncapped InAs QDs grown on InP.

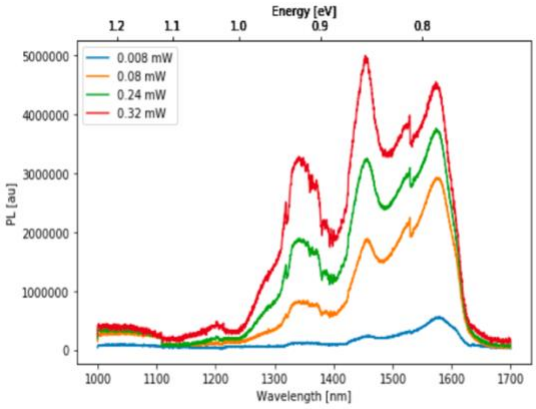

Fig. 2. Room temperature PL emission from single layer InAs/InP quantum dots.

[1] S. L. Portalupi et al., *Semiconductor Science and Technology*, 34(5), p.053001, 2019. [
2] S. Chen et al., *Nature Photonics* 10 (5), p.307, 2016.
[3] D. Jung et al., *Applied Physics Letters* 111 (12), p.122107, 2017.
[4] J. Norman et al., *IEEE Journal of Quantum Electronics*, 55(2), p. 2000511, 2019.

Abstracts

Session 2: Materials Development II

A21_03 InGaAs/AlAs Asymmetric Spacers RTDs for THz Imaging Applications

A AlQurashi and M. Missous

Department of Electrical and Electronic Engineering, the University of Manchester, United Kingdom

Terahertz radiation (THz) has become very attractive to many researchers and companies in the fields of imaging and wireless communications due to its capability to offer high resolution, high data rates and high speed [1]. The resonant tunnelling diode is one of the best candidates for the generation of useful THz radiation because of its high speed, its low fabrication cost, its minimal size, and its ability to operate at room temperature [2]. Double-barrier quantum-well regions were designed with precise resonant energy levels and introducing spacer layers in the RTD is used to prevent the diffusion of dopants from the heavily-doped n-InGaAs into the AlAs barrier. Increasing the oscillation frequency of the RTD has been the main goal for many previous studies, so different methods such as reducing the mesa area of the RTD and increasing the collector spacer thickness have been proposed [2]. Reducing the mesa area of the RTD would decrease the negative differential conductance (NDC), and increasing the thickness of the collector spacer would increase the peak voltage, which could lead to an increase in power dissipation. One of the proposed ways to lower the peak voltage is introducing a thick spacer layer in the emitter region; consequently, the PVCR will increase at the cost of a lower current density [3].

This work presents three asymmetric spacers RTDs with different thicknesses of the quantum well and different percentages of the Indium in the quantum well. Table 1 shows the epi-layer structure of the three proposed asymmetric spacer RTDs. The DC and RF characteristics of asymmetric spacers InGaAs/AlAs RTD have been studied. The quantum well thickness was varied from 2.5 nm to 3.5 nm in 0.5nm step. The Indium percentage was increased from 80% to 90% in 5% step. The negative differential conductance (NDC) increased because of a reduction in the quantum well thickness, as shown in Fig 1(a) so that the output power also increases. The carrier transit time of the asymmetric spacer RTDs becomes shorter as the Indium percentage increases, which results in higher speed operation and higher operating frequency as depicted in Fig 1(b). These results will be discussed in details.

Layer	Material	Doping (cm^{-3})	Thicknes s (nm)
Ohmic layer	$In_{0.53}Ga_{0.47}As$(n++)	2E+19	45
Collector	$In_{0.53}Ga_{0.47}As$(n+)	3E+18	25
Spacer	$In_{0.53}Ga_{0.47}As$	undoped	5
Barrier	AlAs	undoped	1.2
Quantum Well	$In_xGa_{1-x}As$	undoped	t_w
Barrier	AlAs	undoped	1.2
Spacer	$In_{0.53}Ga_{0.47}As$	undoped	10
Emitter	$In_{0.53}Ga_{0.47}As$(n+)	3E+18	25
Ohmic layer	$In_{0.53}Ga_{0.47}As$(n++)	2E+19	400
Substrate	InP		

Table 1. The epi-layers structure of asymmetric spacer RTDs with different quantum well thicknesses and different percentages of Indium.

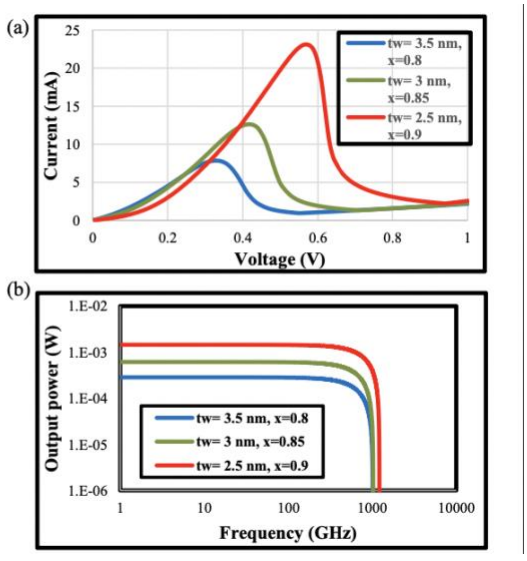

Fig 1: (a) The I-V characteristics of asymmetric spacer RTDs with different quantum well thicknesses and different percentages of Indium. (b) The output power of asymmetric spacer RTDs as a function of oscillation frequency.

[1] Yu, C., et al., The potential of terahertz imaging for cancer diagnosis: A review of investigations to date. Quant Imaging Med Surg, 2012. 2(1): p. 33-45. [2] Maekawa, T., et al., Oscillation up to 1.92 THz in resonant tunneling diode by reduced conduction loss. Applied Physics Express, 2016. 9(2). 3] Mizuta, H., T. Tanoue, and P. Cambridge University, The physics and applications of resonant tunnelling diodes. Cambridge studies in semiconductor physics and microelectronic engineering. 1995.

A21_53 Uni-polar carrier transport in InGaN quantum well systems: From alloy fluctuations to quantum corrected drift-diffusion calculations

M. O'Donovan*[1,2], P. Farrell[3], T. Streckenbach[3], D. Chaudhuri[1], T. Koprucki[3] and S. Schulz[1]

[1] Tyndall National Institute, University College Cork, Cork, T12 R5CP, Ireland
[2] Department of Physics, University College Cork, Cork T12 NY60, Ireland
[3] Weierstrass Institute (WIAS), Mohrenstr. 39, 10117 Berlin, Germany
*email: michael.odonovan@tyndall.ie

InGaN-based quantum wells (QWs) have found widespread applications in light emitting diodes (LEDs) operating in the visible spectral range [1]. To fully exploit the potential of these devices, understanding and tailoring their fundamental properties is of key importance. Especially understanding the carrier transport in InGaN-based devices attracts significant research interest given its importance for optimizing the device performance. Standard drift-diffusion models, which do not include quantum effects, consistently overestimate quantities such as the turn-on voltage of a device. Recent studies revealed the origin of this shortcoming and highlighted that alloy fluctuations and quantum corrections play a major role in correctly modelling transport properties of InGaN-based devices [2]. However, in general these features are not captured in most commercial software packages targeting carrier transport in LEDs.

In this work we present a 3-D multiscale simulation framework that captures random alloy fluctuations on a microscopic level and connects this information to a quantum corrected transport (drift-diffusion) solver. More specifically, we apply an atomistic tight-binding model [3] from which we extract an energy landscape that accounts for alloy and resulting internal built-in field fluctuations on a microscopic level [4]. We transfer this energy landscape through finite element/finite volume meshing to the drift-diffusion solver ddfermi [5]. Moreover, to take into account both random alloy fluctuations and quantum corrections in the transport calculations, we apply the so-called localization landscape theory (LLT) [2].

To visualize the impact of alloy fluctuations and quantum corrections on the carrier transport in an InGaN-based device, and to disentangle these effects from radiative and non-radiative recombination of electrons and holes, we study uni-polar InGaN QW systems. The results are compared to outcomes of a "standard" drift-diffusion solver, similar to the set up found in many (commercial) software packages. In such a standard approach, alloy fluctuations are neglected and the InGaN well is described by a virtual crystal (average material parameters). Our calculations confirm that when alloy fluctuations and quantum corrections are taken into account, the turn-on voltage of the device is shifted to lower values as compared to a virtual crystal approximation (VCA) (cf. figure 1). Thus, the developed multiscale framework provides an ideal starting point for investigations of InGaN-based LEDs, and for guidance to improve their performance further.

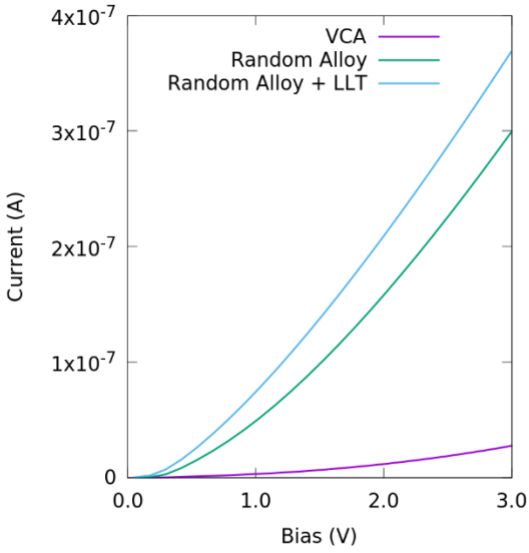

Figure 1. I-V curve for a uni-polar $In_{0.1}Ga_{0.9}N$ single quantum well device in 3 different settings: a) Virtual Crystal Approximation (VCA) (purple) b) Random alloy calculation (green) c) Random alloy calculation with the inclusion of quantum corrections via localization landscape theory (blue).

References

[1] C.J. Humphreys, MRS Bulletin, **33,** (4)**,** p. 459470 (2008); [2] C.-K. Li *et al*, Phys. Rev. B, **95**, p. 144206 (2017); [3] S. Schulz *et al*, Phys. Rev. B, **91**, p. 035439 (2015); [4] D. Chaudhuri *et al* (in press); [5] D.H. Doan *et al*, http://doi.org/10.20347/WIAS.SOFTWARE.DDFERMI (2016)

A21_19 Temperature dependent JV analysis of GaAsBi p-i-n diodes

R. D. Richards, F. Harun, M. R. M Nawawi, Y. Liu, T. B. O. Rockett, J. P. R. David.

Department of Electronic and Electrical Engineering, University of Sheffield, UK

The dark current characteristics of a series of GaAsBi p-i-n diodes were interrogated as functions of voltage, temperature, and band gap. In almost all cases, the complete behaviour could be described by an ideality factor of ~1.6–1.7. However, when growth temperature was used to alter the Bi content (and band gap), the dark currents increased more rapidly than expected with reducing band gap. The results indicate that Bi does not negatively affect the dark current of a device, although care must be taken to grow GaAsBi devices at an appropriate temperature.

GaAsBi is a candidate material for telecommunication lasers [2], multi-junction solar cells [3], and terahertz devices [4]. It is critical to understand the material's dark current behaviour, especially considering the hybridisation of the valence band with Bi-induced, localised states, which causes an enhanced band gap reduction (~ 75 meV/% Bi) [5].

Here we report on the dark current characterisation of a series of GaAsBi p-i-n devices with 100 nm i-regions grown by molecular beam epitaxy. The GaAsBi growth conditions were varied throughout the series to produce devices with a range of Bi contents.

The dark current characteristics of the devices were analysed using the standard Shockley diode equation (see [6] ch2apter 2 for the equation derivation and term meanings):

$$J = q\sqrt{\frac{D}{\tau}}\frac{{n_i}^2}{N}\,exp\left[\frac{qV}{k_BT}\right] + \frac{qW_Dn_i}{2\tau}exp\left[\frac{qV}{2k_BT}\right] \approx C'\left[exp\left(\frac{qV-E_g}{nk_BT}\right)\right]$$

Several weakly temperature dependent terms were assumed to be temperature-independent. This equation characterises a diode's voltage, temperature, and band gap dependence with a single ideality factor (*n*). A representative device's temperature and voltage dependence is shown in figure 1. Up to 0.5 V, the diode behaves predictably, with an ideality factor of 1.58. The band gap dependence data shows that increasing Bi content does not affect the dark currents *per se*, but the growth conditions are critical for maintaining the best material quality.

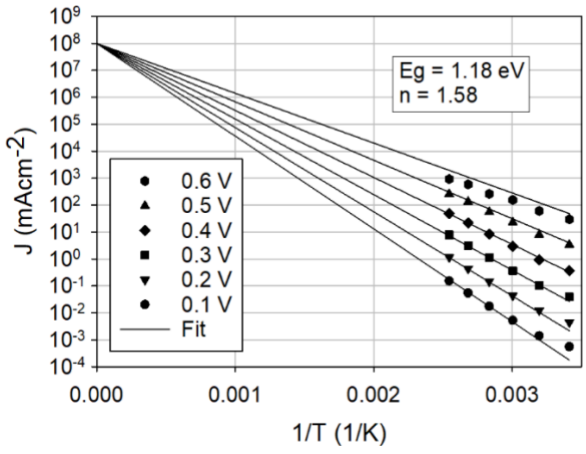

Arrhenius plot of the JV characteristic of one of the devices. The fitting lines all use a common band gap (inferred from [1]) and ideality factor (varied to fit the data).

1. Rockett, T.B.O., et al., Journal of Crystal Growth, 2017. **477**: p. 139-143.
2. Sweeney, S.J. and S.R. Jin, Journal of Applied Physics, 2013. **113**(4): p. 043110.
3. Richards, R.D., et al., Solar Energy Materials and Solar Cells, 2017. **172**: p. 238-243.
4. Pačebutas, V., et al., Semiconductor Science and Technology, 2007. **22**(7): p. 819.
5. Broderick, C.A., et al., Semiconductor Science and Technology, 2013. **28**(12): p. 125025.
6. Sze, S.M., *Physics of Semiconductor Devices*. 2 ed. 1981: John Wiley & Sons, Inc.

A21_65 3D mapping of nanoscale physical properties of VCSEL devices

A. Niblett[1], M. Mucientes[1], S. Shutts*[2], L. Forcieri[1], S. Jarvis[1], I. Eddie[3], W. Meredith[4], M. Haji[5], P. Smowton[2], and O. V. Kolosov*[1]

[1]Physics Department and Materials Science Institute, Lancaster University, LA1 4YB, UK [2]School of Physics and Astronomy, Cardiff University, Cardiff, CF24 3AA, UK, [3]CST Global Ltd, Glasgow, UK, [4]Compound Semiconductor Centre, Cardiff, UK, [5]Time and Frequency Metrology, National Physical Laboratory, Teddington, UK
o.kolosov@lancaster.ac.uk, ShuttsS@cardiff.ac.uk

There is clear lack of methods that allows studies of the nanoscale structure of the VCSEL devices[1] that are mainly focused on the roughness of the DBR, or using FIB cross-sectioning and TEM analysis of failed devices to observe the mechanism of the degradation. Here we present a recently developed advanced approach that combines Ar-ion nano-cross-sectioning with material sensitive SPM[2] to reveal the internal structure of the VCSEL across the whole stack of top and bottom DBR including active area. We report for the first time the direct observation of local mechanical properties, electric potential and conductance through the 3D VCSEL stack. In order to achieve this, we use beam exit cross-section polishing that creates an oblique section with sub-nm surface roughness through the whole VCSEL structure that is fully suitable for the subsequent cross-sectional SPM (xSPM) studies. We used three different SPM measurement modes – nanomechanical local elastic moduli mapping via Ultrasonic Force Microscopy (UFM) [3], surface potential mapping via Kelvin Probe Force Microscopy (KPFM) and mapping of injected current (local conductivity) via Scanning Spreading Resistance Microscopy (SSRM). xSPM allowed to observe the resulting geometry of the whole device, including active cavity multiple quantum wells (MQW), to obtain profiles of differential doping of the DBR stack, profile of electric potential in the active cavity, and spatial variation of current injection in the individual QW in MQW area. Moreover, by applying forward bias to the VCSEL to initiate laser emission, we were able to observe distribution of the potential in the working regime, paving the way to understanding the 3D current flow in the complete device. Finally, we use finite element modelling (FEM) that confirm the experimental results that of the measurements of the local doping profiles and charge distribution in the active area of the VCSEL around the oxide current confinement aperture. While we show that the new xSPM methodology allowed advanced in-situ studies of VCSELs, it establishes a highly efficient characterisation platform for much broader area of compound semiconductor materials and devices.

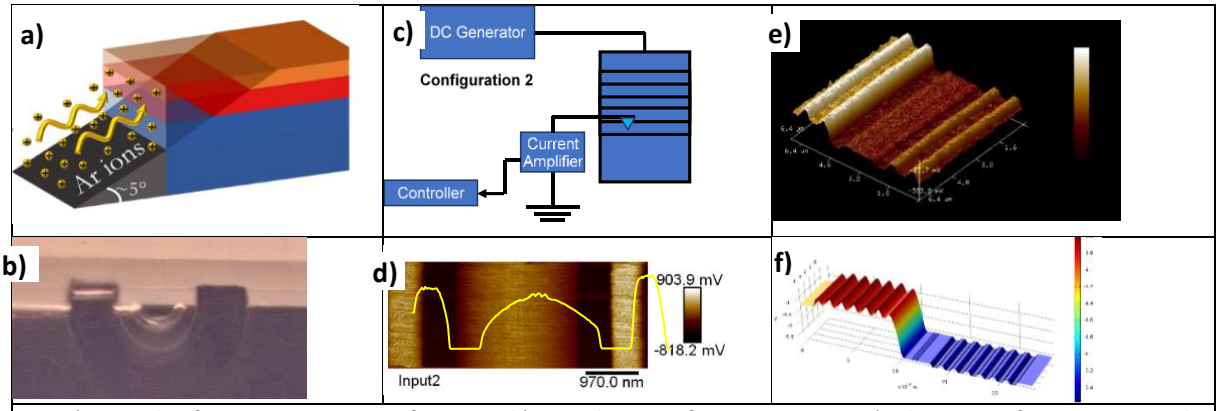

Fig1. a) Principle of nano-crossectioning for xSPM. b) optical image of VCSEL x-section, c) schematics of Scanning Spreading Resistance Microscopy (SSRM) electrical transport measurements, and d) SSRM nano-map of VCSEL active area; e experimental measurements and f) simulation of potential distribution in VCSEL device in the active area and adjacent DBR layers via Kelvin Probe Force Microscopy (KPFM).

1.D. T. Mathes, R. Hull, K. Choquette, K. Geib, A. Allerman, J. Guenter, B. Hawkins and B. Hawthorne, in *Vertical-Cavity Surface-Emitting Lasers Vii*, edited by C. Lei and S. P. Kilcoyne (2003), Vol. 4994, pp. 67-82.
2. A. J. Robson, I. Grishin, R. J. Young, A. M. Sanchez, O. V. Kolosov and M. Hayne, Acs Applied Materials & Interfaces **5** (8), 3241-3245 (2013).
3.. L. Bosse, P. D. Tovee, B. D. Huey and O. V. Kolosov, Journal of Applied Physics **115** (14), 144304 (2014).

A21_05 Colloidal Quantum Dots Visible Light Communication Mediated by Ligand-assisted Interface Modulation

Shijie Zhan[1], Hao Wang[1], Xiangbin Fan[1], Nikos Bamiedakis[1], Richard Penty[1], Ian White[1], Jong Min Kim[1], Bo Hou[1,2*]

1 – University of Cambridge, Department of Engineering, 9 JJ Thomson Ave, Cambridge CB3 0FF, UK
*2 – Cardiff University, Department of Physics and Astronomy, The Parade, Cardiff CF24 3AA, UK *Corresponding Email Address: bh478@cam.ac.uk (Bo Hou)*

The semiconductor light-emitting diodes (LEDs) are potential alternatives to semiconductor lasers for on-chip light sources for the growing demand of short-distance interconnection in the data centre, communication on vehicle, internet of things applications because of their advantages of low cost, high efficiency and scalability. Among various light-emissive materials, colloidal quantum dots (QDs) hold benefits in terms of wavelength tunability from ultraviolet to infrared, low cost, high efficiency and excellent flexibility [1-3]. Over the past decade, progressive improvement has been made to enhance the performance of CdSe, InP, CuInS and perovskite-based quantum dot LEDs (QLEDs) [4-7]. However, the research into the direct utility of QLEDs for communication purposes has lagged while QDs have only been adopted as down-conversion materials working in photoluminescence (PL) mode[8-10]. In this work, the first Cd-free QLED based communication source was demonstrated. Different from free-space visible light communication, this work applied QLED for waveguide communication. To improve the bandwidth, alkane dithiol ligand (1,4-butanedithiol (BDT)) assisted passivation process was utilised which not only enable the disassociation of original surface ligands during the solvent (ACN) treatment but also successfully passivated the accompanying generated interface defects. Moreover, as-prepared CuInZnS QLED shows significant improvement in bandwidth up to ~5MHz, which is more than five times higher than the original bandwidth. This result demonstrates the promising roles of CuInZnS QLEDs in future communication applications and the possible way of bandwidth improvement via surface ligand modulation.

References

[1] X. Dai, Y. Deng, X. Peng, and Y. Jin, Adv Mater **29** (2017).
[2] S. B. Brichkin and V. F. Razumov, Russian Chemical Reviews **85**, 1297 (2016).
[3] J. M. Pietryga, Y. S. Park, J. Lim, A. F. Fidler, W. K. Bae, S. Brovelli, and V. I. Klimov, Chem Rev **116**, 10513 (2016).
[4] W. Ki Bae, J. Kwak, J. W. Park, K. Char, C. Lee, and S. Lee, Advanced Materials **21**, 1690 (2009).
[5] X. Dai, Z. Zhang, Y. Jin, Y. Niu, H. Cao, X. Liang, L. Chen, J. Wang, and X. Peng, Nature **515**, 96 (2014).
[6] J. Lim, M. Park, W. K. Bae, D. Lee, S. Lee, C. Lee, and K. Char, ACS Nano **7**, 9019 (2013).
[7] B. Chen *et al.*, Advanced Functional Materials **22**, 2081 (2012).
[8] I. Dursun *et al.*, ACS Photonics **3**, 1150 (2016).
[9] S. Mei, X. Liu, W. Zhang, R. Liu, L. Zheng, R. Guo, and P. Tian, ACS Appl Mater Interfaces **10**, 5641 (2018).
[10] C. Ruan, Y. Zhang, M. Lu, C. Ji, C. Sun, X. Chen, H. Chen, V. Colvin, and W. Yu, Nanomaterials **6**, 13 (2016).

Abstracts

Session 3: Posters I

A21_61 Modelling bistability in 1D array of coupled micro-ring resonators

Ghada Alharbi, Sang Soon Oh*

School of Physics and Astronomy, Cardiff University, Cardiff, CF24 3AA, United Kingdom.
** E-mail: OhS2@cardiff.ac.uk*

Photonic topological insulator has been studied intensively creating a field called "topological photonics" since Haldane and Raghu's proposal of photonic quantum-Hall effect [1]. These photonic materials are characterized by their edge modes protected by time reversal symmetry with no back-scattering or dissipation even in the presence of the large non-magnetic impurities. Recent study demonstrated that these edge modes can be utilized for photonic topological insulator lasers such as in a 1D Su-Schrieffer-Heeger (SSH) array and in 2D photonic quantum spin-Hall or quantum valley-Hall structures [2,3].

Bistabiity is one of the important nonlinear effects which can be demonstrated using Kerr nonlinear materials. Almost 40 years ago, Kaplan et al. showed theoretically the appearance of bistability in a single ring resonator and the chiral symmetry is broken[4]. More recently, the bistability and the chiral symmetry breaking in a micro-ring resonator has been demonstrated experimentally [5].

In this work, we present a theoretical model that describes a nonlinear system of multi coupled micro-ring resonators in one dimension (Fig. 1(a)). Here we consider the Kerr effect which gives the self-phase modulations and cross phase modulations and the coupling coefficients between ring resonators that alternate from *v* to *w*. The mode intensities of each rings are denoted as $a_{i,\pm}, b_{i,\pm}$, for the clockwise (+) and counter-clockwise (-). We investigate the bistability of the coupled modes in the SSH array (Fig. 1(b)). We describe this model by using the coupled mode theory and solve it by the fourth-order Runge-Kutta method in the time domain. Further, we will present how the bistability changes for different Kerr nonlinearity coefficients.

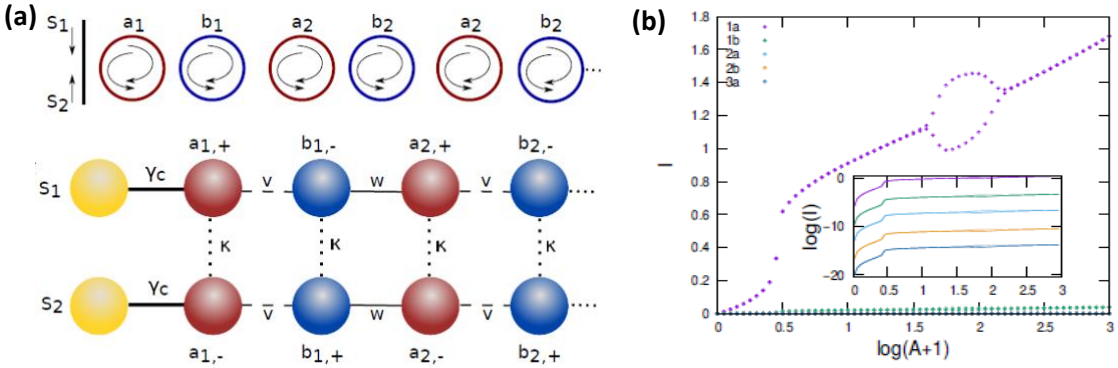

Figure **1 (a)** A schematic of the SSH model of coupled ring resonators with Kerr nonlinearity coefficient κ *a* ,*b* and *s* are the amplitudes of ring resonator and incident beams respectively.
(b) Illustration of the bistabilty in multi coupled ring resonators (5 ring resonators). The inset figure is shown in logarithm scale.

References

[1] S. Raghu and F. D.M. Haldane, Phys. Rev. B, vol. 78, 033834, 2008.
[2] M. Saba, S. Wong, M. Elman, S. S. Oh, and O. Hess, Phys. Rev. B, vol. 101, 054307, 2020.
[3] Y. Gong, S. Wong, A. J. Bennett, D.L. Huffaker, and S. S. Oh, ACS Photon, vol. 7, 2089, 2020.
[4] A. E. Kaplan and P. Meystre, Opt. Commun, vol. 40, 229, 1982.
[5] L. Del Bino, J. M. Silver, S. L. Stebbings, and P. Del'Haye, Sci. Rep. vol. 7, 43142, 2017.

A21_13 Analytical model for cantilever optimization towards photoacoustic energy harvesting enhancements with capacitive transduction.

W. Trzpil [1], N. Maurin[1], D. Ayache, R. Rousseau [1], A. Vicet[1] and M. Bahriz [1]

[1] *IES, Univ. Montpellier, CNRS, F-34000 Montpellier, France*

Gas sensing find tremendous applications in various fields like medicine, air quality, food processing or security and defense. The main challenge in industry is to create an integrated and compact sensor while maintaining its performance and power consumption. Photoacoustic spectroscopy (PAS) gains particular interest in this field due to its excellent selectivity while maintaining compactness. In tunable laser diode absorption spectroscopy (TDLS) the signal is proportional to optical path. Sensitivity in photoacoustic spectroscopy is proportional to the power of the laser, which allows to keep a good sensitivity even with small gas cells. The use of mechanical resonator with high quality factor allows to improve the signal-to-noise ratio and avoid the use of an acoustic chamber [1] as is the case for microphone-based PAS. Micro-electro mechanical systems (MEMS) fabricated in silicon technology remain a reasonable choice to realize a compact and integrated sensor, including laser source and electronics. Cantilever enhanced PAS (CEPAS) [2] offers integrated solution; however, it suffers from the lack of compactness due to optical read out mechanism. Therefore, as a replacement of optical detection we propose a capacitive transduction method, which can be easily integrated, compact and highly sensitive [3]. Nevertheless, to improve capacitive signal it is advantageous to enlarge the capacitor surface which leads to a rise in viscous damping and abbreviates device performance. Undoubtedly, for parameters characterized by opposite trends an optimization based on a theoretical model seems to be a first step towards sensor performance improvement.

Therefore, as a solution, we propose an analytical model for geometry optimization of silicon cantilever for photoacoustic wave collection using capacitance as a transduction mechanism. The study was carried out using silicon cantilever as a model, which brings the opportunity to obtain an analytical solution for all physical parameters. The goal of this research stands maximization of energy harvesting from a photoacoustic wave using cantilever with capacitive transduction mechanisms. To reach this objective we studied the creation of photoacoustic wave in order to find the optimal cantilever geometry for photoacoustic wave energy collection, which includes cantilever resonance frequency related with molecule relaxation time and the relative position of the laser beam and cantilever. In the next step, we optimized energy conversion from photoacoustic force to mechanical movement, thus mechanical sensitivity of the system. This stage focuses on the cantilever mechanical susceptibility enhancement which comprises quality factor, effective mass and favorable resonance frequency. The study for quality factor increasement considers the following losses mechanisms: acoustic, thermoelastic, support and viscous. The last step covers maximization of the capacitive transduction mechanism.

Conducted study gives a solution of cantilever dimensions and frequency for integrated compact gas sensor performance enhancement. Obtained results support the hypothesis that focusing on one aspect, like increasement of quality factor, is insufficient to enhance the performance of the whole device. Finally, it brings valuable insight for further system optimization since it can be extended to more complex structures which is a further perspective.

[1] Kosterev, A. A., Bakhirkin, Y. A., Curl, R. F., & Tittel, F. K. (2002). Quartz-enhanced photoacoustic spectroscopy. Optics letters, 27(21), 1902-1904.

[2] Kauppinen, J. (2007). U.S. Patent No. 7,208,737. Washington, DC: U.S. Patent and Trademark Office.

[3] Alam, A. H. M. Z., Arfah, N., Khan, S., & Islam, M. R. (2010). Design of capacitance to voltage converter for capacitive sensor tra**ns**ducer. American Journal of Applied Sciences, 7(10), 1353

A21_33 Efficient optical modulator based on D-shaped photonic crystal fiber

Nada Yazeed M. Dawood[1,2], B. M. Younis[1,3], Nihal F. F. Areed[2], Mohamed Farhat O. Hameed[3,4,5*], and S. S. A. Obayya[3*]

[1] *Electronics and Communications Department, Misr Higher Institute for Engineering and Technology (MET), Mansoura, Egypt.*
[2] *Electronics and Communications Department, Faculty of Engineering, Mansoura University, Mansoura 35516, Egypt.*
[3] *Centre for Photonics and Smart Materials, Zewail City of Science and Technology, October Gardens, 6th of October City, Giza 12578, Egypt.*
[4] *Nanotechnology and Nanoelectronics Engineering Program, Zewail City of Science and Technology, October Gardens, 6th of October City, Giza 12578, Egypt.*
[5] *Mathematics and Engineering Physics Department, Faculty of Engineering, Mansoura University, Mansoura 35516, Egypt.*
**Corresponding author: sobayya@zewailcity.edu.eg , mfarahat@zewailcity.edu.eg*

In this paper, a novel optical modulator based on D-shaped photonic crystal fiber (D-PCF) is proposed and analyzed. A vanadium dioxide (VO_2) layer is added above the etched surface of the D-PCF as shown in Fig. 1. The VO_2 is used to control the switching process thanks to its transition from the dielectric phase (ON state) with low optical loss to metallic phase (OFF state) with high optical loss. The VO_2 can be controlled by applying an external electric field of 6.5×10^7 V/m [1] at 300° K. The TM mode will be highly attenuated in the OFF state, while it can be propagated with low loss in the ON state. The full vectorial finite element method (FVFEM) is used to analyse the proposed design in terms of the effective index and loss in the dielectric/metallic phases of the VO_2 material. The proposed D-PCF modulator has a relatively low insertion loss of 0.16 dB and high extinction ratio of 30.8 dB at operating wavelength of 6.0 µm with a compact device length of 60 µm. Additionally, the suggested design is based on rectangular lattice which can be fabricated by the well-known stack and draw method [2].

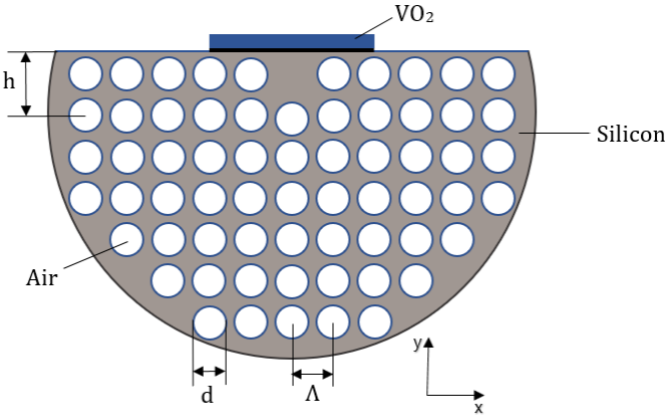

Fig.1. Cross-section of the suggested D-PCF optical modulator

References

[1] B. Wu, A. Zimmers, H. Aubin, R. Ghosh, Y. Liu, and R. Lopez, "Electric-field-driven phase transition in vanadium dioxide," Phys. Rev. B - Condens. Matter Mater. Phys., vol. 84, no. 24, pp. 2–5, 2011, doi: 10.1103/PhysRevB.84.241410.
[2] PYSZ *et al.,* Stack and draw fabrication of soft glass microstructured fiber optics Bull. Pol. Ac.: Tech. 62(4) 2014

A21_35 Dual-Arm Horn Nano-Antenna for Wireless Communications

Mohamed Elsaid [1,2], K. R. Mahmoud[3], Mohamed Hussein[1,2,4], Mohamed Farhat O. Hameed[1, 5, 6*], S. S. A. Obayya[1*]

[1]*Centre for Photonics and Smart Materials, Zewail City of Science and Technology, October Gardens, 6th of October City, Giza, 12578 Egypt.*
[2] *Department of Physics, Faculty of Science, Ain Shams University, Abbassia 11566, Cairo, Egypt.*
[3]*Electronics, Communications, and Computers Department, Faculty of Engineering, Helwan University, Cairo, Egypt*
[4]Light Technology Institute, Karlsruhe Institute of Technology, Engesserstrasse 13, 76131 Karlsruhe, Germany
[5]*Nanotechnology and Nanoelectronics Engineering Program, Zewail City of Science and Technology, October Gardens, 6th of October City, Giza, 12578 Egypt.*
[6]*Mathematics and Engineering Physics Department, Faculty of Engineering, Mansoura University, Mansoura, Egypt*
**Corresponding author: sobayya@zewailcity.edu.eg , mfarahat@zewailcity.edu.eg*

An optical horn nanoantenna (NA) with dual arm is introduced and numerically studied for the wireless communication purposes. Figure 1 (a) shows the proposed NA design. It may be seen that the radiator of the dual arm horn NA resembles W-shape. It consists of two symmetric dual arms with arm lengths l_1 = 722 nm and l_2 = 660 nm with thickness of t = 100 nm. The flaring angle of the horn NA is θ = 22.7°. The NA feeding through two parallel rectangular waveguides with length *a = 1000 nm* and cross section *b×c = 100×50*. The two rectangular waveguides are separated with distance g = 30. The W-shape horn NA is made from sliver. The NA is completely encapsulated in silicon dioxide with refractive index of n=1.44. The proposed optical NA is operating at wavelength of λ=1550 nm. The proposed design is simulated using finite integration technique (FIT) [1]. The performance of the proposed design is analyzed in terms of directivity, radiation efficiency and electric field distribution. The suggested NA achieves high directivity and realized gain of 17.4 and 8.5 are achieved, respectively. The achieved directivity has an improvement of 12.25% compared to the conventional horn NA reported in [2]. This is attributed to multiple tips in the suggested structure that accumulate the current and maximize the electric field. Fig.1 (b) illustrates the electric field distribution of the suggested NA. Additionally, a radiation efficiency of 77% is accomplished. Overall, the obtained radiation characteristics of the designed NA are satisfied for the wireless nano-links and wireless applications.

(a) **(b)**

Fig.1 (a) 2D geometrical structure of the suggested NA and (b) the electric field distribution of the reported dual arm NA.

References

[1]] M. Clemens and T. Weiland, "Discrete electromagnetism with the finite integration technique," Progr. Electromagn. Res. (PIER), vol. 32, pp. 65–87, (2001).

[2] Y. Yang *et al.*"Plasmonic sectoral horn nanoantennas," Opt. Lett. Vol 39, PP 3204–3207, 2014.

A21_36 Highly Sensitive 1D Photonic crystal Hemoglobin Biosensor

Mahmoud Salman. S. Ibrahim[1], Mohamed. Tarek[1], S. S. A. Obayya[2], Mohamed Farhat O. Hameed[2, 3,4]

[1]Physics Department, Faculty of Science, El-Arish University, El-Arish, Egypt
[2]Centre for Photonics and Smart Materials, Zewail City of Science and Technology, Zewail City of Science and Technology, October Gardens, 6th of October City, Giza, 12578, Egypt
[3] Nanotechnology and Nanoelectronics Engineering Program, Zewail City of Science and Technology, October Gardens, 6th of October City, Giza, 12578, Egypt
[4]Mathematics and Engineering Physics Department, Faculty of Engineering, Mansoura University, Mansoura, Egypt
**Corresponding authors: sobayya@zewailcity.edu.eg , mfarahat@zewailcity.edu.eg*

In this paper, highly sensitive 1D Si/air photonic crystal (PhC) biomedical sensor is introduced for the detection of the hemoglobin concentration (0-300 g/L). The proposed design, as shown in Fig. 1, has a defect layer filled by the blood sample where its refractive index is related to the hemoglobin concentration. Therefore, the resonance wavelength changes accordingly. In order to optimize the sensor sensitivity, the PhC geometrical parameters are studied by full vectorial finite element method. The suggested design achieves high sensitivity and quality factor of 341 nm/RIU and 450097, respectively for the TE polarized mode. Additionally, the TM mode offers high sensitivity and quality factor of 314 nm/RIU and 35977, respectively which are higher than those reported in the literature [1, 2]. Further, detection limit and linearity of 3.09×10^{-7} RIU and 1.00 are obtained by the TE mode while 4.93×10^{-6} RIU and 0.99983 for the TM polarized mode.

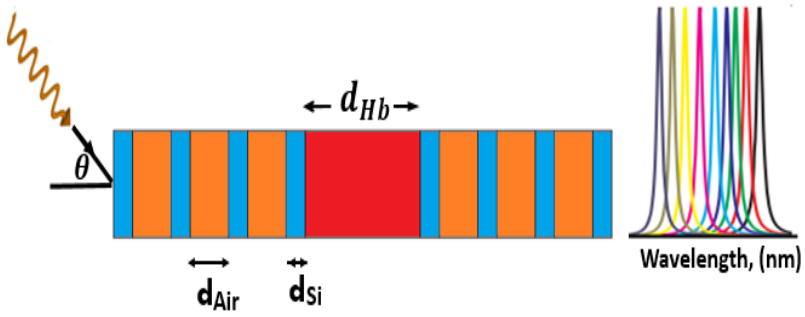

Fig.1. Cross-section of the proposed 1D Si/air PhC hemoglobin sensor. The red region represents the blood sample defect

References

[1] S. Olyaee, M. Seifouri, H. Mohsenirad, "Label-free detection of glycated haemoglobin in human blood using silicon-based photonic crystal nanocavity biosensor", *Journal of Modern Optics*, Vol. 63, No. 13, 2016.
[2] M. M. Abadla, H. A. Elsayed, "Detection and sensing of hemoglobin using one-dimensional binary photonic crystals comprise

A21_04 Intermittent Dynamics Switching in Discrete-mode Semiconductor Lasers with Long External Cavity Optical Feedback

Zhuqiang Zhong[1], Da Chang[1], Wei Jin[1], Min Won Lee[2], Jianming Tang[1], and Yanhua Hong[1]

[1] School of Computer Science and Electronic Engineering, Bangor University, Wales, LL57 1UT, UK, 2 Laboratoire de Physique des Lasers CNRS UMR 7538, Universit´e Paris 13, Sorbonne Paris Cit´e, 93430 Villetaneuse, France.

Intermittent dynamic, characterised by laminar and turbulent phases, is widely reported in semiconductor lasers subject to optical feedback. Most of this research focus on the intermittence between two dynamic states when an external-cavity lasers (ECLs) operates slightly above its threshold current. However, the studies of intermittency on the route to chaos of a semiconductor laser with long external cavity and the laser biases well above the threshold current are scarce.

In this paper, intermittent dynamics of a special type of semiconductor laser - discrete-mode (DM) semiconductor laser is investigated. The length of external cavity is very long with a feedback round trip time of ~216 ns. The results show two types of intermittent dynamics switching. One is the regular intermittent dynamics switching between stable state and period-one oscillation possessing a square-wave envelope. The other is the irregular intermittent dynamics switching between stable state and multi-state and chaos for higher feedback ratio at a relative high bias current. Fig. 1(a) illustrates a time trace of the DM laser operating at 30mA (threshold current is 12mA) with a feedback ratio of 0.07. The result demonstrates that the DM laser is at an intermittent dynamic, which includes laminar (steady) and turbulent (period-one) phases. While unlike the results of random appearance of laminar and turbulent phases in most published papers, the occurrence of laminar and turbulent phases is very regular. When the bias current increases to 70mA, more complex intermittent dynamics are observed, as shown in Fig. 1(b). Some stochastic irregular bursts of intensity away from the laminar phases can be observed, and the dynamical state switches randomly from stable state to multi-state and chaotic state. In addition, similar evolution route containing intermittent dynamics can be observed at wide ranges of bias currents and feedback ratios.

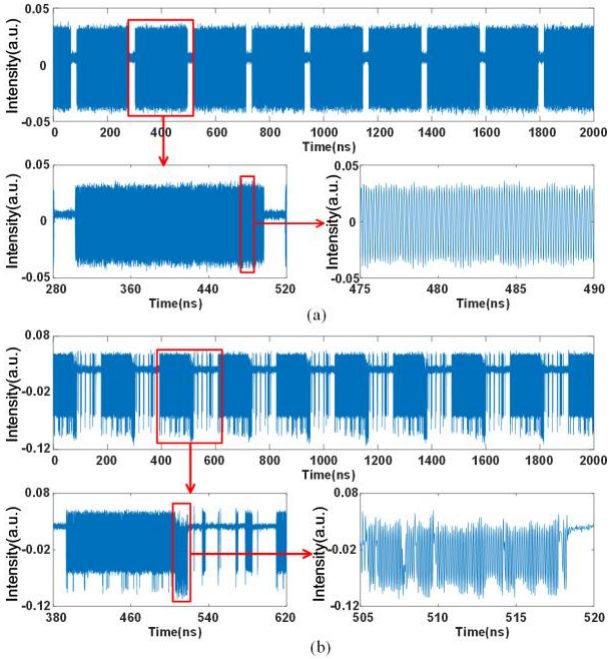

Fig.1. Time traces of a discrete mode laser output at the bias current and feedback ratio of (a) 30mA and 0.07, (b) 70mA and 0.57, respectively.

Acknowledgements

This work was supported in part by research projects of the DSP Centre funded by the European Regional Development Fund (ERDF) through the Welsh Gov

A21_10 Mode selection in L40 photonic crystal cavities via spatial pumping

Lingfang Wang [1], Yunran Wang[2], Henry Francis[2], Ri Lu [1], Mingjun Xia [1], Feng Liu [1], Xing Lin [1], Mark Hopkinson[2] and Chaoyuan Jin[1*]

[1] *College of information Science and Electronic Engineering, Zhejiang University, China* [2] *Department of Electronic and Electrical Engineering, University of Sheffield., UK Correspondence Author:* jincy@zju.edu.cn

Abstract. Recently, the effective manipulation of mode oscillation based on parity- time symmetry effects and spatial injection has gained remarkable research attention. While the single-mode selection can be understood by the spatially modulated gain, the underneath physics of the single-mode lasing has not been discussed. Here, we develop a rate equation model which considers the spatially modulated gain and spontaneous emission, which are inherently governed by the ripple of the vacuum electromagnetic field in a Fabry-Pérot (FP) microcavity. By manipulating the interplay between the spatial oscillation of the vacuum field and external spatial optical injection, single longitudinal mode operation is observed in a FP-type microcavity with a side mode suppression ratio (SMSR) exceeding 40 dB. In the experiment (Fig. 1), one of six FP- type modes is selected for lasing by spatially pumping a L40 PhC cavity, the SMSR is increased from 3.85dB to 17.48dB compared to the same input power under uniform pumping.

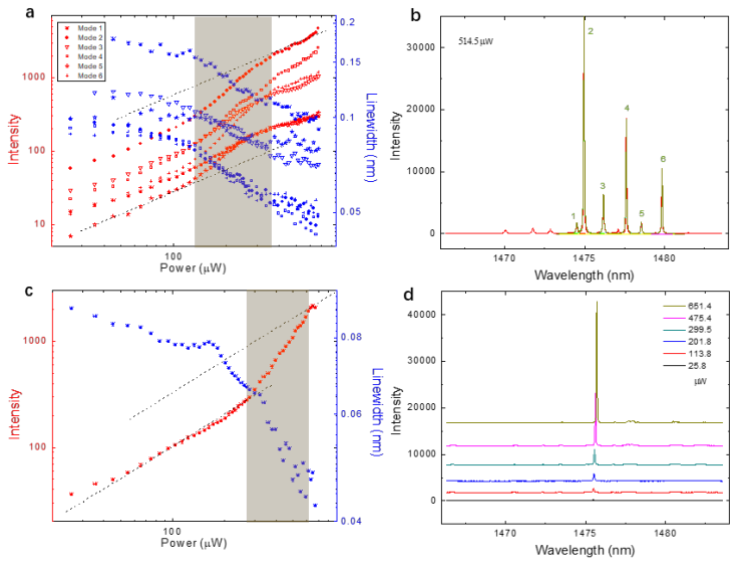

Fig.1 Experiment results in the same L40 PhC cavity via spatial pumping. a b. six lasing modes in uniform pumping. c d. one lasing mode in spatial pumping.

A21_66 Gain measurement of Vertical Cavity Surface Emitting Lasers using Segmented Contact Technique

Curtis Hentschel[1], Craig P. Allford[1], Sara-Jayne Gillgrass[1], Zhibo Li[1], Josie Nabialek[1], Wyn Meredith[2], Iwan Davies[3], Samuel Shutts[1] and Peter M. Smowton[1]

[1]EPSRC Future Compound Semiconductor Manufacturing Hub, School of Physics and Astronomy, Cardiff University, Cardiff, UK; [2]Compound Semiconductor Centre, UK; [3]IQE plc, Newport, UK.

A large growth in the vertical cavity surface emitting laser (VCSEL) market is expected to continue over the next few years, particularly in sensing applications, such as face and gesture recognition. In addition, the emergence of specialised miniature atomic sensors, require VCSELs which meet stringent requirements. Test and verification of VCSEL epitaxial structures is necessary to ensure the desired specifications are met. This can be achieved by a combination of growth calibrations - such as room temperature photoluminescence and cavity resonance reflectance measurements - plus fabrication of full VCSEL structures to give laser output characteristics, tested at the wafer-level. However, making informed decisions on appropriate changes to the epitaxial structure to optimise device performance is challenging. One of the key factors to consider is the gain-peak to cavity resonance detuning. To ensure efficient operation, with low threshold current, the gain-peak should coincide with the cavity resonance; this is complicated since each of these parameters has a different temperature dependence.

Currently, there is no direct way of measuring the gain-peak wavelength in VCSEL structures. The highly reflecting Bragg mirrors, forming the vertical cavity, make it difficult to prevent lasing and apply traditional gain measurement techniques. Test wafers can be grown with a nominally identical active region, but this cannot be used to evaluate the actual wafer that VCSEL devices would be fabricated from. Photovoltage spectroscopy (PVS) can be used to assess quantum-well transition energies and cavity resonance, as a function of temperature, but it does not indicate what occurs under forward bias and cannot be used to measure the optical gain.

Here, we investigate the optical gain characteristics of VCSEL material using a stripe-length method (typically used on edge-emitting laser structures), to measure the in-plane modal-gain as a function of carrier injection, for a range of operating temperatures. By measuring the transverse electric (TE) polarised in-plane modal gain, the gain of the vertical cavity mode can be found by accounting for the differences in the confinement factor of the modes. In addition to the gain magnitude and gain peak wavelength values that are routinely obtained for edge emitting structures, measurements also contain information relating to the vertical cavity resonance.

Acknowledgements: C. Hentschel would like to acknowledge support from an EPSRC Industrial-CASE Award co-funded by IQE plc.

A21_02 Self-Catalyzed AlGaAs Nanowires and AlGaAs/GaAs Nanowire-Quantum Dots on Si Substrates

Giorgos Boras,[†,||] Xuezhe Yu,[†,||] H. Aruni Fonseka,[‡] George Davis,[§] Anton V. Velichko,[§] James A. Gott,[‡] Haotian Zeng,[†] Shiyao Wu,[⁑] Patrick Parkinson,[⌞] Xiulai Xu,[⁑] David Mowbray,[§] Ana M. Sanchez[‡] and Huiyun Liu[†]

[†]*Department of Electronic and Electrical Engineering, University College London, London WC1E 7JE, United Kingdom*
[‡]*Department of Physics, University of Warwick, Coventry CV4 7AL, United Kingdom*
[§]*Department of Physics and Astronomy, University of Sheffield S3 7RH, United Kingdom*
[⁑]*Institute of Physics, Chinese Academy of Science, Beijing 100190, China*
[⌞]*Department of Physics and Astronomy and the Photon Science Institute, University of Manchester, Manchester M13 9PL, United Kingdom*

Abstract

Self-catalyzed approach for the synthesis of AlGaAs nanowires (NWs) and AlGaAs/GaAs nanowire quantum dots (NWQDs) is an advantageous growth technique in comparison to the regularly employed Au-catalyzed method, as it eliminates Au contamination issues that form mid-gap states. Hence, the structures are rendered compatible with CMOS technology applications and drive electronics. In the current work, we report the growth of AlGaAs NWs and NWs with a GaAs dot axially embedded, monolithically on Si (111) substrates via solid-source molecular beam epitaxy, by employing the self-catalyzed method. Structural studies reveal the spontaneous formation of an Al-rich AlGaAs shell, thicker at the NW base and thinning towards the tip, with the opposite trend observed for the NW core. Wide alloy fluctuations in the shell are conspicuously observed. AlGaAs NWs with nominal Al contents of 10%-30% have robust room temperature photoluminescence emission in the range of 1.5 to 1.72 eV. Individual structures with an embedded 4.9 nm-thick GaAs segment exhibit clear quantum dot behavior, with spatially localized emission, exciton and biexciton recombination lines and an exciton linewidth of roughly 490 μeV at low temperature. Our results demonstrate the properties and behaviour of AlGaAs NWs and AlGaAs/GaAs NWQDs grown via the self-catalyzed approach for the first time and display their potential for a range of novel applications such as nanolasers and non-classical light emitters, including single photon sources.

A21_70 Large-scale metamaterial thermal emitters for infrared heating application

Yongkang Gong and Sang Soon Oh*
School of Physics and Astronomy, Cardiff University, Cardiff, CF24 3AA, United Kingdom.
* *E-mail: OhS2@cardiff.ac.uk*

Space heating is a huge source of energy consumption in cold/cool climate. In the UK, for instance, energy consumption for space heating are 28,728 and 10,084 thousand tonnes of oil equivalent in domestic and service sectors[1], which accounts for >50% of total energy use. New approaches to energy efficiency heating are key to reduce fuel poverty to aid our society in transition to low carbon economy. As an alternative to air heating technolgy (i.e, heat is generated and dissipated into air) that is very inefficient as it convects heat to the whole space, infrared heating can be used to heat objects locally and instantly without having to warm up air in whole space and can consume >30% less energy[2]. Commercial infrared panels, typically made of tungsten, nichrome alloys, ceramic materials etc, emit infrared electromagnetic wave based on grey-body radiation and their power depends on operating temperature and optical emissivity of heating panel materials. There are two major issues that have inhibited the market penetration to industry and homeowners: dazzling red glare and low electric-light conversion efficiency.

Thermal emitters based on metamaterials have recently attracted a great attention[3, 4]. Here we report a new kind of electrically controlled layered-metamaterial thermal emitters (LTEs) composed of multiple dielectric/metallic nanolayers[5]. In contrast to the other reported nanophotonic thermal emitters, the proposed LTEs are thermal-photonic integrated and have advantage of tailoring thermal radiation with selectively enhanced emissivity in a broadband infrared regime and effectively suppressed emissivity at the visible wavelengths. We design and analyze the optical characteristics of the LTEs both analytically and numerically, and experimentally investigate their optical and thermal properties including angular dependent emissivity, spectral radiation, thermal photonic properties, and electro-optical conversion efficiency. Our study offers a cost-effective, spectrally selective, and integrated infrared source solution that could possibly overcome the drawbacks of the existing infrared heater technologies (i.e., dazzling glare and low emissivity at the infrared wavelengths).

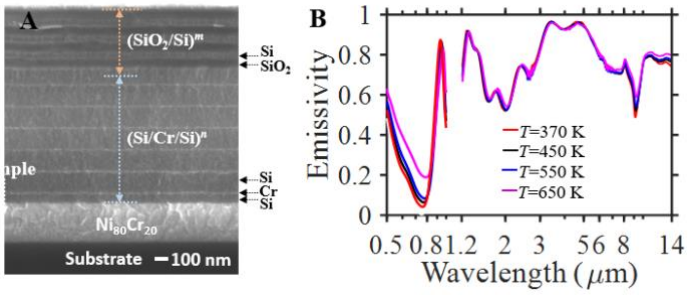

Figure 2 (A) SEM image of the cross section of the LTEs that consists of two 1D photonic lattices with structures of $(Si/Cr/Si)^n$ and $(SiO_2/Si)^m$ lying on top of a $Ni_{80}Cr_{20}$ nanolayer. (B) The measured emissivity at the angle of $\theta = 45^\circ$ under different structure temperature obtained by controlling the voltage applied to the $Ni_{80}Cr_{20}$ layer.

References

[1]. Estimates of heat use in the United Kingdom in 2013; https://www.gov.uk/government/statistics/energy-trends-september-2013-special-feature-articles-estimates-of-heat-use-in-the-united-kingdom-in-2012
[2]. K, Roth, et al., "Emerging Technologies: Infrared Radiant Heaters," ASHRAE, June 2007.
[3]. Y. Gong, et al., "Highly efficient and broadband mid-infrared metamaterial thermal emitter for optical gas sensing," Opt. Lett. 42, 4537-4540 (2017)
[4]. Y. Gong, et al., "Coherent emission of light using stacked gratings," Phys. Rev. B. 87, 205121 (2013)
[5]. Y. Gong, et al., "Integrated and spectrally selective thermal emitters enabled by layered metamaterials," Nanophotonics, 2021, https://doi.org/10.1515/nanoph-2020-0578

A21_59 Improved performance of 1.3 µm quantum dot by direct Si doping

Huiwen Deng[1], Mingchu Tang[1], Peter Smowton[2], Chaoyuan Jin[3], Alwyn Seeds[1], Huiyun Liu[1]

[1]*Department of Electronic and Electrical Engineering, University College London, London, WC1E 7JE, UK*
[2]*School of Physics and Astronomy, Cardiff University, Cardiff, CF10 3AT, U.K.*
[3] *College of Information Science and Electronic Engineering, Zhejiang University, Hangzhou 310007, China*

InAs/GaAs QDs have been researched intensively due to their superior advantages such as ultra-low threshold current density, recorded high temperature lasing, and the insensitivity to the temperature and dislocations. In order to further improve QD performance, doping techniques are introduced. Modulation p-doped technique can improve the high-temperature performance, the differential gain and small-signal modulation response. While the direct n-doped technique is found to yield better uniformity, to enhance photoluminescence (PL) and to suppress the thermal quenching. In this letter, direct Si-doped technique for InAs/GaAs QDs is investigated.

The InAs/GaAs QD calibration samples for lasers used in this study were grown on n-type GaAs substrates by molecular beam epitaxy. Figure (a) depicts the sample structure with 8 stacked QD layers as the active region. Each of the calibration samples consisted of a 200-nm n-GaAs buffer, a 100-nm Al0.4Ga0.6As layer, a 50-nm GaAs layer, the active region, a 100-nm upper Al0.4Ga0.6As layer, a 50-nm GaAs buffer layer, and an InAs QD layer without capping. Each InAs QD layer in the active region composed a 2.85 monolayer of self-assembled InAs QDs in 6-nm In0.16Ga0.84As quantum well with direct n-type doping and without doping and a 42.5-nm GaAs spacer layer. To optimised the Si doping level of InAs/GaAs QDs, three samples with different doping concentrations, nominally 1.5 electrons per dot, 3 electrons per dot and 5 electrons per dot, were grown under the similar conditions. Figure (b) presents the room temperature PL of four samples, in which the inset figure gives atomic force microscopy (AFM) result of the 1 〖µm〗^2 centre area for the 3-electron-per-dot QD calibration sample. Figure (c) shows the PL lifetime of the ground state at 80K for all samples. It clearly shows that the n-doped technique increases the PL lifetime.

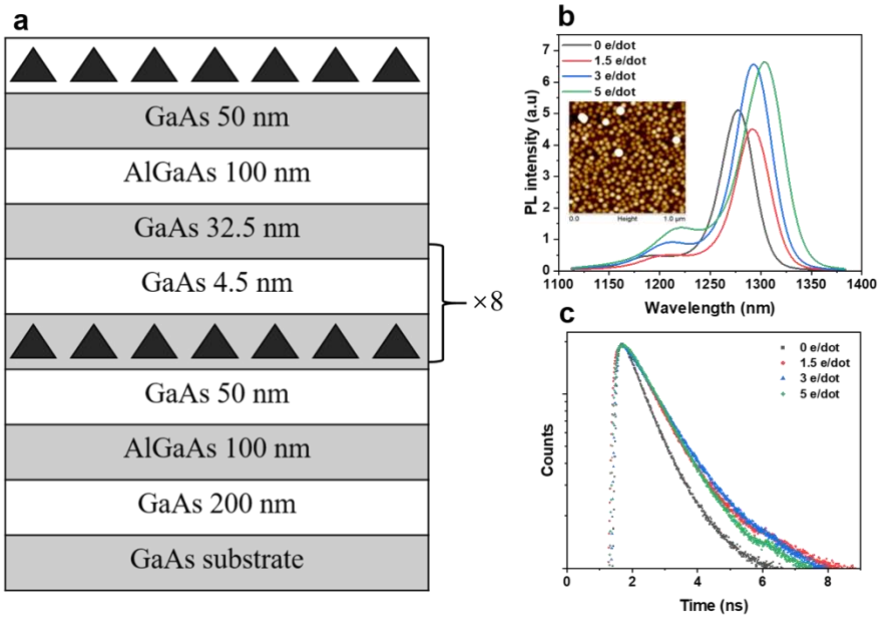

Figure a. Schematic of the layer structure grown on the GaAs substrate. Figure b. RT PL results for samples. Figure c. The AFM result of 1 〖µm〗^2 centre area for the 3-electron-per-dot QD calibration sample

A21_29 Cross-shaped-silicon nanowires for highly efficient solar cell

R. El-Bashar,[1,2] M. Hussein,[1,3,4] S. F. Hegazy,[1.2] Y. Badr,[2] S. S. A. Obayya [1,*] Mohamed Farhat. O. Hameed,[1,5,6*]

[1]Centre for Photonics and Smart Materials, Zewail City of Science and Technology, October Gardens, 6th of October City, Giza 12578, Egypt
[2]National Institute of Laser Enhanced Sciences (NILES), Cairo University, Giza 12613, Egypt
[3]Department of Physics, Faculty of Science, Ain Shams University, Abbassia 11566, Cairo, Egypt
[4]Light Technology Institute, Karlsruhe Institute of Technology, Engesserstrasse 13, 76131 Karlsruhe, Germany
[5]Nanotechnology and Nanoelectronics Engineering Program, Zewail City of Science and Technology, October Gardens, 6th of October City, Giza 12578, Egypt
[6]Mathematics and Engineering Physics Department, Faculty of Engineering, Mansoura University, Mansoura 35516, Egypt
**Corresponding author: sobayya@zewailcity.edu.eg , mfarahat@zewailcity.edu.eg*

An innovative design of cross-shaped (CS) silicon nanowire (NW) is presented for thin film solar cell applications. The small filling ratio of the proposed design reduces the surface reflection with improved light absorption. Figure 1 (a) shows the unit cell of the proposed NW. The optical characteristics of the CS NW are studied by using finite difference time domain (FDTD) via Lumerical software package [1]. Further, the particle swarm optimization (PSO) technique is utilized to optimize the geometrical parameters to maximize the light absorption. Figure 1 (b) shows the absorption spectrum of the thin film SC, conventional cylindrical NW and the suggested CS NW. It may be seen that the reported NW has better absorption than the other studied SCs. The proposed CS NW SC has an ultimate efficiency of 34.6 % and short circuit current density of 28.4 mA/cm^2 with an enhancement of 22 % over the cylindrical NW counterpart. This is due to the geometry of the CS NW which produces multiple light scattering between the NWs. Additionally, multiple cavities are produced between the adjacent NWs with improved absorption. The optical ultimate efficiency of the reported NW SC is improved to 41% by adding a bottom substrate. This is owing to the coupling between the modes supported by the NW and that of the substrate.

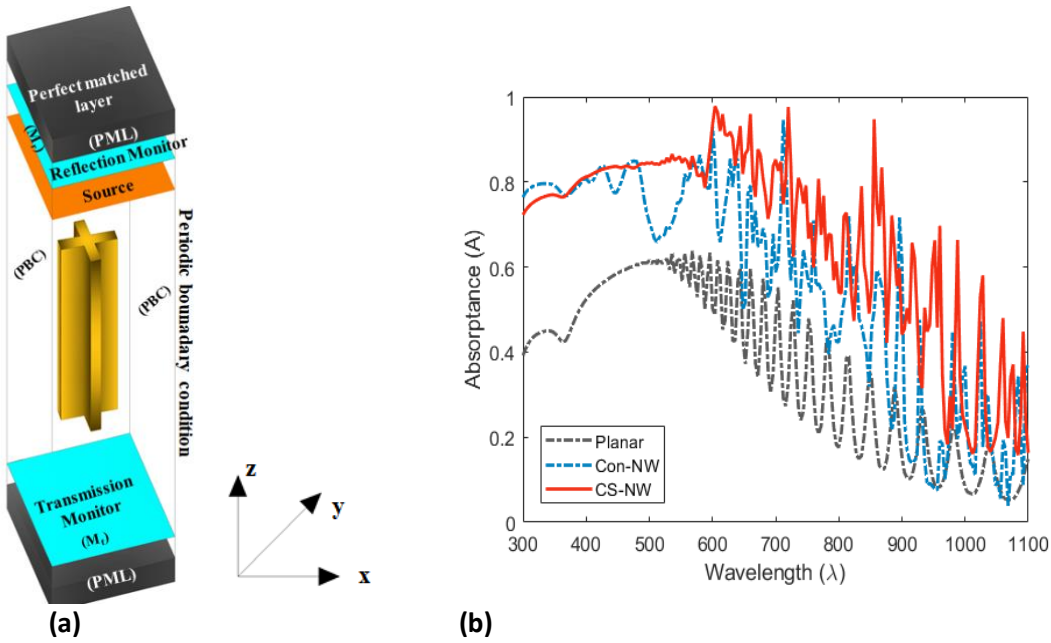

Fig. 1 (a) Schematic diagram of the unit cell of the CS NW and (b) the absorption spectrum of the planar thin film SC, conventional cylindrical NW and CS NW

References

[1] I. Lumerical Solution, ", Inc., https://www.lumerical.com."

A21_30 Enhanced light trapping in thin film solar cell

Mahmoud A. Elrabiaey [1], Mohamed Hussein[1,2,3], Mohamed Farhat O. Hameed [1,4,5*], and Salah S. A. Obayya [1]

[1] Centre for Photonics and Smart Materials, Zewail City of Science and Technology, October Gardens, 6t[h] of October City, Giza 12578, Egypt.
[2]Department of Physics, Faculty of Science, Ain Shams University, Abbassia 11566, Cairo, Egypt
[3]Light Technology Institute, Karlsruhe Institute of Technology, Engesserstrasse 13, 76131 Karlsruhe, Germany
[4]Nanotechnology and Nanoelectronics Engineering Program, University of Science and Technology, Zewail City of Science and Technology, Giza 12578, Egypt.
[5]Mathematics and Engineering Physics Department, Faculty of Engineering, Mansoura University, Mansoura 35516, Egypt,
**Corresponding authors: sobayya@zewailcity.edu.eg , mfarahat@zewailcity.edu.eg*

In this study, a novel thin film solar cell (TFSC) is reported with a thickness of 1.0 µm. In order to improve the light trapping in the suggested design, a dielectric nanowire (NW) is embedded through the C-Si active layer. The generated photocurrent density of the proposed TFSC is calculated using finite-difference time-domain (FDTD) vai Lumerical software package [1]. Further, the geometrical parameters are optimized using particle swarm optimization (PSO) technique to maximize the absorption through the SC. Figure 1(a) shows the schematic diagram of the proposed C-Si TFSC, with a thickness of 1 µm and 75 nm of Si_3N_4 as an anti-reflective coating. Further, 200 nm of aluminum back reflector is used. In order to increase the reflection of the back reflector, a trapezoid grating is etched in the aluminum layer with an upper (L_{tu}) and lower (L_{tb}) bases. The embedded NW has an elliptical shape with a minor and major radii of r_1 and r_2, respectively. The NW is embedded in the active layer at a depth of Z_o from the surface of the SC with a rotation angle of θ from the x-axis. The modified design offers an absorption enhancement of 72% over the conventional TFSC. Further, the photocurrent density (J_{ph}) of 30.22 mA/cm^2 is achieved by the proposed design as shown in Fig.1.(b). This enhancement is due to the presence of NW that produces a volume light scattering in the active layer with improved absorption.

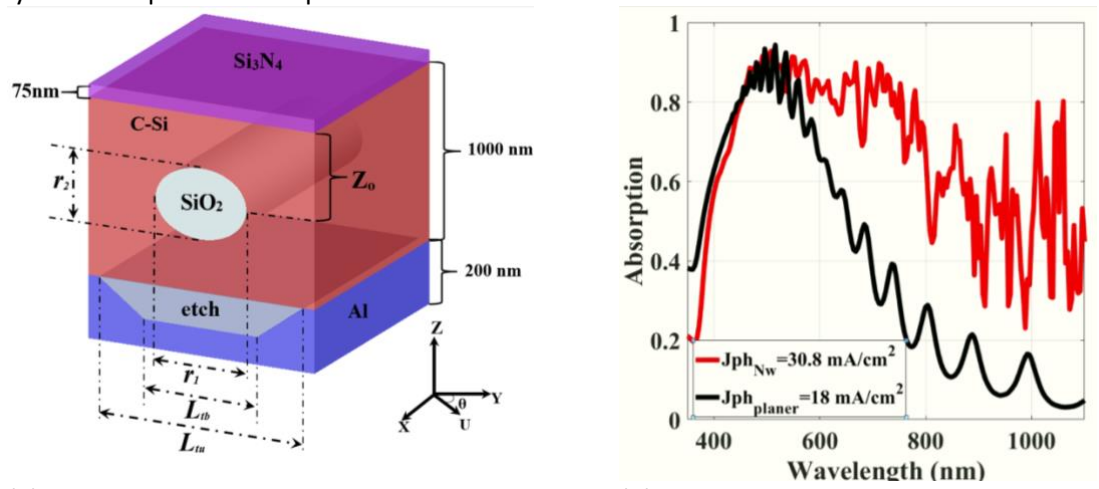

(a) (b)

Fig. 1.(a). Schematic diagram of C-Si TFSC with an embedded SiO_2 NW, and (b) Absorption spectra of the planer C-Si TFSC (black line) and the proposed design with embedded NW (red line).

References:

[1] "Lumerical: High-Performance Photonic Simulation Software." [Online]. Available: https://www.lumerical.com/products/.

A21_49 Design and Analysis of GaAs-based Asymmetric SPAcer-layer Tunnel (ASPAT) Diodes for Microwave/mm-wave detection

A. Salhi[a,*], A. Hadfield[a], S. G. Muttlak[a], J. Sexton[a], M. J. Kelly[b], and M. Missous[a]

*[a]School of Electrical and Electronic Engineering, University of Manchester, Manchester M13 9PL, U.K [b]Department of Engineering, University of Cambridge, Cambridge CB1 1EG, U.K. *Corresponding author:E-mail address: abdelmajid.salhi@manchester.ac.uk*

In the last few years, high data rate wireless networks and ultra-high-speed wireless communication have expanded enormously [1]. The tunneling diode could fulfill the demands of wireless ultra-low power and high-speed mixed-signal integrated circuit [2]. A key factor of such a device is its temperature-insensitive current-voltage characteristics. GaAs-based diodes, which incorporate a single tunnel barrier of AlAs in a crystal of GaAs with asymmetric doping profiles, are an excellent example of fast, cost-effective, and efficient tunnel diodes [3]. The asymmetric spacer layers design produces an asymmetric I-V characteristic making it suitable for use as a zero- bias detector. Although this tunneling device was demonstrated experimentally, the reported curvature coefficient at zero bias is still lower than the one reported for high-performance Schottky diode of 40V-1. Furthermore, there is a lack of inclusive structure design and modeling, in which the effect of multiple physical design parameters on the critical device parameters is dependent (In particular, the junction resistance Rj ,curvature coefficient Kv and junction capacitance Cj and how these characteristics can be optimized). In this work, we have thoroughly investigated the design of Asymmetric SPAcer-layer Tunnel (ASPAT) diodes using numerical modeling employing SILVACO Atlas software. The developed SILVACO physical models were reproduced and validated using experimental data obtained from fabricated ASPAT diodes. Afterwards, they have been used to evaluate the effect of different structure designs on three key parameters, namely the junction resistance, curvature coefficient and junction capacitance Cj at zero bias. The impact of the variation in the spacer layers thicknesses, emitter, collector, their doping profile, and the barrier width was thoroughly explored. It was found that the spacers and the barrier thickness are the most critical design parameters affecting the junction resistance and curvature coefficient. The insertion of an InxGa1-xAs QW layer adjacent to the AlAs barrier, combined with the proper choice of spacers and AlAs barrier thicknesses, contributed to an increase in the curvature coefficient by a factor of three while maintaining a low junction resistance. The cut-off frequency of a 4×4µm2 ASPAT device is predicted to be >500GHz at zero bias. A thorough study is presented to guide researchers working on ASPAT devices, providing valuable prediction for appropriate design parameters toward maximizing the microwave/mm-wave device performance.

[1] N. Oshima, K. Hashimoto, S. Suzuki, and M. Asada Electron. Lett., 52 (2016), p. 1897, DOI: 10.1049/el.2016.3120.
[2] M. Missous, M. J. Kelly, and J. Sexton IEEE Electron Device Lett., 36 (2015), p. 543, DOI: 10.1109/LED.2015.2427335.
[3] R. T. Syme, M. J. Kelly, R. S. Smith, A. Condie, and I. Dale Electronics Lett., 27 (1991), p. 2192, DOI: 10.1049/el:19911356.

A21_41 Large Optical Bandwidth InGaAs/InAlAs/GaAs metamorphic-PIN Photodiode Suitable for over 20Gb/s Optical Communication Systems

Saad G. Muttlak[1], A. Salhi[1], M. Sadeghi[2], Kawa Ian[3] and M. Missous[1]

[1]School of Electrical and Electronic Engineering, University of Manchester, UK , [2]Advanced Hall Sensors Ltd, Manchester, UK, [3]Integrated Compound Semiconductors, Manchester, UK saad.muttlak@manchester.ac.uk and saad.muttlak.uk@gmail.com

The rapid growth in data traffic trends due to the massive-demands for high speed optical systems is a key-driver for developing low-cost and wide-bandwidth PIN/APD photodiodes. This has resulted in a deployed 10Gb/s Ethernet Passive Optical Network, EPON (IEEE 802.2av, ratified September 2009) in late 2013, exploiting fibre-to-the-home, FTTH optical architecture system[1]. An optical rack to rack interconnections with 25Gb/s was also proposed for server systems in data centres, providing an effective solution for space reduction in short communication distances reaching several cm in off-chip applications[2]. A wide optical bandwidth characteristic for an integrated photodiode is, therefore, of vital importance to efficiently satisfy such optical system requirements. Of course, a reasonable absorption layer thickness can prudently stabilize the trade-off between the RC time constant and carrier transit delay time of the photodiode. Taking these into consideration, a low-cost and mass-produced PIN-PD based on InP technology capable of supporting optical bandwidths exceeding 20GHz is still a challenge at least at the present.

The work reported here is concerned with demonstrating an InGaAs/InAlAs/GaAs metamorphic-PIN (mPIN) photodiode targeted for intercity optical link operating at over 20Gb/s. The device was grown on a semi-insulating GaAs substrate utilizing Solid Source Molecular Beam Epitaxy (SSMBE). A 0.5µm thick InAlAs graded buffer layer was used to reduce the threading dislocations impact, thereby further improve the device DC and RF performances. Two mPIN-PDs were grown at two different temperatures [440 and 500°C] and denoted as sample XMBE#468 and #469 respectively. The devices were fabricated and the measured results revealed that the high temperature grown sample X469 device had a much lower leakage current of <10nA when fully depleted (i.e. at a voltage bias of -5V) while it was >50nA for the low temperature grown sample X468. There was a 44% decrease in the intrinsic capacitance of the mPIN sample X469 in comparison with the results found for X468. The electrical equivalent circuit models were extracted from experimental S- parameter data obtained using on-wafer probing up to 40GHz. A measured 11.2 and 19.7GHz optical bandwidth were achieved for the low and high temperature grown mPINs respectively with an optical window size of 20µm. The outstanding results of sample X469, which are identical to similar structures grown on InP substrates, are adequate for 25Gb/s optical system operation. Detailed growth process, characterization and relevant analysis regarding the mPIN photodiodes will be presented.

[1] K. Tanaka, A. Agata, and Y. Horiuchi, "IEEE 802.3 av 10G-EPON standardization and its research and development status," *Journal of Lightwave Technology,* vol. 28, no. 4, pp. 651- 661, 2010.
[2] H. T. J. Meier, "Design, characterization and simulation of avalanche photodiodes," ETH Zurich, 2011.

A21_32 Efficient Nanowire Solar Cell with Surface Texturing

Ghada Yassin Abdelatif, [1,2] M. F. O. Hameed, [1,3,4*] M. Hussein, [1,5,6] S. S. A. Obayya, [1*]

[1]Centre for Photonics and Smart Materials, Zewail City of Science and Technology, October Gardens, 6th of October City, Giza, 12578, Egypt.
[2] Department of Electronic and Communication Engineering, MISR Higher Institute for Engineering and Technology, Mansoura Ring Road, Mansoura, 35516, Egypt.
[3] Nanotechnology and Nanoelectronics Engineering Program, Zewail City of Science and Technology, October Gardens, 6th of October City, Giza, 12578, Egypt.
[4]Mathematics and Engineering Physics Department, Faculty of Engineering, Mansoura University, Mansoura 35516, Egypt.
[5] Department of Physics, Faculty of Science, Ain Shams University, Abbassia 11566, Cairo Egypt.
[6]Light Technology Institute, Karlsruhe Institute of Technology, Engesserstrasse 13, 76131 Karlsruhe, Germany
**Corresponding authors: sobayya@zewailcity.edu.eg , mfarahat@zewailcity.edu.eg*

The surface roughness is a promising way to enhance the light trapping in solar cells. In particular, nanowire (NW) with surface texturing can reduce the reflection by coupling the reflected light into the adjacent NWs which enhances the light absorption. In this paper, the effect of the composing material Si, a-Si:H and GaAs, of star-shaped NWs is reported and analyzed using finite difference time domain (FDTD) via Lumerical software package [1]. Figure 1 shows the unit cell of a periodic star-shaped Si NWs. The optimized star-shaped NWs offer high optical ultimate efficiency of 41.93%, 33.28% and 30.5% using Si, a-Si:H and GaAs, respectively. The corresponding short current density of 34.31, 21.02 and 15.69 mA/cm^2 are achieved. This is due to the star surface textures which allow multiple light scattering between the NWs.

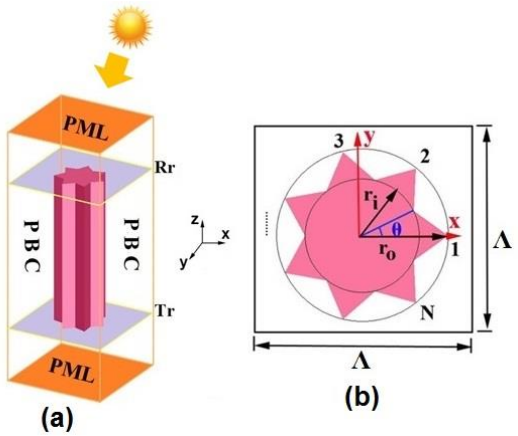

Fig. 1 (a) unit cell and (b) top view of the proposed star-shaped NW [2]

References

[1] I. Lumerical Solution, ", Inc., https://www.lumerical.com."
[2] G. Y. Abdel-Latif, M. F. O. Hameed, M. Hussein, M. A. Razzak, and S. S. Obayya, "Characteristics of highly efficient star-shaped nanowires solar cell," *Journal of Photonics for Energy,* vol. 8, no. 4, p. 047001, 2018.

A21_72 Characterisation and Design of InP QD Material for Passively Mode-locked Lasers

Reem Alharbi[1,2], Zhibo Li[1], Craig Allford[1], Samuel Shutts[1], Adam Forrest[3,] Andrey Krysa[4], Maria Ana Cataluna[3], Peter M. Smowton[1]

[1]EPSRC Future Compound Semiconductor Manufacturing Hub, School of Physics and Astronomy, Cardiff University, Cardiff, UK
[2]Department of Physics, King Abdulaziz University, Jeddah 21551, Saudi Arabia
[3]Institute of Photonics and Quantum Sciences, School of Engineering and Physical Sciences, Heriot-Watt University, Edinburgh, EH14 4AS, United Kingdom
[4]EPSRC National Centre for III-V Technologies, University of Sheffield, Sheffield, S1 3JD
E-mail: Alharbirs@cardiff.ac.uk

Mode-locked quantum-dot (QD) monolithic laser diodes are promising ultrafast laser sources due their advantageous spectrally broad optical gain/absorption (due to the fluctuation of dots' sizes), ultra-fast dynamics of both absorption and gain, high efficiency, low cost and compact size. These characteristics can be harnessed in QD lasers to generate ultrashort pulses in the picosecond or sub-picosecond range. In addition, QD lasers can be operated at a low power consumption due to their low threshold current density, and as a consequence there is typically no requirement for water cooling.
InP QD diode lasers, with a broad optical gain in this range of wavelengths from 690nm to 780nm, aim to achieve ultrashort pulse generation with durations in the picosecond and sup-picosecond range. Therefore, these have the potential to replace the Ti-Sapphire mode-locked lasers at this range of wavelengths (690nm to 780nm) in some biomedical imaging applications, in particular for lab-on-chip devices.
The laser structures were grown by MOVPE on n-GaAs (100) substrates oriented 10° off toward <111>. Self-assembled InP QDs were covered by slightly tensile strained GaInP quantum wells and separated by AlGaInP barriers, with AlInP cladding layers. Broad-area oxide-isolated stripe non-lasing segmented-contact devices were fabricated to measure the optical modal gain as a function of carrier density and modal absorption spectra.
Here we aim to establish a new method/calculation to characterise and design QD materials for passive mode-locking. We do this by measuring the modal absorption under reverse bias and determine its convolution with the modal gain spectrum to replicate the conditions of a laser under a mode-locked regime. We investigate appropriate conditions for mode-locking under the influence of different gain current and for a range of reverse bias voltage. From these measurements, we design the mode-locked laser structures, in particular, the absorber to gain length ratios and also the total cavity length. We compared the results of the modal gain and absorption measurements to those from an InP QD mode-locked laser, from which achieved a repetition frequency of ~12.5 GHz and a pulse width of ~6 picoseconds

Abstracts

Session 4: New Approaches for Datacom / Telecom Wavelength lasers

A21_63 Single Mode Nanolaser Monolithically Grown on On-axis Si substrate

Mingchu Tang[1,*], Taojie Zhou[2], Siming Chen[1], Zhaoyu Zhang[2], Huiyun Liu[1]

[1] *Department of Electronic and Electrical Engineering, University College London, London, WC1E 7JE, United Kingdom*
[2] *School of Science and Engineering, The Chinese University of Hong Kong, Shenzhen, Guangdong, 518172, P.R. China*
**mingchu.tang.11@ucl.ac.uk*

The recent exponential growth in data traffic requires a more efficient on-chip optical interconnect with a lower energy consumption and higher integration density. In this regard, nanoscale laser device with photonic crystal (PhC) cavity with ultra-small mode volume and low energy consumption is one of the most promising architectures for integrated nanoscale devices. Monolithic integration of efficient III-V light emitting sources on planar on-axis Si (001) has been recognized as an enabling technology for realizing Si-based photonic integrated circuits. In addition, zero-dimensional quantum dots (QDs) monolithically grown on Si platform as gain materials provides various advantages, including low lasing threshold, reduced temperature sensitivity, and hence have been widely investigated in last few years.

Here, we present the ultra-small InAs/GaAs QD PhC membrane lasers monolithically grown on CMOS-compatible Si substrate as presented in the fig 1(a), (b) and (c). The PC laser with a small mode volume of 0.88 $(\lambda/n)^3$ was continuous wave optically pumped under room temperature and exhibits an ultra-low lasing threshold of ~0.6 μW as seen in fig 1(d) and (e) at room temperature. A wavelength range of 70 nm is obtained by changing the parameters of PhC cavity, as shown in fig 1(f). The demonstrated Si-based PC lasers with a small footprint as well as low power consumption are expected to play an important role in the next-generation nanoscale Si photonics.

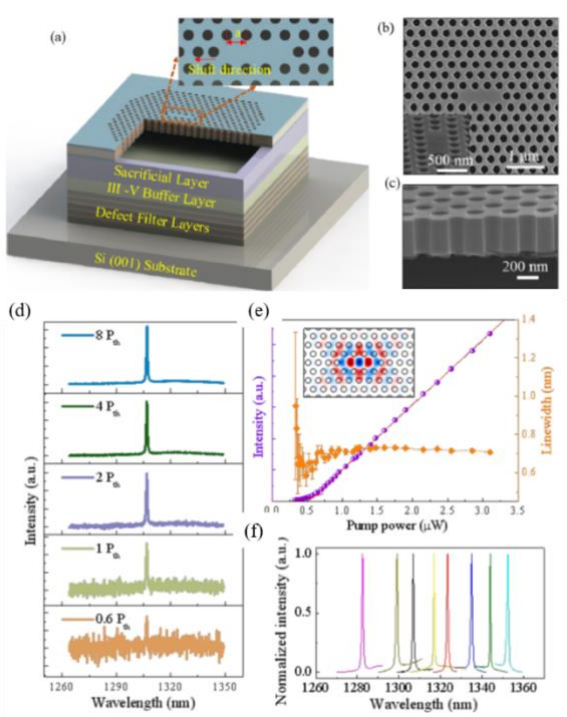

Fig.1 (a) Schematic diagram of the fabricated InAs/GaAs QD PC laser epitaxially grown on on-axis Si (001) substrate. (b) Top-view and (c) tilted cross-section view SEM images of the fabricated PC cavity. (d)Measured spectra under various input pumping powers of the PC laser (e) Collected L-L curve and linewidth of the lasing peak at 1306 nm. (f) Normalized PL spectra from representative PC lasers above lasing threshold.

A21_27 Low-threshold strain-compensated InGaAs/(In,Al)GaAs multi-quantum well nanowire lasers emitting near 1.3 µm

Paul Schmiedeke[1], Andreas Thurn[1], Markus Döblinger[2], Sonja Matich[1], Jonathan J. Finley[1] and Gregor Koblmüller[1]

[1]Walter Schottky Institut and Physics Department, Technical University of Munich, Garching, Germany [2]Department of Chemistry, Ludwig-Maximilians-Universität München, Munich, Germany Paul.Schmiedeke@wsi.tum.de

Abstract— We demonstrate lasing from single GaAs-based core-shell nanowires with coaxial InGaAs multiple quantum well (MQW) using a novel strain compensating InAlGaAs buffer layer. The buffer layer between the GaAs core and the MQW active region effectively reduces the compressive strain in the InGaAs MQW, which red-shifts the lasing energy. Using this structure, a lasing emission wavelength near 1.3 µm at room temperature was achieved.

Semiconductor nanowire (NW) lasers are nanoscale coherent light sources that exhibit a small footprint, low threshold lasing characteristics, and properties suitable for monolithic integration onto silicon (Si) photonic circuits. In order to achieve long propagation lengths in a Si waveguide, the lasing emission has to be tuned below the silicon bandgap of 1.12 eV to a wavelength above 1100 nm.

In this presentation, we demonstrate the lasing of GaAs-based NWs, which were overgrown with a multishell consisting of a highly strained buffer layer and InGaAs multiple quantum wells (MQW) as active gain medium. Compared to previous work [1], we replaced the ternary Al0.3Ga0.7As buffer layer and barriers with quaternary InxAlxGa1-2xAs, with x=0.3 in the buffer and x=0.23 in the barriers (blue layers in Figure 1 (b). For an In content of 30 % in the QW, the emission energy of the first lasing mode shifts from 1.18 eV to 1.12 eV due to the quaternary buffer. In the case of a lattice-matched buffer (AlGaAs), the InGaAs quantum-well is compressively strained due to its larger lattice constant compared to the (Al)GaAs barrier and core. If a strained buffer layer (InAlGaAs) is used, that is thick enough to cause a tensile strain in the GaAs core, the compressive strain in the InGaAs is reduced accordingly. This reduction in strain in the MQW reduces its bandgap and therefore also the lasing energy. We use numerical simulation to calculate the system's ground state transition including strain and find a close match with the experimental lasing energy. Additionally, the NWs with InAlGaAs buffer have a strongly reduced lasing threshold compared to NWs with AlGaAs barrier.

Reducing the strain also allows incorporation of higher In contents in the MQW. We demonstrate NWs with multimodal lasing emission as low as 0.96 eV (1292 nm) at room temperature, highlighting the positive effect of the reduced strain and the applicability for GaAs based NW lasers for telecom band lasing.

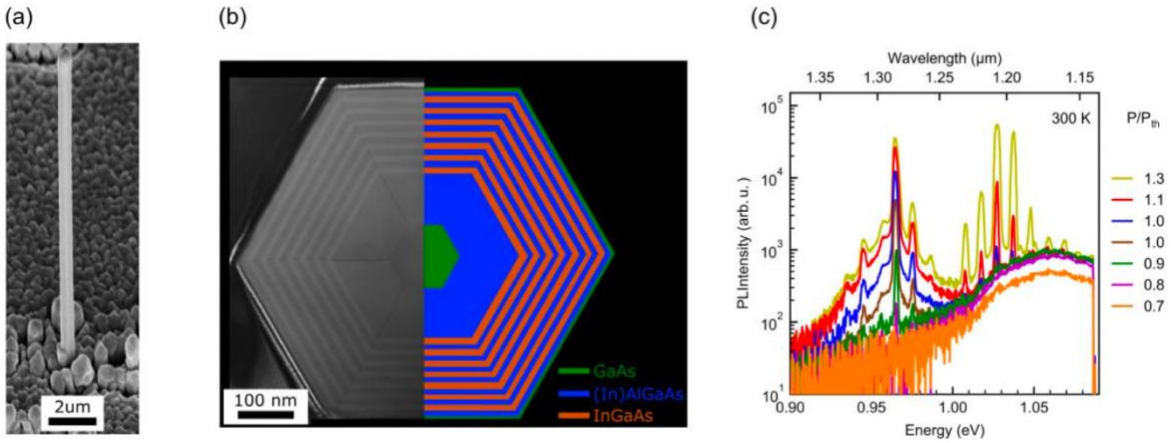

InAlGaAs buffer overlaid with a schematic illustration of the core-shell MQW heterostructure. (c) Pump power dependent µ-PL spectra of a single optically pumped NW laser with nominal In-molar fraction of 40% in the MQW (at 300 K).

1. T. Stettner, et al., Nano Lett., 18 (10), pp. 6292-6300 (2018)

A21_64 Low Threshold Type-II GaInAs/GaAsSb "W"-Lasers Operating in the 1.2-1.3µm Wavelength Range

Dominic A. Duffy[1], Igor P. Marko[1], Christian Fuchs[2], Timothy D. Eales[1], Jannik Lehr[2], Wolfgang Stolz[2] and Stephen J. Sweeney[1]

[1] Advanced Technology Institute and Department of Physics, University of Surrey, Guildford, GU2 7XH, United Kingdom
[2] Materials Sciences Center and Department of Physics, Philipps-Universität Marburg, Renthof 5, 35032, Marburg, Germany

The development of higher efficiency and temperature stable semiconductor lasers in the near-infrared (NIR) is important for the future of lower energy-consuming data communications networks. Lasers based on type-II "W"-quantum well heterostructures (QWHs), where electrons and holes are spatially separated in the active region, exhibit unique properties that offer the possibility of improved device characteristics over existing type-I lasers[1,2]. These properties have been well demonstrated in the mid-infrared and include more flexible control of operating wavelength and band structure parameters[1], as well as some evidence of reduced Auger recombination rates[2]. These structures have also been demonstrated in the near-infrared with (GaIn)As/Ga(AsSb) type-II "W"-QWH lasers (see Fig.) emitting in the 1.2-1.3µm range[3]. However, much of the physics underpinning the current understanding of type-II structures is not well-established, with most theoretical models based upon theory developed for simpler type-I structures which may not always be applicable to type-II structures. Thus, in order to further improve the performance of these structures an improved understanding of the characteristics and main limiting processes occurring in these "W"-QWHs is essential.

In this work, we investigate the radiative and non-radiative processes occurring in (GaIn)As/Ga(AsSb)-based "W"-lasers operating at 1255nm as a function of temperature and current, comparing and contrasting their performance with standard type-I lasers emitting at similar wavelengths. The devices exhibit low room temperature threshold current densities (J_{th}) of around 200-300 A cm^{-2}, pulsed output powers exceeding 1 W for 100mm-wide stripes, and a reduced temperature dependence of the threshold lasing wavelength when compared to conventional type-I lasers. The physical mechanisms driving the observed device characteristics will be discussed alongside routes for further optimisation.

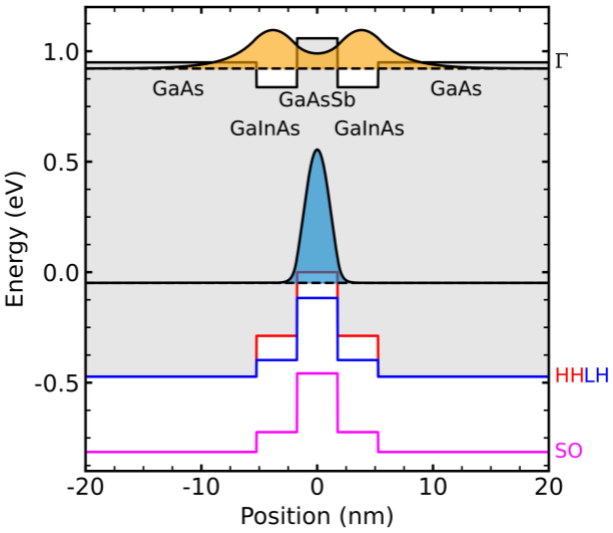

[1] J. R. Meyer et al., *Appl. Phys. Lett.*, vol. 67, p. 757, 1995.
[2] G. G. Zegrya and A. D. Andreev, *Appl. Phys. Lett.*, vol. 67, no. 18, p. 2681, 1995.
[3] C. Fuchs *et al.*, *Sci. Rep.*, vol. 8, no. 1, pp. 8–13, 2018.

A21_07 All-MBE grown InAs/GaAs quantum dot lasers with thin Ge buffer layer on Si substrates

Junjie Yang[1,5,*], Zizhuo Liu[1,5], Pamela Jurczak[1,*], Mingchu Tang[1,*], Keshuang Li[1], Shujie Pan[1], Ana Sanchez[2], Richard Beanland[2], Jin-Chuan Zhang[3], Huan Wang[3], Fengqi Liu[3], Zhibo Li[4], Samuel Shutts[4], Peter Smowton[4], Siming Chen[1], Alwyn Seeds[1], Huiyun Liu[1,*]

[1]*Department of Electronic and Electrical Engineering, University College London, Torrington Place, London, WC1E 7JE, UK*
[2]*Department of Physics, University of Warwick, CV4 7AL Coventry, UK*
[3]*Key Laboratory of Semiconductor Materials Science, Institute of Semiconductors, Chinese Academy of Sciences, Beijing 100083, P. R. China*
[4]*Department of Physics and Astronomy, Cardiff University, Queens Building, The Parade, Cardiff CF24 3AA, UK*

Abstract – A monolithic, high-performance III-V quantum dot (QD) laser grown on Si is one of the most promising candidates for commercially viable Si-based lasers. Great efforts have been made to overcome the challenges, including threading dislocations (TDs) and anti-phase domains (APDs), by growing a more than 2 µm thick III-V buffer layer. However, this relatively thick III-V buffer layer causes the formation of thermal cracks in III-V epi-layers, and hence a low yield obtained of Si-based QD devices. In this paper, we demonstrate the use of a thin Ge buffer layer to replace the initial part of GaAs buffer layer on Si to reduce the overall thickness of the structure, while maintaining the density of defects in III-V layers and maintain the performance of the InAs/GaAs QD laser. A very high operating temperature of 130 °C has been demonstrated for an InAs/GaAs QD laser by this approach.

We have demonstrated a high-performance InAs/GaAs QD laser grown directly on a Si substrate with a reduced overall buffer layer thickness of around 2 µm. With the help of high temperature cyclic thermal annealing of the 300 nm Ge buffer layer, a dramatic reduction in the number of TDs can be observed before they propagate into the DFLs [1]. Fewer repetitions of DFLs, as well as a reduced thickness of the GaAs buffer layer to less than 2 µm, are hence feasible in an InAs QD laser structure. Employing the Ge/Si VS helps to eliminate thermal cracking issues and thus is expected to boost the total yield without causing any negative side effects. In order to test the feasibility of implementing a thin Ge buffer layer in the InAs QD laser structure, an InAs QD laser device was grown directly on the Ge buffer. The laser threshold current density under pulsed operation was measured as 200 A/cm^2, corresponding to 28.6 A/cm^2 for each of the seven QD layers. A maximum output power of ~78 mW was obtained from a single facet. Lasing was observed up to 130 °C. Further improvements in threshold current density and temperature performance are possible with further optimising the growth and fabrication processes.

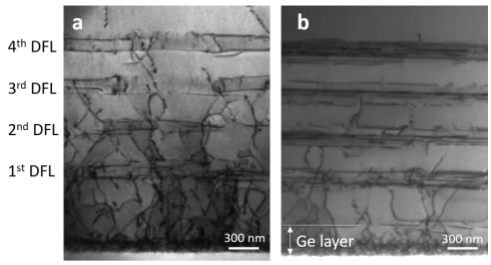

Fig. 1. Cross-sectional TEM results of (a) GaAs buffer layer grown on Si substrate and (b) GaAs buffer layer grown on Ge/Si VS. Both (a) and (b) have the same total thickness and consist of 4-set DFLs.

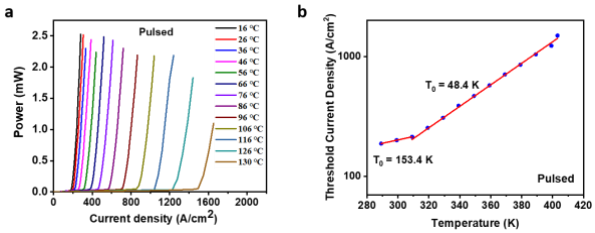

Fig. 2. (a) Light output power against injection current density at various temperatures under pulsed mode. (b) Characteristic temperature measured under pulsed mode from 289 K to 309 K.

[1] J. Yang, P. Jurczak, F. Cui *et al.*, "Thin Ge buffer layer on silicon for integration of III-V on silicon," *Journal of Crystal Growth,* vol. 514, pp. 109-113, 2019.

A21_57 GaSb/GaAs quantum-ring VCSELs operating at telecoms wavelengths

Peter D. Hodgson,[1] Tom J. Wilson,[1] Alex J. Robson,[1,2] Qian D. Zhuang,[1] Stewart McDougall,[3] Kenneth Kennedy,[4,5] Saurabh Kumar[4] and Manus Hayne[1,2]

[1]*Department of Physics, Lancaster University, Lancaster LA1 4YB, UK*
[2]*Lancaster Material Analysis, Department of Physics, Lancaster University, Lancaster LA1 4YB, UK*
[3]*CST Global Ltd, 4 Stanley Blvd, Hamilton International Technology. Park., Glasgow G72 0BN, UK*
[4]*EPSRC National Centre for III-V Technologies, University of Sheffield, Sheffield, S3 7HQ, UK*
[5]*Nanofabrication Core Lab, King Abdullah University of Science and Technology (KAUST), Thuwal 23955-6900, Saudi Arabia*

Hole-confining type-II GaAs/GaSb self-assembled quantum rings (QRs) have potential for applications including solar cells [1] and memory devices [2]. Comparatively less attention has been paid regarding their use in light emitting diodes (LEDs) and lasers [3], mainly due to their type-II nature and the consequent reduction in carrier recombination rates. However, this is mitigated by strong Coulomb binding of electrons arising from multiple charging of the rings with holes [4] and the QR geometry [5], allowing photoluminescence (PL) to be seen up to 400 K. This raises the possibility of their use in the commercially important 1260-1675 nm telecommunications band.

Here we report on recent progress in the developments of GaSb/GaAs QR vertical-cavity surface-emitting lasers (VCSELs). These devices have large area circular mesas with diameters of 100 to 200 µm and were found to emit light even at 380 K, which is the limit of our equipment. Far-field measurements indicated that their emission is highly divergent [see Fig.1 a)], with a FWHM of 70 ± 10˚ and 108 ± 10˚ in the 100 µm and 200 µm devices respectively, suggesting that a large number of higher order transverse modes are supported. It was also found that the cavity emission blueshifts at higher dispersion angles, which is in excellent agreement with optical simulations created using TFCalc software.

Linear polarisation measurements [Fig. 1 b)] showed that emission collected at higher dispersion angles is more strongly polarised than light collected at zero dispersion angle, and is also shifted in polarisation orientation. This suggests that the numerous cavity modes have greatly varying gain characteristics, and mixing of these modes in the emission spectrum reduces the observed linear polarisation degree. Thus, by reducing the number of transverse modes in the next iteration of GaSb QR VCSELs, e.g. by inclusion of an oxide aperture, we expect to achieve higher output power, improved monochromaticity, lower divergence and increased polarisation.

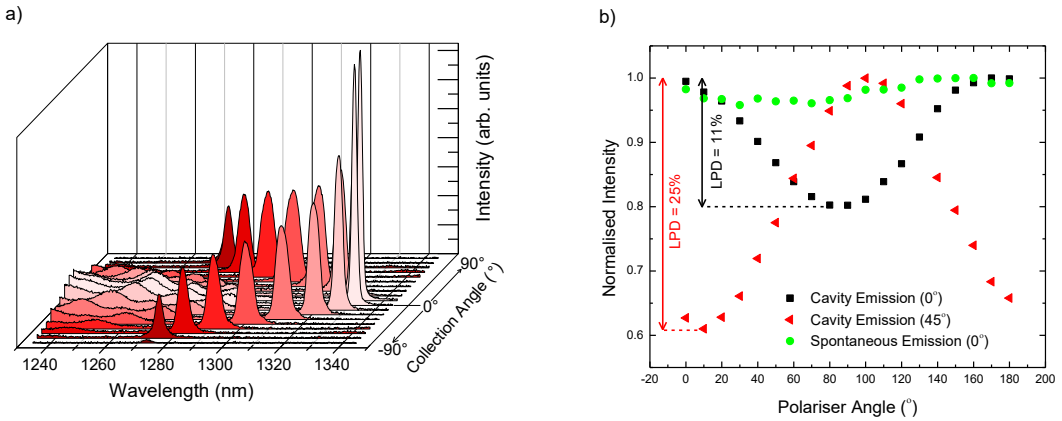

Figure 1. Experimental data from a GaSb QR VCSEL. a) Emission spectra collected at a range of dispersion angles. b) Linear polarisation data with linear polarisation degrees (LPD) labelled. A 90˚ polarisation shift in the cavity emission can be seen at a collection angle of 45˚. Spontaneous emission from the QR ensemble is unpolarised.

[1] R. B. Laghumavarapu et al, Appl. Phys. Lett. 90, 173125 (2007). [2] M. Hayne et al., J. Phys. D: Appl. Phys. 46, 264001 (2013). [3] J. Tatebayashi et al., Appl. Phys. Lett. 90, 261115 (2007). [4] P. D. Hodgson et. al., Appl, Phys. Lett. 105, 081907 (2014). [5] R. J. Young et al., Appl. Phys. Lett. 100, 082104 (2012).

A21_17 Performance of dilute bismide and dilute nitride multiple quantum well lasers at 1.55µm

Zoe C. M. Davidson[1], Judy M. Rorison[1], and Christopher A. Broderick[2,3]

[1]Department of Electrical and Electronic Engineering, University of Bristol, Bristol BS8 1UB, U.K. [2]Tyndall National Institute, University College Cork, Lee Maltings, Dyke Parade, Cork T12 R5CP, Ireland [3]Department of Physics, University College Cork, Cork T12 YN60, Ireland

The continued exponential growth of the internet dictates the need to develop energy-efficient "green" photonics technologies for telecoms. Conventional temperature sensitive 1.55 µm InP-based telecom lasers require external cooling, greatly increasing the energy consumption of optical communication networks. This is due to strong intrinsic losses associated with Auger recombination (AR) and inter-valence band absorption (IVBA), with AR accounting for > 50% of threshold current at room temperature [1]. Several novel material concepts have been proposed as potential routes to enable long-wavelength GaAs- based semiconductor lasers offering enhanced performance compared to conventional InP-based quantum well (QW) laser technologies, including highly-mismatched dilute nitride and dilute bismide alloys [2].

Incorporation of N or Bi in (In)GaAs drives strong band gap reduction in highly-mismatched dilute nitride or bismide alloys [3]. In addition, incorporation of Bi in (In)GaAs causes a strong increase of the valence band spin-orbit splitting energy, offering the potential to reduce temperature sensitivity by suppressing the dominant hot-hole producing CHSH AR pathway involving the spin-split-off band [3]. These novel material concepts offer the potential to develop GaAs-based 1.3 and 1.55 µm QW lasers, and hence to take advantage of the opportunities offered by the GaAs platform. We perform a systematic theoretical study to provide a quantitative comparison between the threshold characteristics of novel GaAs-based 1.55 µm multi-QW lasers to evaluate the potential of the proposed material platforms for 1.55 µm applications.

We perform multi-band k·p calculations for quantum well (QW) laser structures using 10-band (dilute nitride) and 12-band (dilute bismide) Hamiltonians. QW eigenstates obtained from k·p calculations are used directly to compute optical gain for each laser structure (separate confinement heterostructure) [4]. To facilitate quantitative comparison, all material systems are treated on equal footing by assuming equivalent spectral broadening and internal loss in the optical gain calculations. We consider GaAs-based dilute nitride InGaNAs(Sb)/GaAs QWs and dilute bismide GaAsBi/GaAs QWs. In all cases we consider compressively strained QWs having unstrained barriers, and adjust the QW alloy composition to fix the peak of the gain spectrum at 1.55 µm (at threshold injection and temperature T = 300 K). We identify 1.55 µm structures satisfying these criteria as functions of QW thickness, and identify trends in their threshold characteristics via direct calculation supported by detailed analysis of the QW band structure. Using a finite-difference approach to solve the coupled Schrödinger-Poisson equations we analyse carrier drift-diffusion and localisation in multi-QW structures [5, 6].

To optimise performance in a QW laser it is desirable to minimise the threshold carrier density n_{th}, and maximise the differential gain $\frac{dg}{dn}$ at threshold. Minimising nth reduces the AR current density, thereby decreasing threshold current density and its temperature sensitivity. Maximising $\frac{dg}{dn}$ increases modulation bandwidth, while decreasing the linewidth enhancement factor and hence chirp. By increasing the number of QWs we are able decrease n_{th} and increase $\frac{dg}{dn}$ per QW. However,
due to drift-diffusion and localisation of carriers within the QWs under electrical injection, we must examine how many QWs it is feasible to employ in a laser structure without compromising device performance.

Our results are partially summarised in Fig. 1, which shows increasing $\frac{dg}{dn}$ (blue) and decreasing threshold carrier density (red) per QW for increasing the number of 4 nm thick QWs in GaAs-based dilute nitride (solid) and dilute bismide (dashed) QW lasers designed to emit at 1.55 µm.

GaAsBi/GaAs structures display reduced nth compared to InGaNAs(Sb)/GaAs, but with dg being ≈ 10% higher in the latter. The $\frac{dg}{dn}$expected suppression of CHSH AR and IVBA due to the spin-orbit

splitting energy exceeding the band gap makes GaAsBi/GaAs multi- QW structures a more attractive proposition, promising to significantly reduce the threshold current density and its temperature sensitivity, and potentially paving the way for uncooled telecom laser operation [3].

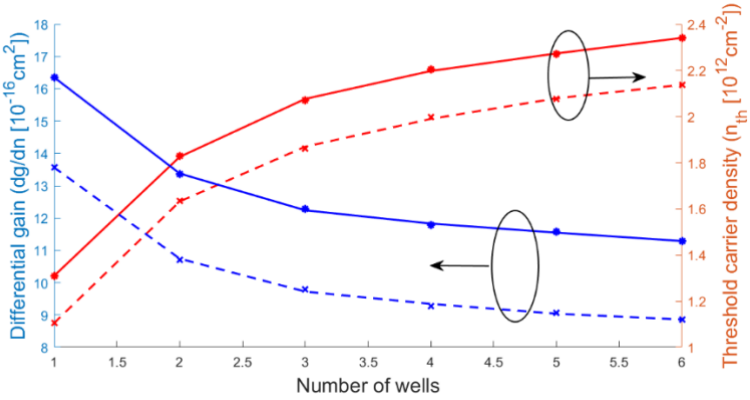

Fig. 1 *Calculated differential gain* $\frac{dg}{dn}$ *(blue) and threshold carrier density (red) per 4nm QW for GaAs-based dilute nitride InGaNAs(Sb)/GaAs (solid) and dilute bismide GaAsBi/GaAs (dashed) 1.55 µm multi-QW lasers vs. number of QWs.*

Our calculations also indicate that there is minimal performance benefit to be achieved by including >4 QWs in GaAsBi/GaAs or InGaNAs(Sb)/GaAs structures. For larger numbers of QWs, charge trapping prevents injected carriers from populating all QWs. This is reflected in the exemplar drift-diffusion calculation of Fig. 2 for a PIN diode structure. Following our gain calculations we inject nth per QW and find a sufficient distribution of electrons and holes across both QWs in a 2 QW structure. For > 4 QWs charge trapping impedes carrier transport to the central QWs. Our calculations therefore suggest that development of temperature insensitive GaAsBi/GaAs QW lasers should focus on multi- QW structures containing 2 - 4 QWs, with QWs of thickness ⍰ 5 nm.

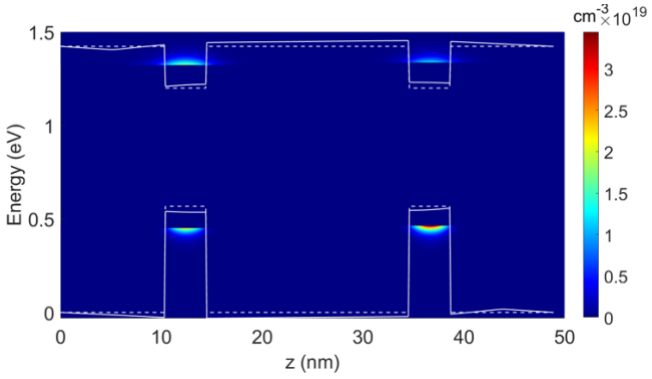

Fig. 2 *Carrier drift-diffusion at threshold injection of electrons (from the left) and holes (from the right) for a 2 MQW GaAsBi/GaAs PIN diode. Dotted white lines show the conduction and valence band edge potentials (inclusive of strain). Solid white lines show the self-consistently calculated conduction and valence band edge energies due to electrostatic attraction from carrier densities.*

Acknowledgements: This work was supported by the University of Bristol (UOB; via a Doctoral Studentship, held by Z.C.M.D.), by Science Foundation Ireland (SFI; project no. 15/IA/3082), and by the National University of Ireland (NUI; via the Post-Doctoral Fellowship in the Sciences, held by C.A.B.).

References

1 A. F. Phillips, S. J. Sweeney et al *IEEE J. Sel. Top. Quantum Electron.*, vol. 5, p. 401, 1999.
2 C.A.Broderick,S.Dasetal*IEEEPhotonicsSocietyNewsletter*,vol.34, p. 6, 2020.
3 C. A. Broderick, M. Usman et al *Semicond. Sci. Technol.*, vol. 27, p. 094011, 2012.
4 C.A.Broderick,P.E.Harnedyetal*IEEEJ.Sel.Top.QuantumElectron.*, vol. 21, p. 1503313, 2015.
5 L. Nevou, "Schrodinger-poisson solver in 1d." https://github. com/LaurentNevou/Q_SchrodingerPoisson1D_demo, 2020.
6 R. A. Jabr, M. Hamad, and Y. M. Mohanna *International Journal of Electrical Engineering Education*, vol. 44, pp. 23–33, 2007.

Abstracts

Session 5: Laser and Laser Systems

A21_01 Improved lateral brightness in 940-nm high-power broad-area diode lasers using enhanced self-aligned structure

M. Elattar, O. Brox, P. Della Casa, A. Maaßdorf, D. Martin, H. Wenzel, A. Knigge, and P. Crump

Ferdinand-Braun-Institut, Leibniz-Institut für Höchstfrequenztechnik, Gustav-Kirchhoff-Str. 4, 12489 Berlin, Germany

We present high-power broad-area diode lasers with improved beam quality, reduced threshold current, and increased efficiency, realized by implementing an enhanced self-aligned lateral structure. GaAs-based broad-area diode lasers (BALs) are used in a variety of applications, where high output power (P), conversion efficiency (η) and beam quality are desirable. In typical BALs operating at 940 nm, the opt E vertical beam profile is close to the ideal diffraction-limited case, while the lateral profile strongly deviates from it, resulting in reduced beam quality (quantified by the beam parameter product BPP). Besides thermal lensing, BPP can be affected by non-thermal mechanisms, such as lateral current spreading and lateral carrier lat accumulation (LCA). Different lateral structuring techniques have been developed for central confinement of current and carriers, such as high-energy deep ion implantation [1,2] as well as buried mesa (BM) [3,4] and lateral buried implant (LBI) [5] structures. However, it remains challenging to reduce BPP while maintaining lat high η , P , polarization purity (quantified by the degree of polarization DOP), and long device lifetime. E opt

Based on the self-aligned structure (SAS) [6,7], we present results of an enhanced lateral current confinement technique "eSAS", integrated within an extreme-triple-asymmetric (ETAS) vertical design with a thin p-side [8]. This enhanced structure uses current-confinement layers outside the laser stripe, whose location, materials, thicknesses, and doping concentrations are varied and precisely defined. Compared to established SAS designs, the eSAS allows smaller residual thickness between the current-confinement layers and the active zone, as well as higher process control and repeatability. In the first eSAS realization, BPP was significantly reduced in lateSAS devices compared to reference devices without current confinement, primarily due to reduced near-field width, as shown in Fig. 1 for single-emitters with stripe width W = 90 µm and resonator length L = 4 mm under continuous-wave (CW) operation at 25°C (BPP reduced by 20% at P = 10 W). Threshold lat opt current Ith is also strongly reduced in eSAS devices, as shown in Fig. 2 as a function of W for over 30 single- emitters. Following the approach in [9], these data points can be used to estimate current loss at device edges due to current spreading. Linear fits of the points are taken, and the y-intercepts at W = 0 represent empirical estimates of the current loss in each case. Using this approach, we estimate a 59.5% reduction of current loss by implementing the eSAS. Very high DOP (> 99%) and comparable slope values were demonstrated from eSAS and reference devices, and peak ηE was slightly higher in eSAS devices (~1.03 ×). In conclusion, it has been demonstrated that the eSAS enables a significant enhancement of lateral brightness $B = P/BPP$ without lat opt lat compromising other performance aspects, and can therefore achieve better overall performance than other lateral structuring techniques. The design, simulation, processing, and measurement results of eSAS BALs are described in more detail in [10].

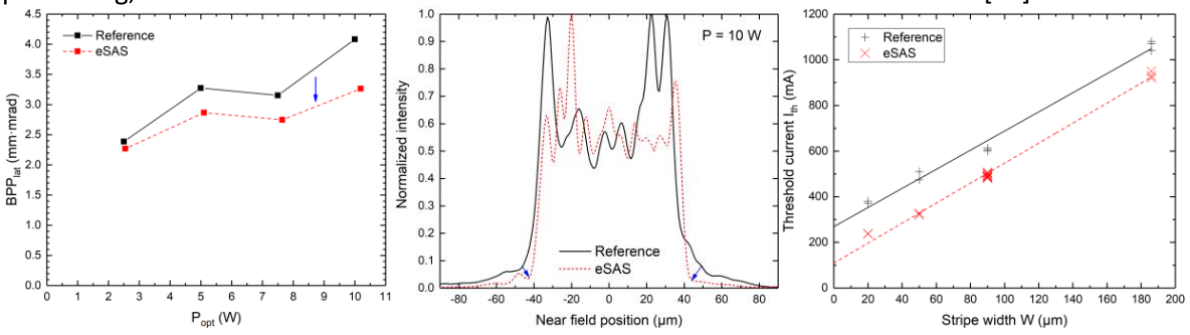

***Fig. 1**: BPP as a function of P* lat opt *and normalized optical intensity as a* function of near-field position at P_{opt} = 10 W *for mounted reference and eSAS single-emitters with W = 90* µm *and L = 4* mm *(CW, 25*℃

***Fig. 2:** I as a function of stripe width W for over 30 reference and eSAS single-emitters (CW, 25°C).*

We thank TRUMPF Laser GmbH for supporting this work.

[1] M. Winterfeldt et al., IEEE Photon. Technol. Lett. 27, pp. 1809–1812, (2015) [2] M.M. Karow et al., CLEO/Europe-EQEC 2019, paper cb_5_4 (2019)
[3] P. Della Casa et al., Semicond. Sci. Technol. 32, 065009 (2017)
[4] V.V. Shamakhov et al., Quantum Electron. 49, 1172 (2019)
[5] P. Della Casa et al., Semicond. Sci. Technol. 34, 105005 (2019)
[6] Y. Yamagata et al., Proc. SPIE 9348, 93480F (2015)
[7] Y. Kaifuchi et al., Proc. SPIE 10900, 109000F (2019)
[8] T. Kaul et al., IEEE J. Sel. Top. Quantum Electron. 25, 1501910 (2019)
[9] H. Wenzel et al., Semicond. Sci. Technol. 15, 557 (2000)
[10] M. Elattar et al., Semicond. Sci. Technol. 35, 095011 (2020)

A21_47 High pulsed power output in the eye-safe wavelength range from a double-asymmetric-structure laser diode with a bulk active layer

L. Hallman[(a)], B.S. Ryvkin[(a,b)], E.A.Avrutin[(c)], J.T. Kostamovaara[(a)]

(a) Dept of Electrical and Information Engineering, University of Oulu, Finland; emails lauri.hallman@oulu.fi ; juha.kostamovaara@oulu.fi (b) A.F.Ioffe Physico-Technical Institute, St.Petersburg, Russia; email ryvkin@switch.ioffe.ru
(c) Dept of Electronic Engineering, University of York, UK, email eugene.avrutin@york.ac.uk

High power broad area pulsed diode lasers operating in the eye-safe wavelength range (λ= 1.4-1.7 μm) are indispensable for applications including medical instrumentation and range finding/LIDAR systems [1]. An attractive approach to design of such lasers is the use of waveguide and active layer position asymmetries. The use of these asymmetries for high power λ~ 1.5 μm lasers was investigated theoretically in [2]. It was predicted [2] and demonstrated [3] that structures of this kind can select a single fundamental transverse mode while simultaneously suppressing carrier accumulation and hence free carrier absorption in the optical confinement layer (OCL) at high currents. In particular, current-induced spatially nonuniform OCL carrier accumulation is suppressed most efficiently when the active layer is located near the p-cladding [2,3]. Such location (double waveguide asymmetry [3]) allows also to decrease thermal and electrical laser resistance. The use of a bulk active layer was shown to be advantageous for realizing short cavity designs for improved output efficiency [4]. In our recent work [5][6], experimental characterization of short cavity double asymmetric laser structures (Fig.1) with a bulk active layer and a relatively short cavity has been reported. Total pulsed power output of about 18 W reported at the bias current of 80 A from a w=90 μm wide stripe laser with uncoated facets, mounted p-side up with conducting glue.

Here, we report first measurements of single-facet pulsed power from an AR/HR coated sample, mounted p-side down with solder for improved thermal properties. Output power levels of 19W have been measured at substantially lower currents than in [5] (~ 60 A, Fig.2). Pumping (and hence optical) pulses £ 20 ns long, relevant to LIDAR applications, were used.

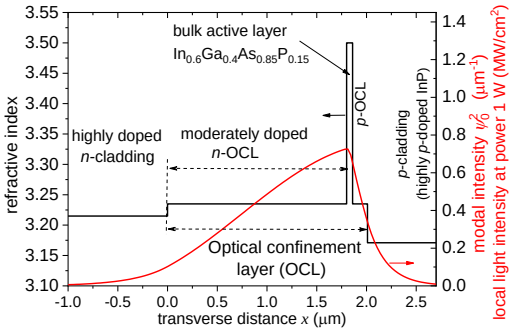

Figure 1. Structure schematic.

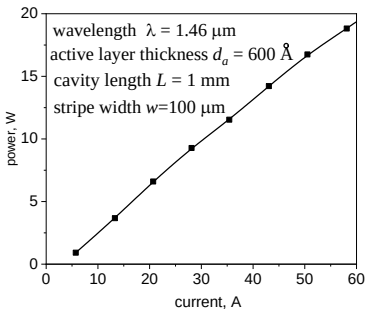

Fig.2. Measured pulsed light-current dependence

Further experimental and theoretical results will be presented at the conference.

[1]V. Molebny, G. Kamerman, O. Steinvall, "Laser radar: from early history to new trends," *Proc. SPIE 7835*, 2010, 7835023.[2] B. S. Ryvkin and E. A. Avrutin, "Asymmetric, nonbroadened large optical cavity waveguide structures for high-power long-wavelength semiconductor lasers," *J. Appl. Phys.,* vol. 97, no. 11, p. 123103, Jul. 2005 [3]P. Crump *et al.*, "Efficient high-power laser diodes," *IEEE JSTQE*, vol. 19, no. 4, p. 1501211, Jul.–Aug. 2013.[4]B.S.Ryvkin, E.A.Avrutin, and J.T.Kostamovaara, "Asymmetric-waveguide, short cavity designs with a bulk active layer for high pulsed power eye-safe spectral range laser diodes", *Semicond. Sci. Technol.*, 2017, **35** (2020) 085008. [5]L.W. Hallman *et al.,* "High power 1.5μm pulsed laser diode with asymmetric waveguide and active layer near *p*-cladding", *IEEE PTL*, 2019, **31** (30), pp. 1635-1638. [6]L.W. Hallman, *et al.,* "Double asymmetric structure 1.5μm high power pulsed laser diodes", in Proc. 2019 IEEE Conference on High Power Laser Diodes and Systems (HPLDS), Coventry, UK, Sep. 2019, IEEE. 2019, pp. 19-20

A21_68 Master-Oscillator Power-Amplifier system emitting at 626 nm: Increasing the laser power for future 9Be+ cooling applications

Gunnar Blume, Ali Koyucuoglu, Morten Drees, Johannes Pohl, David Feise, Alexander Sahm, and Katrin Paschke

Ferdinand-Braun-Institut gGmbH, Leibniz-Institut für Höchstfrequenztechnik (FBH), Gustav-Kirchoff-Str. 4, 12489 Berlin,Germany

Ultracold beryllium ions are used for various quantum technologies such as e.g. qubits [1] or optical clocks [2]. Its cooling requires laser light at 313 nm, which is usually generated via the second harmonic of light at 626 nm. The wavelength of 626 nm in turn requires either dye lasers or a complex set of solid state or fibre lasers, which are difficult to miniaturise. Here an all semiconductor laser solution would be much preferable. Hence, a few solutions have already been developed recently, either using external cavity diode lasers (ECDLs) directly [3] or in a master-oscillator power amplifier (MOPA) [4].
We previously reported on distributed Bragg reflector ridge waveguide laser (DBR-RWL) for the wavelength of 626 nm [5]. We now improved on their design by adding grating heaters (GH) for electric wavelength tuning. Furthermore, we developed tapered amplifier (TPA) to amplify the optical output power in an MOPA configuration.
In a benchtop experiment more than 300 mW of optical output power were obtained, when the TPA was cooled to 5°C (see Fig. 1, left). It emitted near 626 nm with a side mode suppression exceeding 30 dB (centre).

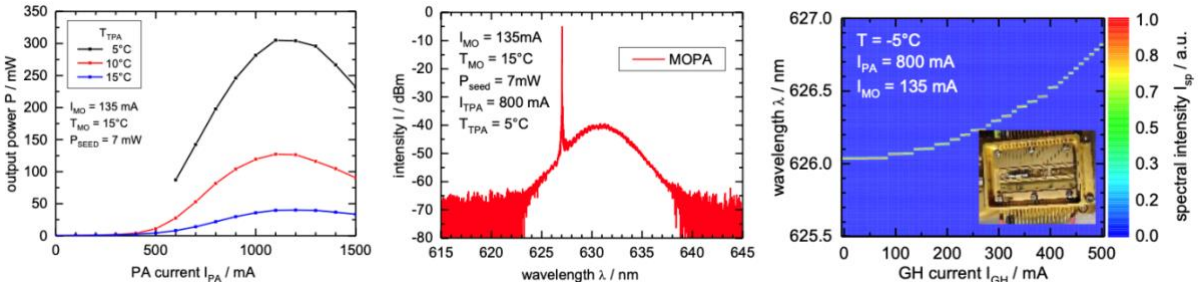

Fig. 1 Benchtop MOPA: output power as a function of temperature (left), emission spectra at 200 mW (centre); and miniaturized MOPA (picture as inset): spectral mapping of the lasing peak as a function grating heater current

The MOPA was also miniaturized and assembled in a closed package (see inset in Fig. 1, right). Here chips as well as beam shaping optics and a custom optical isolator [6] were mounted onto a micro-optical bench with a total length of about 50 mm. The internal temperature was held at about -5°C during assembly of the optics. The package was constantly purged with nitrogen and sealed afterwards to prevent condensation.
At currents of IMO = 135 mA and IPA = 800 mA an optical output power of about 80 mW, somewhat less than in the benchtop experiment. The laser wavelength can be tuned via the grating heater e.g. with IGH = 280 mA to 626.26 nm (see Fig. 1, right). Further cooling to internal temperatures of -15°C yielded optical output powers up to 200 mW at 626 nm.
This should allow generation of 313 nm light in the mW-range using frequency doubling as in [4] and hence allow a small sized laser cooling system for beryllium ions.

References [1] C. Langer, R. Ozeri, J. D. Jost, J. Chiaverini, B. DeMarco, A. Ben-Kish, R. B. Blakestad, J. Britton, D. B. Hume, W. M. Itano, D. Leibfried, R. Reichle, T. Rosenband, T. Schaetz, P. O. Schmidt, and D. J. Wineland, "Long-lived qubit memory using atomic ions," Phys. Rev. Lett. 95, 060502 (2005).[2] T. Rosenband, P. O. Schmidt, D. B. Hume, W. M. Itano, T. M. Fortier, J. E. Stalnaker, K. Kim, S. A. Diddams, J. C. J. Koelemeij, J. C. Bergquist, and D. J. Wineland, "Observation of the $^1S_0 \rightarrow {}^3P_0$ clock transition in $^{27}Al^+$," Phys. Rev. Lett. 98, 220801 (2007). [3] F. M. J. Cozijn, J. Biesheuvel, A. S. Flores, W. Ubachs, G. Blume, A. Wicht, K. Paschke, G. Erbert, and J. C. J. Koelemeij, "Laser cooling of beryllium ions using a frequency-doubled 626 nm diode laser," Opt. Lett. 38(13), 2370–2372 (2013).[4] N. Ohmae and H. Katori, "626-nm single-frequency semiconductor laser system operated near room temperature for mW- level second-harmonic generation at 313 nm," Review of Scientific Instruments 90, 063201 (2019). [5] G. Blume, O. Nedow, D. Feise, J. Pohl, and K. Paschke, "Monolithic 626 nm single-mode AlGaInP DBR diode laser," Optics Express 21 (18), 21677-21684 (2013).[6] Miniaturized optical isolator prototype based on CdMnTe with T_1 = -4 dB and T_2 = -38 dB kindly provided by Toptica Photonics AG.

A21_18 Experimental Implementation of Ultrafast Photonic Recurrent Neural Networks using Reservoir Computing and Semiconductor Lasers

Julián Bueno, Joshua Robertson, Matěj Hejda, and Antonio Hurtado

Institute of Photonics, Dept. of Physics, University of Strathclyde, Technology and Innovation Centre, Glasgow, UK

Artificial neural networks (ANN) have proven to be extremely successful to solve highly complex problems for which classical computing architectures struggle. Photonic technologies have enabled highly hardware-friendly system realizations [1,2]. Among photonic ANNs, Reservoir Computing techniques have undergone considerable attention [3] since they substantially simplify the learning stages and create intrinsic memory inside the ANN (an extremely helpful feature for a wide variety of processing tasks). Moreover, Reservoir Computers (RC) can be implemented using a single nonlinear element and a delay line [4]. These concepts have been extremely useful to develop experimentally multiple photonic and optical neural networks implemented in hardware using different devices including semiconductor lasers [5,6]. Yet, to date these have been mostly based on in-plane laser sources, and have not focused on vertical-cavity surface emitting lasers (VCSELs). Only recently, the first reports have emerged indicating enhanced performance in VCSEL-based reservoir computing ANNs [7]. In this work, we experimentally explore the properties and capabilities of an RC ANN system based on a VCSEL emitting at the important telecom wavelength of 1550 nm and its dependence on different experimental parameters.

The experimental setup used to build the VCSEL-based RC ANN is depicted in Fig. 1. It consists of off-the-shelf fibre-optic components, including a VCSEL emitting a main lasing mode (parallel-polarised mode) and a subsidiary attenuated mode (orthogonally-polarised mode), separated by 14.5 GHz. The delay feedback time was measured to be 65.0 ns. A tunable laser provides CW light and information is encoded by modulating its intensity with a Mach-Zehnder modulator. Two sets of Variable Optical Attenuator (VOA) and a Polarization Controller (PC) are used to control the intensity and polarization (parallel or orthogonally-polarised) of the optical feedback and the optical injection. The injected signal consists of a temporal mask that is continuously iterated every delay time (65.0 ns) multiplied by the value we want to compute. The mask consisted of 325 random values in the range of [-1,+1], modulated at 5 GSa/s using a 5 GHz Arbitrary Waveform Generator. This creates an ANN with 325 virtual nodes inside the delay feedback loop. Output weights are computed offline via a supervised learning algorithm, considering an output layer with one node.

To evaluate the performance of the VCSEL RC system of this work we initially use the Mackey-Glass Prediction Task using the NMSE (Normalized Mean Square Error), where it has to predict the next value in a chaotic time-series based on its previous history. Fig. 2 shows the performance of the VCSEL RC system. The polarization of the optical injection and delayed feedback light was set parallel (PAR) or orthogonally rotated (ROT) with respect to that of the main lasing mode of the VCSEL. Fig. 2 shows that for very low injected powers the error is large regardless of the operating conditions. As power increases, the error reduces quickly reaching low values of NMSE = 0.012 for ROT and PAR thanks to the VCSEL quickly locking to the external-injection and its nonlinear properties [8]. Fig. 2 also shows that for lower currents, the system exhibits better performance under lower optical injection powers. This is due to the lower power requirements needed to achieve injection locking as bias current reduces. These results experimentally demonstrate that VCSEL-based RC neural networks exhibit successful performance on general prediction tasks on a broad parameter region including low power injection conditions. In this talk I will explain the concepts of recurrent neural networks, reservoir computing, and how they can be applied to a photonic system under delayed feedback to create an entire reservoir and use it to process information at GHz speeds. Full details on the VCSEL RC performance, the effect of key system's parameters, its intrinsic memory and operation for different tasks will be provided during the talk.

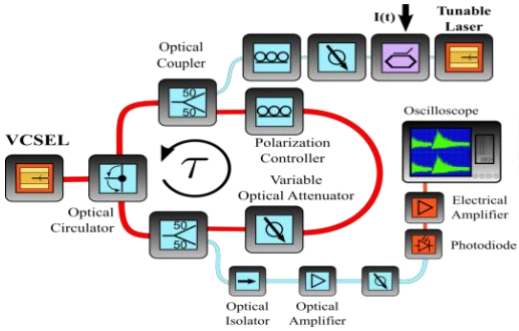

Figure 1: Diagram of the experimental setup used

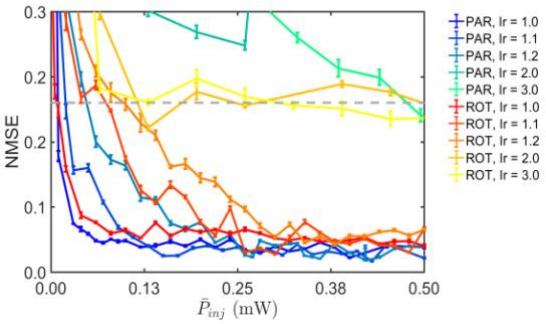

Figure 2: Performance of the VCSEL RC to build a RC system with a 1550nm VCSEL. system for the Mackey-Glass prediction task

[1]. J. Feldmann, N. Youngblood, C. D. Wright, H. Bhaskaran, and W. H. P. Pernice, "All-optical spiking neurosynaptic networks with self-learning capabilities," Nature **569**(7755), 208–214 (2019).
[2]. X. Lin, Y. Rivenson, N. T. Yardimci, M. Veli, Y. Luo, M. Jarrahi, and A. Ozcan, "All-optical machine learning using diffractive deep neural networks," Science **361**(6406), 1004–1008 (2018).
[3]. H. Jaeger and H. Haas, "Harnessing Nonlinearity: Predicting Chaotic Systems and Saving Energy in Wireless Communication," Science **304**(5667), 78–80 (2004).
[4]. L. Appeltant, M. C. Soriano, G. Van der Sande, J. Danckaert, S. Massar, J. Dambre, B. Schrauwen, C. R. Mirasso, and I. Fischer, "Information processing using a single
[5]. dynamical node as complex system," Nat. Commun. **2**(1), 1–6 (2011).
[6]. D. Brunner, M. C. Soriano, C. R. Mirasso, and I. Fischer, "Parallel photonic information processing at gigabyte per second data rates using transient states," Nat. Commun.
[7]. **4**(1), 1–7 (2013).
[8]. J. Vatin, D. Rontani, and M. Sciamanna, "Experimental reservoir computing using VCSEL polarization dynamics," Opt. Express **27**(13), 18579–18584 (2019).
[9]. J. Vatin, D. Rontani, and M. Sciamanna, "Enhanced performance of a reservoir computer using polarization dynamics in VCSELs," Opt. Lett. **43**(18), 4497–4500 (2018).
[10]. J. Bueno, D. Brunner, M. C. Soriano, and I. Fischer, "Conditions for reservoir computing performance using semiconductor lasers with delayed optical feedback," Opt.
[11]. Express **25**(3), 2401–2412 (2017).

A21_58 Ultrafast non-equilibrium dynamics in GaAs-based nanowire lasers

A. Thurn[1], J. Bissinger[1], S. Meinecke[2], P. Schmiedeke[1], S. S. Oh[3], W. W. Chow[4], K. Lüdge[2], G. Koblmüller[1], and J.J. Finley[1]

1 – Walter Schottky Institut, Technische Universität München, Am Coulombwall 4, 85748 Garching, Germany
2 - Institut für Theoretische Physik, Technische Universität Berlin, Hardenbergstraße 36, 10623 Berlin, Germany
3. School of Physics and Astronomy, Cardiff University, Cardiff CF24 3AA, UK,
4 - Sandia National Laboratories, Albuquerque, New Mexico 87185-1086, USA. andreas.thurn@wsi.tum.de

Nanowires (NW) provide a highly attractive route to integrate III-V compounds onto silicon. Due to the nonplanar growth, they exhibit a small footprint, strongly alleviating lattice mismatch restrictions and leading to a high structural quality. Moreover, their intrinsic one-dimensional geometry facilitates low-loss waveguiding, low- threshold lasing and site selective integration onto silicon photonic circuits. To assess the potential of NW lasers for future nanoscale opto-electronic devices, an understanding of the mechanisms influencing their ultrafast temporal lasing dynamics is of key importance. Previous studies laid out the groundwork by studying fundamental aspects of gain dynamics [1, 2] and by demonstrating the potential of NW lasers for ultrafast external modulation by optically injecting carriers, with frequencies of up to ~200 GHz [3]. In this work we build on this foundation and address open questions that still remain to be answered. In particular, it is currently unclear what the microscopic mechanisms and dynamic processes are that govern and potentially limit the ultrafast behaviour of NW lasers. To shed light on this issue we use non-resonant degenerate pump-probe spectroscopy to investigate the temporal dynamics of single GaAs-AlGaAs core-shell NW lasers [4]. In this contribution we report on unexpected NW laser dynamics occurring over few picosecond timescales. These findings are supported by microscopic numerical simulations based on both a k-resolved semiconductor Bloch equation model [5] and a quantum statistical model [6] which provide excellent qualitative and quantitative agreement with our experiments. Our results show that the observed ultrafast laser dynamics correspond to a non-equilibrium analogue of relaxation oscillations caused by the intricate interplay of carrier heating and cooling in the electron hole plasma of the lasing NWs and further reveal how these dynamics are tied to their unique resonator geometry. This suggests that it is possible to engineer nanolasers with the aim to optimize and later on also utilize their ultrafast dynamics in the non-equilibrium regime.

1. T. P. H. Sidiropoulos *et al*., Ultrafast plasmonic nanowire lasers near the surface plasmon frequency. *Nature Physics*. **10**, 870 (2014). 2. R. Röder *et al*., Ultrafast Dynamics of Lasing Semiconductor Nanowires. *Nano Letters.* **15**, 4637 (2015). 3. B. Mayer *et al*., Long-term mutual phase locking of picosecond pulse pairs generated by a semiconductor nanowire laser. *Nature Communications.* **8**, 15521 (2017).
4. A. Thurn, et al., to be submitted (2021).
5. W.W. Chow, S. W. Koch, and M. Sargent, Semiconductor-Laser Physics. (Springer-Verlag Berlin Heidelberg, 1994). 6. F. Jahnke & S. W. Koch, Many-body theory for semiconductor microcavity lasers. *Phys. Rev. A.* **52**, 1712 (1995).

A21_51 Study of the randomness of the dynamics in a laser diode subject to optical feedback with stimulated Brillouin scattering

Leidy Johana Quintero-Rodríguez[1], Ignacio Enrique Zaldívar-Huerta[1], Yanhua Hong[2], Cristina Masoller[3] and Min Won Lee[4]

1 Departamento de Electrónica, Instituto Nacional de Astrofísica, Óptica y Electrónica, Puebla 72000, Mexico, 2 School of Computer Science and Electronic Engineering, Bangor University, Wales, LL57 1UT, UK, 3 Departament de Física, Universitat Politècnica de Catalunya, St. Nebridi 22, 08222, Terrassa, Barcelona, Spain 4 Laboratoire de Physique des Lasers CNRS - UMR7538, Université Sorbonne Paris Nord, 93430 Villetaneuse, France

Chaotic dynamics in laser diodes subject to optical feedback has widely been studied for decades. The periodicity imposed by the external cavity frequency (the so-called "time delay signature") is challenging to eliminate and it is a drawback for some applications, such as all-optical random signal generation, that require random signals. This has motivated the search for alternative ways of generating optical chaos with diode lasers.

In this paper, a new configuration of optical feedback using stimulated Brillouin scattering is proposed and the level of randomness of the laser output is quantified using the permutation and Kolmogorov entropies. As stimulated Brillouin scattering is a random process, it has potential for generating, all-optically, fully random signals. In order to stimulate Brillouin backscattering, a high-power incoherent laser diode emitting at 1450 nm is used together with a standard 4km optical fibre (the maximum free-running power is 270 mW for a pump current of 1000 mA). The light backscattered from the fibre is injected back into the laser diode as stimulated Brillouin scattering optical feedback (SBSOF). For comparison, conventional optical feedback (COF) is also studied with a similar configuration (Fig. 1), but only the light transmitted through the fibre is injected back into the laser diode (the time delay is 21 μs). When varying the feedback strength and the laser current, both the configurations show a rich variety of complex dynamics.

Because in the SBSOF configuration the feedback light is the light backscattered from a long fibre, therefore, it is the superposition of light reflected from an infinite number of external cavities and the time delay signature in the SBSOF configuration is fully suppressed [1]; whereas it is strong, as expected, when the light transmitted through the fibre is re-injected into the laser. In order to compare the complexity of the two chaotic signals, SBSOF and COF, the permutation entropy (PE) and the Kolmogorov entropy (KE) have been computed from experimental time traces as a function of the feedback ratio and laser current. While the PE values are only slightly larger in the SBSOF setup than those in the COF setup [Figs. 1(a) and (b)], the KE values are significantly higher in the SBSOF case than those in the COF case [Fig.1(c) and (d)], which clearly demonstrates that the signals generated with the SBSOF setup have much higher degree of randomness, as compared with conventional feedback.

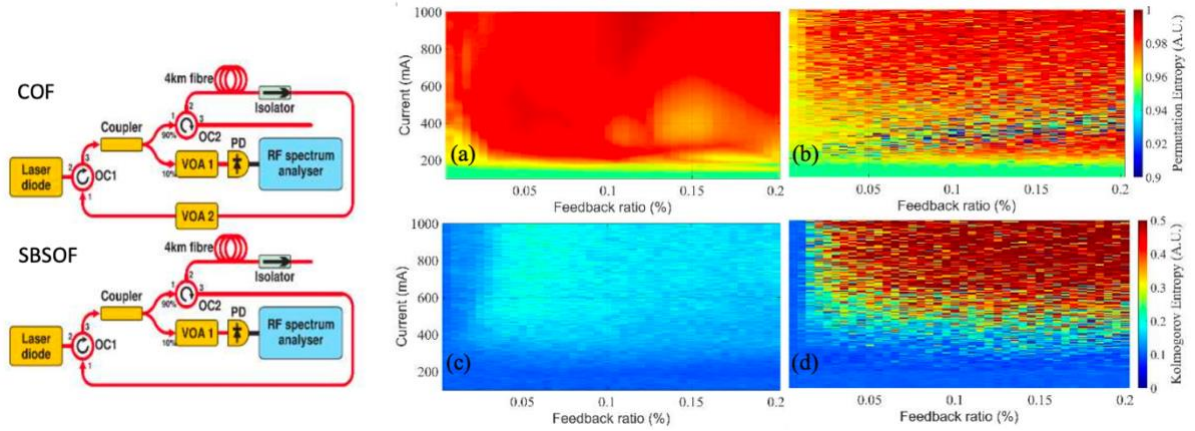

Fig. 1 Experimental setup (described in Ref. [1]); permutation entropy (a,b) and Kolmogorov entropy (c,d) of chaotic optical signals generated via conventional optical feedback (a,c); stimulated Brillouin scattering optical feedback (b, d).

To summarize, we have studied experimentally two optical feedback configurations, and quantified the degree of randomness of the diode laser output using permutation and Kolmogorov entropies. We have shown that when the feedback light is the stimulated Brillouin backscattered light from a standard optical fibre, it can generate signals with a higher degree of randomness as compared to those when the feedback light is the one transmitted through the fibre.

Acknowledgements M. W. Lee and I. E. Zaldívar-Huerta thank the ECOS-Nord programme (N° M19P03) for the support. L. J. Quintero-Rodríguez wishes to thank the Mexican Consejo Nacional de Ciencia y Tecnología (CONACyT) for the student scholarship (no. 465594) and the research stay in France.

References

[1] A. G. Correa-Mena, M. W. Lee, I. E. Zaldívar-Huerta, Y. H. Hong, A. Boudrioua, “Investigation of the dynamical behavior of a high-power laser diode subject to stimulated Brillouin scattering optical feedback”, IEEE J. Quantum Electron., 56(1), 1 – 6 (2020).

A21_12 Image Edge Detection with Spiking VCSEL Neurons

J. Robertson,[1*] Y. Zhang,[1,2] M. Hejda,[1] J. Alanis,[1] J. Bueno,1 S. Xiang,[2] and A. Hurtado[1]

*[1]Institute of Photonics, Dept. of Physics, University of Strathclyde, Technology and Innovation Centre, Glasgow, UK [2]State Key Laboratory of Integrated Service Networks, Xidian University, Xi'an 710071, China. *joshua.robertson@strath.ac.uk*

Fast spiking Vertical Cavity Surface Emitting Laser (VCSEL) neurons are used to reveal edge feature information in digital images. Image convolution is demonstrated with a photonic system where a VCSEL-neuron showcases the ability to both integrate and threshold optical inputs, resulting in a convolved image output with a fast spiking representation.

The functionality of computer vision aims at creating processing systems that recognize and understand complex images and patterns as humans do. Using convolution and the scanning of kernel operators (masks), convolutional neural networks (CNNs) detect and extract distinctive features from source images to provide identification [1,2]. Using vertical-cavity surface-emitting lasers (VCSELs), neuromorphic devices that have demonstrated the ability to operate using spiking signals with different neuronal functionalities (interconnectivity, thresholding [3], leaky integrate-and-fire (LIF) operation for pattern recognition [4]), we will show two experimental methods (threshold- and-fire and integrate-and-fire) for implementing spiking edge-feature detection in digital images. Utilizing time- multiplexing and optical injection, we trigger fast (sub-ns long) neuronal spikes to reveal target feature information in a single VCSEL-neuron system, and demonstrate the high prospects of these devices for applications in future novel CNN architectures for future spiking computer vision systems in the optical domain.

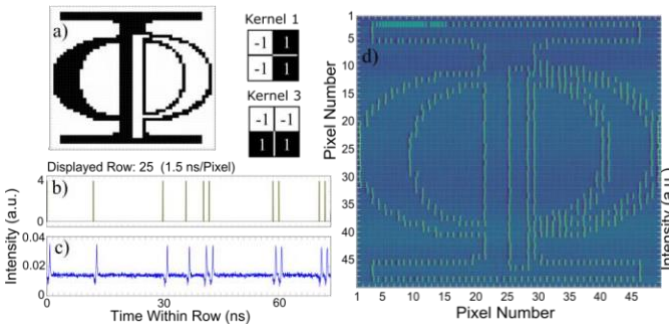

Fig. 2: Method 1-Threshold-and-activate. **a** 50x50 source image (Strathclyde's Institute of Photonics logo), **b** input *(Kernels 1&3 applied)*, **c** VCSEL output and **d** image reconstruction

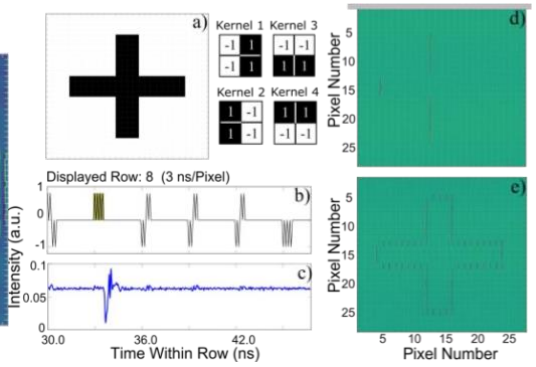

Fig. 3: Method 2-Integrate-and-fire. **a** 28x28 source 'cross' image, **b** input *(Kernel 1)*, **c** VCSEL output, **d** & **e** reconstructed images *(Kernel 1 & Kernels 1-4)*

Figures 2a & 3a plot respectively the source images used for the demonstrations of each method, threshold- and-fire (the Institute of Photonics logo, 50x50 pixels) and integrate-and-fire (a cross pattern, 28x28 pixels). Both Figs. 2 & 3 show the method-varying input signal generated and injected into the VCSEL-neuron (b), and the kernels used to extract the edge information. The time series and temporal maps of the VCSEL responses are plotted (c & d) to demonstrate the detection of edge features with fast spiking dynamics. In method 1, inputs generated by Kernels 1 & 3 are combined to detect changes in gradient magnitude. Hence, following the injection of the signal, the VCSEL thresholds each input pulse and activates a spiking response for the sufficiently strong inputs that constitute large changes in pixel gradient magnitude (edge features). In method 2 the image input is calculated by applying a single Kernel, element-wise, to the source image. The image input injected into the VCSEL-neuron consists of bursts of input pulses that correspond to the 4 values produced during convolution. In response to the injection of this input, as shown in the recorded time series (Fig. 3b), the VCSEL-neuron activates a spike for the burst corresponding to the target edge feature only (green highlight). The VCSEL-neuron utilizes its ability to optically integrate 4 short pulses into a larger total input, allowing the system to activate a fast spiking response. Complete edge detection of the

image (Fig. 3e) is achieved when all four kernels are run. This integrate- and-fire method therefore demonstrates that part of the convolution (summation into a destination pixel) can be achieved within the photonic system, where the output is fast (sub-ns) spiking directly in the optical domain. During the conference, we will expand upon these results by demonstrating the detection of further target features in a diversity of source images, as well as the detection of multiple image edge features in one experimental run towards the realization of compact, hardware friendly, photonic spike-based computer vision systems.

3. References

[1]. M. El-Sayed, et al., *Int. J. Adv. Comput. Sci. Appl*., vol. 4, no.10, 11-17 (2013).
[2]. D. Marr, *Proc. R. Soc. Lond*. B, vol. 207, 187-217 (1980).
[3]. J. Robertson, et al., *IEEE J. Sel. Top. Quantum Electron*., vol. 26, no. (1), 7700715 (2020).
[4]. J. Robertson, et al., *Sci. Rep*, vol. 10, 6098 (2020).

Abstract

Session 6: Invited Speaker I

Invited **p-doping in quantum dot lasers**

Weng W. Chow[1], Zeyu Zhang[2], Justin Norman[2], John E Bowers [2], Juan Duan[3] and Federic Grillot [3]

[1]Sandia National Laboratories, Albuquerque, New Mexico, USA
[2]Materials and Electrical and Computer Engineering Departments, University of California, Santa Barbara, California USA
[3]Telecom Paris, Institut Polytechnique de Paris, France

Unlike quantum-well lasers, optimizing performance by strain engineering is not practical in QD lasers. The reason is that strain also greatly affects QD formation. Instead, p-doping serves as an alternative, by roughly equalizing the electron and hole populations. However, other effects, e.g. defect loss, have to be taken into account. This talk describes experimental and theoretical investigations into the effects of p- doping in InAs quantum-dot lasers. Examples involving gain, linewidth enhancement factor and four-wave mixing susceptibility will be discussed.

Abstracts

Session 7: Compound Semiconductors on Silicon

A21_22 APB annihilation of III-V materials monolithically grown on on-axis silicon (001)

Keshuang Li[1*†], Junjie Yang[1*], Ying Lu[1*], Mingchu Tang[1*], Pamela Jurczak[1], Zizhuo Liu[1], Xuezhe Yu[1], Jae-Seong Park[1], Huiwen Deng[1], Hui Jia[1], Manyu Dang[1], Ana M. Sanchez[2], R. Beanland[2], Wei Li[3], Xiaodong Han[3], Jin-Chuan Zhang[4], Huan Wang[4], Fengqi Liu[4], Siming Chen[1], Alwyn Seeds[1], Peter Smowton[5] and Huiyun Liu[1]

[1] Department of Electronic and Electrical Engineering, University College London, London, WC1E 7JE, United Kingdom [2] Department of Physics, University of Warwick, Coventry, CV4 7AL, United Kingdom, [3] Institute of the Microstructure and Properties of Advanced Materials, Beijing University of Technology, 100124, Beijing, China, [4] Key Laboratory of Semiconductor Materials Science, Institute of Semiconductors, Chinese Academy of Sciences, Beijing 100083, China, [5] Department of Physics and Astronomy, Cardiff University, Queens Building, The Parade, Cardiff, CF24 3AA, United Kingdom

Monolithic growth of III-V materials on complementary metal-oxide-semiconductor (CMOS) compatible on-axis Si (001) enables a high integration level of photonic integrated circuits (PICs). However, due to the polarity difference between group III-V and group VI materials, directly growing III-V materials on Si substrate will cause anti-phase boundary (APB) which could severely degrade the performance of device developed upon it. APB is a kind of planner defect that arises from the interface between III-V materials and Si. They intensively impact the material quality and thus need to be eliminated prior to integration of III-V optoelectronic integrated circuits onto Si platform. In this paper, we demonstrate a technique to achieve APB-free GaAs materials directly grown on on-axis Si (001) substrates by molecular beam epitaxy (MBE), without use of any intermediate layers, patterned substrates or substrates with intentionally selected offcut angles. By combining a periodic array of single-atomic height Si steps shown in Fig. 1(a) and a strict GaAs growth method, the APBs can nucleate on the parallel, straight Si steps which could confine the movement of defects that arise from the interface. In addition, the probability of APB self-annihilation process during the subsequent GaAs growth is also dramatically enhanced. Eventually, a repeatable APB-free GaAs growth method is achieved in the absence of dominated double atomic-height Si step. The APB-free surface of 1µm thickness GaAs grown by this method is shown in the inset image of Fig. 1(a). By using the high-quality, low-surface-roughness APB-free GaAs buffer layer as a platform for the monolithic integration of III-V optoelectronics on CMOS compatible Si (001), a 1.3µm InAs quantum dot (QD) laser was successfully developed. Inset image of Fig. 1(b) shows InAs QDs grown on our platform with high density of $5.4\times10^{10}cm^{-2}$. In addition, room temperature PL measurement was performed for five repeats of QD layers grown on our APB-free GaAs/Si platform and non-optimized GaAs/Si platform. The result is shown in Fig. 1(b), realising a four-fold improvement on our platform. The peak wavelength is similar for both samples at ~1288nm. The full width-half-maximum for InAs QDs on APB-free GaAs/Si (001) is as low as ~28meV. Broad-area lasers were fabricated for subsequent pulsed characterisation. As shown in Fig. 1(c), a low threshold current density of $83.3A/cm^2$ was achieved at room temperature. The highest operation temperature was over 120°C. Moreover, the slope efficiency of the single-facet emission was ~130mW/A at 20 °C and remained stable when temperature increased, showing a good temperature reliability for the InAs QD laser on our APB-free GaAs/Si (001) platform. This confirms the suitability of this platform for the integration of optoelectronic devices with current CMOS technology. Our results indicate that APBs will no longer be a fundamental issue for the monolithic integration of polar III-V on non-polar group IV and form a basis of combing monolithic integration of Si photonics with mature CMOS technology in the future.

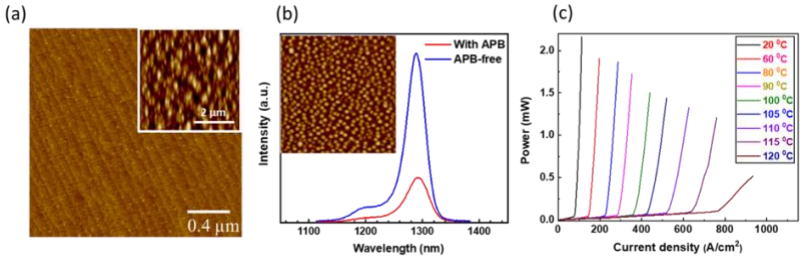

Figure. 1. (a) 2 µm × 2 µm AFM image of Si buffer layer surface showing alternating S step pairs; inset: 5 µm × 5 µm AFM image of APB-free GaAs on on-axis Si (001). (b) Comparison of room temperature PL for QD grown on two different platform; (inset: $1\times1\mu m^2$ AFM image of uncapped QD in high density. (c) Temperature dependent Light-current curve for 1.3µm QD laser grown on CMOS compatible Si substrate.

A21_15 Linewidth enhancement factor measurement by using phase modulation method for epitaxial quantum dot laser on silicon

Shihao Ding [1, §], Bozhang Dong [1], Heming Huang [1], John E. Bowers [2], and Frédéric Grillot [1, 3]

1 LTCI, Télécom Paris, Institut Polytechnique de Paris, 91120 Palaiseau, France
2 Institute for Energy Efficiency, University of California, Santa Barbara, California 93106, USA
3 Center for High Technology Materials, The University of New-Mexico, Albuquerque, NM 87106, USA §
shihao.ding@telecom-paris.fr

The amplitude-phase coupling, namely the dynamic change of the active medium refractive index in relation to changes of the gain, commonly characterized by the linewidth enhancement factor (αH factor) reflects a basic characteristics of semiconductor lasers [1]. Here, we measured the above-threshold αH from the amplitude-phase coupling in a silicon-based epitaxial quantum dot (QD) laser using an optical phase modulation (OPM) method [2]. The laser under study is an InAs/GaAs Fabry–Perot (FP) laser made with five QD layers grown on an on-axis (001) Si wafer [3]. In the set-up depicted in Fig.1(a), the bias current of laser is set to twice the threshold (72 mA). The QD laser was modulated by the RF generator with a modulation frequency of 8.5 GHz. Meanwhile, the phase modulator was also modulated by the same frequency. The optical delay line (ODL) is used to control the delay between the optical and electrical signals at the input of the phase modulator. The frequency dependence of the amplitude phase coupling reads as $\alpha(fm)= \alpha H[1+(fc/fm)2]1/2$ with fc the corner frequency and fm the modulation frequency [1]. The analysis of the side mode dynamic on the optical spectrum is used for extracting the amplitude phase coupling and subsequently the αH factor at $fm>>fc$. Fig. 1(b) depicts the optical spectrum and the corresponding αH factors extracted for 19 longitudinal modes near the gain peak. We demonstrate very low values of the above threshold αH factors in such epitaxial QD lasers hence ranging between ~1.0 and ~1.6 across the optical spectrum. Such results confirm the high quality of the material along with the narrow inhomogeneous broadening [4]. This work is important for integrated technologies on silicon. Last but not least, this OPM method can be applied to any types of semiconductor laser either single-mode, multi-mode, or with complex structures.

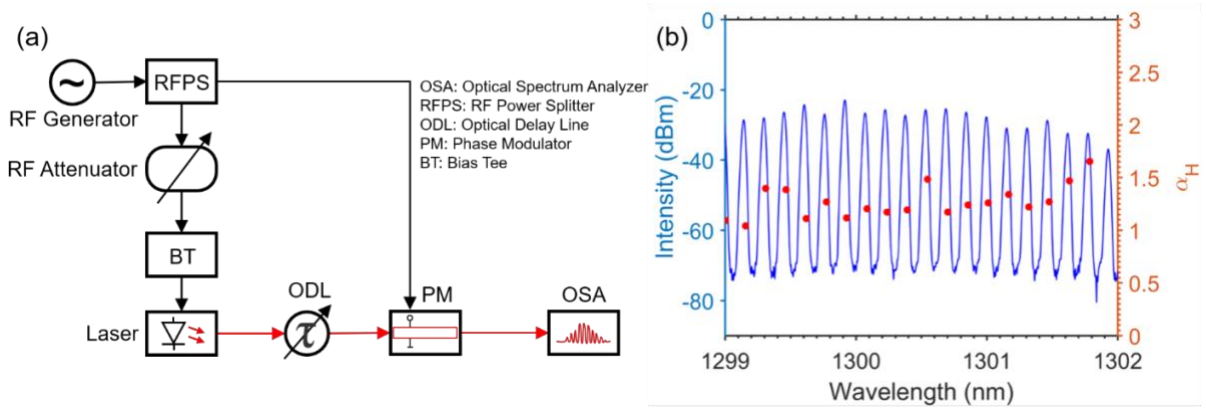

Figure 1. (a) Schematic of the experimental set-up, (b) Free running spectrum (blue line) and spectral dependence of the αH factor (red dots) for the silicon-based epitaxial QD laser.

References

1. J-G Provost, and F. Grillot, IEEE Photonics Journal, 3(3), 476-488, 2011.
2. J. G. Provost, et al., Optics Express. 19(22) 21396-21403, 2011.
3. J. Duan, et al., Photonics Research. 7(11), 1222-1228, 2019.
4. W. W. Chow, et al., Applied Physics Letters. 5, 026101, 2020.

A21_60 Carrier Transport in Quantum Dot Laser on Silicon: impact of traps and p-type modulation doping on laser performance

M. Gioannini,M.Saldutti.A.TibaldiandF.Cappelluti

Departement of Electronics and Telecommunication, Politecnico di Torino, Italy

The monolithic integration of Quantum Dot (QD) lasers on silicon is the ultimate solution to epitaxially integrate laser sources in silicon photonic integrated circuits [1]. The mismatch in the lattice constants between Si and III-V materials causes threading dislocations (TDs), which act as non-radiative recombination centres. The achievable TD density (Nd) is still around 107 cm−2 [1].

We present a theoretical investigation on how the TDs limit the performance of QD lasers epitaxially grown on silicon. The approach is based on a transport model including drift-diffusion of electrons and holes in the entire heterostructure, Shockley-Read-Hall (SRH) recombination in the traps caused by TDs, carrier dynamics in the QD states and photon rate equations [2]. Overcoming the traditional lumped formulations based on rate equations, our approach can simulate the power vs current (P-I) and voltage vs current (V-I) characteristics of the QD laser diode from the description of materials, doping, and geometry. As example we consider a device with stack taken from [3]. For the laser diode emitting only from the ground state (GS), Fig.1 shows the degradation of the threshold current and slope efficiency due to the increased Nd in both the barrier layers and in the quantum well of the dot-in-well structure (DWELL). Whereas TDs in the barrier layers between DWELLs do not degrade the P-I, the major part of the degradation is due to TDs in the well or wetting layers. The coupling of the transport model with rate equations for photons emitted from the GS and excited state (ES) also permits the simulation of the double laser emission from GS and ES, with consequent quenching (or not) of the GS power. In [2] we demonstrated for first time how the competition for photons between GS and ES is driven by the different mobilities of electrons and holes in the barrier layers and the consequent very ununiform distribution of holes in the different layers of QDs. Such a behaviour can be partially mitigated by p-type modulation doping that, as shown in Fig. 2a-c, changes the relative position of the GS and ES thresholds and the variation of GS power increasing current. Fig. 2d demonstrates how the separation between GS and ES threshold can be arranged by a proper doping level, but also how it is very dependent on the Nd. When Nd is too high, SRH recombination partially shadows the effect of doping. In conclusion we have shown a simulation platform to achieve deeper understanding of the device operation with the aim of designing devices with improved performance.

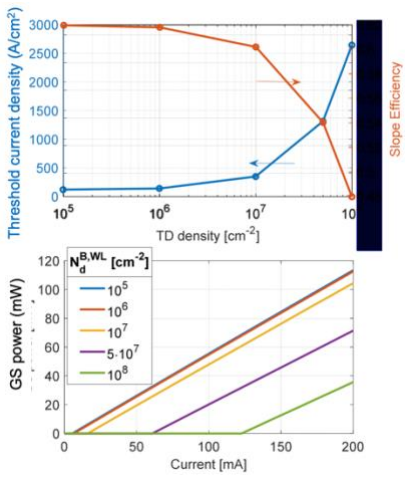

Fig.1 (top) GS laser threshold current and slope efficiency ; (bottom) P-I characteristic varying Nd

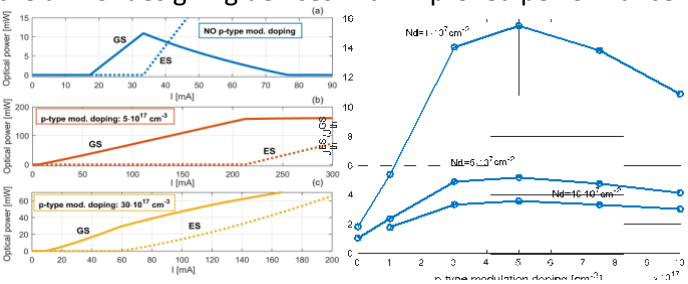

Fig.2 (a-c) Double lasing from GS and ES at different doping levels and (d) ratio between GS and ES threshold current varying doping level and dislocation density Nd.

[1] A. Y. et al. ” IEEE J. Sel. Top. Quantum Electron. 24, 6000412 (2018).
[2] M. Saldutti et al. Photonic Research, 8,1388-1397, (2020) [3] D. Jung, et al. ACS Photonics 5, 1094–1100 (2018).

A21_40 Stable 25.5 GHz mode-locked quantum dot lasers operating up to 120 °C

S. Pan[1*], J. Huang[2], L. Ponnampalam[1], Z. Zhou[1], K. Balakier[1], M. Tang[1], Z. Cao[2], Z. Liu[1], A. Seeds[1], H. Liu[1], and S. Chen[1] shujie.pan.14@ucl.ac.uk

[1]Departement of Electronic and Electrical Engineering, University College London, London WC1E 7JE, United Kingdom;
[2]Department of Electronic and Electrical Engineering, Eindhoven University of Technology, Eindhoven 5612AZ, Netherland;

Mode-locked semiconductor lasers, motivated by the ability to generate stable and cost-effective ultrafast, high-repetition-rate and low-noise optical pulses, have led to significant advances in a range of applications from optical-communications, clock distribution/recovery to sampling. Quantum dot (QD) structures have, for many years, been regarded as one of the most promising materials systems for ultrafast science and technology [1]. Given their inherent properties, such as ultrabroad gain bandwidth as well ultrafast carrier dynamics, the progress in mode-locked QD lasers has been awe-inspiring since X. Huang *et al.* first demonstrated mode-locking at a repetition rate of 7.4 GHz with a duration of 17 ps, using a passive mode-locking technique [2], and mode-locked QD lasers have now been proved to be a superior alternative to the bulk and quantum well counterparts in terms of pulse duration, linewidth, noise performance, and peak power.

Temperature resilience has long been the hallmark of QDs, mainly due to their delta-function-like density of states. This opens up new avenues for the ultimate deployment of cost-effective, uncooled mode-locked lasers for many applications, particularly in ultrafast optical communications. While high-temperature continuous-wave operation up to 220 °C has been demonstrated from edge-emitting Fabry–Perot InAs QD lasers, turning this prediction into reality for QD MLLs limited to not only the thermal mechanisms but also the mutual interdependence of the gain section and the saturable absorber in the two-section passive devices. Given that, the work of Cataluna and co-works first emphasised the stability of mode-locking in 20 GHz InGaAs QD MLLs at elevated temperatures and, unfortunately, the device exhibited unstable mode-locking operation over 70 °C evidenced by RF signal- to-noise quenching and RF linewidth broadening [3]. Stable mode-locking from 20 °C to 110 °C has also been demonstrated from two-section passive InAs QD MLLs [4]. However, mode-locking switching between the ground state (GS) and the first excited state (ES1) appears at temperatures over 93 °C due to the carrier escape from the GS with increasing temperature, and the long laser cavity of 8-mm employed in their work limited the fundamental repetition rate to only 5 GHz. Achieving large mode spacing from a single frequency comb light source with ultra-stable mode spacing over an extremely broad temperature range remains a key challenge at the present time.

In this work, by engineering the QD active region with a high optical model gain and a large quantised-energy difference between the GS and the ES1 and optimising the passively two-section laser structure. We demonstrate stable mode-locking at temperatures ranging from 20 °C to 120 °C (Fig. 1a) in a 25.5 GHz passively mode-locked InAs QD laser with a marginal change (Δ~0.07 GHz) in the repetition rate over this entire temperature range (Fig. 1b), exclusively from the GS transition (Fig. 1c). To the best of our knowledge, this is the highest mode-locking operation temperature ever reported to date for any types of MLLs.

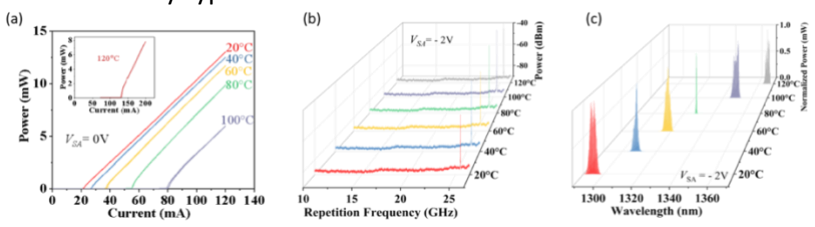

Figure 1 (a) Temperature-dependent *L-I* characteristics with *VSA* = 0 V. (b) RF spectra as a function of temperature with *VSA* = -2 V. The spectra were measured at 49, 60, 64.7, 85, 148.5, and 210 mA at 20, 40, 60, 80, 100, and 120 °C, respectively (RBW: 1 MHz, VBW: 10 kHz). (c) Optical spectra under the same conditions as shown in (b).

1.E. U. Rafailov et al., Nat. Photon. 1, 295 (2007). 2. X. Huang et al., Appl. Phys. Lett. 78, 2825 (2001) 3.M. A. Cataluna et al., IEEE Photon. Tech. Lett. 18, 1500 (2006) 4. J. K. Mee et al, Appl. Phys. Lett. 101, 071112 (2012)

A21_39 Investigation of edge coupling between quantum dot laser-to- silicon waveguide via micro transfer printing

Ali Uzun1, Fatih Atar1, John Justice1, Peter Ossieur2, Ruggero Loi3, Igor Krestnikov4, Brian Corbett1

1 Tyndall National Institute, University College Cork, Ireland.
2 imec-IDLab and Ghent University, Ghent, Belgium.
3 X-Celeprint Ltd, Lee Maltings, Cork, Ireland.
4 Innolume GmbH, Konrad-Adenauer-Allee 11; 44263 Dortmund, Germany.

Si based photonic integration circuit (PIC) platforms provide a powerful route to scaling the performance (bandwidth, energy consumption) of transceivers while reducing the manufacturing cost. These circuits need an integrated solution for the light source which we propose to achieve via micro transfer printing (µTP) of lasers. In particular, when compared to quantum wells laser diodes having quantum dots (QD) in their active region mitigate the negative effect of temperature on the device characteristics while keeping a low threshold current density and reduced feedback sensitivity. In order to exploit those unique features an optimised low-loss coupling structure to the PIC platforms is crucial. In our approach the laser will be butt-coupled to the Si waveguide using the imec 220 nm silicon photonics platform with a 2 µm buried oxide and a 3.6 µm SiO2 over-cladding. One particular challenge for coupling from QD lasers to Si waveguides structures is the strong transverse mode confinement effect that leads to coupling loss due to the mode-size mismatch between that of the laser diode and the Si waveguides. Thus, the Si waveguide coupler needs to be precisely designed in order to minimise the loss.

In this work, the 1300 nm wavelength QD laser structure contains an active region comprising of a stack of 12 InAs QD layers separated by GaAs spacers. The waveguide is clad by 1.2 µm thick p- and n-doped AlGaAs layers. Inverse tapered Si edge couplers with various tip configuration are designed and simulated for 2 and 3 µm wide ridge waveguide lasers. Multiple tip couplers (double and triple tips studied in this work), similar to that of a trident fork, show improvements both in terms of coupling efficiency and misalignment tolerance between the laser and Si waveguide in the lateral direction compared with a single tip coupler design with the same tip width. In order to achieve a coupler that gives maximum performance with a low- loss optical coupling and flexible alignment tolerance, Si waveguide dimensions including tip width, spacing between adjacent waveguides, and taper length have been simulated for each design. A triple trident configuration with a tip width of 150 nm, gap of 800 nm and taper length of 100 µm shows the best performance. An overall coupling efficiency of 80% (-1dB) is simulated for transverse electric (TE) mode with a lateral misalignment tolerance (for a 3dB loss penalty) of ± 1.5 µm. All designs have a vertical misalignment tolerance of ± 0.5 µm which is rather smaller than that in horizontal direction as a result of the strong vertical mode confinement in the QD region.

The integration of quantum dot laser coupons with Si waveguide coupler will be carried out using the µTP technique utilizing a PDMS elastomeric stamp to pick the lasers from the source substrate and precisely place them with respect to the Si coupler. To achieve this, a 500 nm thick Al0.95Ga0.05As layer is added to the epitaxial structure between substrate and the n-AlGaAs layer in order to permit the release the device from the native wafer. A diluted HCl etchant has been developed to selectively undercut the Al0.95Ga0.05As release layer.

A21_21 Etched-facets Mid-IR laser on on-axis Silicon substrate for photonic integrated circuits

Laura Monge Bartolomé, Marta Rio Calvo, Michaël Bahriz, Jean-Baptiste Rodriguez, Laurent Cerutti and Eric Tournié.

IES, Univ. Montpellier, CNRS, 34000 Montpellier, France. Contact: laura.monge-bartolome@umontpellier.fr ; eric.tournie@umontpellier.fr

Silicon photonics has recently made great progress, particularly with the integration of passive devices such as (de)multiplexer or beam splitter among others. However, an efficient light source is still missing, because silicon has an indirect bandgap. Consequently, there is high interest for the integration of efficient III-V semiconductor laser sources compatible with the well-developed silicon platforms. This would open the way to compact, robust and affordable sensors based on silicon photonics integrated circuits (PICs). Although two approaches, bonding and direct epitaxy, are possible, direct epitaxy appears as the most promising approach for large scale integration. Therefore, this work is focused on the demonstration of mid-infrared Sb-based laser diodes (LDs) suitable for Si PICs for sensing applications.

The actual integration of lasers on PICs first requires, on one hand, the epitaxy of high performance LDs on on-axis Si substrates and, on the other hand, the fabrication of a laser cavity without resorting to the cleavage step used with discrete devices. In this communication we will focus on facet fabrication. We have developed a technology process to obtain good quality cleavage-free laser facets by using standard lithography and dry etching techniques. We first focus on GaSb-based laser diodes grown on GaSb substrates and emitting at 2.3 µm. We compare different geometries of the etched facets, T-shape and square shape, as well as shallow and deep ridge etching and we benchmark them with cleaved facets. The LD performances are very similar, which means that facet etching does not increase the optical losses. Then we transfer the optimized facet etching technological process to GaSb-based laser diodes grown on Silicon substrates. CW operation was achieved with similar threshold as discrete devices.[1]

These results represent a step forward towards mid-infrared GaSb-based devices monolithically integrated on silicon for smart, compact and robust sensors on PICs.

Part of this work has been supported by the H2020 program (REDFINCH, GA 780240) and the trench program on “Investments for the Future” (EquipEx EXTRA, ANR-11-EQPX-0016).

[1] L. Monge Bartolomé, T. Cerba, D. Diaz-Thomas, M. Bahriz, M. Rio Calvo, G. Boissier, T. Baron, J.-B. Rodriguez, L. Cerutti, and E. Tournie, "Etched-cavity GaSb laser diodes on a MOVPE template grown on a 300-mm Silicon wafer," Opt. Express 28(14), 20785–20793 (2020).

Abstracts

Session 9: Detectors and Related Materials

A21_11 Colloidal Quantum Dots for Indoor and Concentration Solar Cells Applications

Dr Bo Hou

School of Physics and Astronomy, Cardiff University https://www.cardiff.ac.uk/people/view/1756484-hou-bo Email: houb6@cardiff.ac.uk

Colloidal metal chalcogenide quantum dots (QDs) have excellent quantum efficiency in light- matter interactions and good device stability. Although QDs have been brought to the forefront as viable building blocks in bottom-up assembling semiconductor devices, the development of QD solar cell (QDSC) is still confronting considerable challenges comparing to other QD technologies due to their low performance under natural sunlight, as a consequence of untapped potential from their quantized density-of-state and inorganic natures.1-3 This talk is about our recent works on addressing this long-standing challenge by accessing the feasibility of using QDSC for indoor and concentration PV (CPV) applications. We found that bandgap photon energy irradiation of QD solids can generate high densities of excitons via multi-photon absorption (MPA) and multiple exciton generation (MEG) and these excitons are not limited to diffuse by Auger recombination up to 1.5*1019 cm-3 densities irradiance. Based on these findings, we demonstrated a 19.5% (2000 lux indoor light), and an 11.6% efficiency (1.5 Suns) QDSCs could be facilely realized from an ordinary QDSCs (9.55% under 1 Sun). To further illustrate the MPA's potential in QDSCs, a 21.29% efficiency polymer lens CPVs (4.08 Suns) and viable sensor networks powered by indoor QDSCs matrix have been demonstrated5.

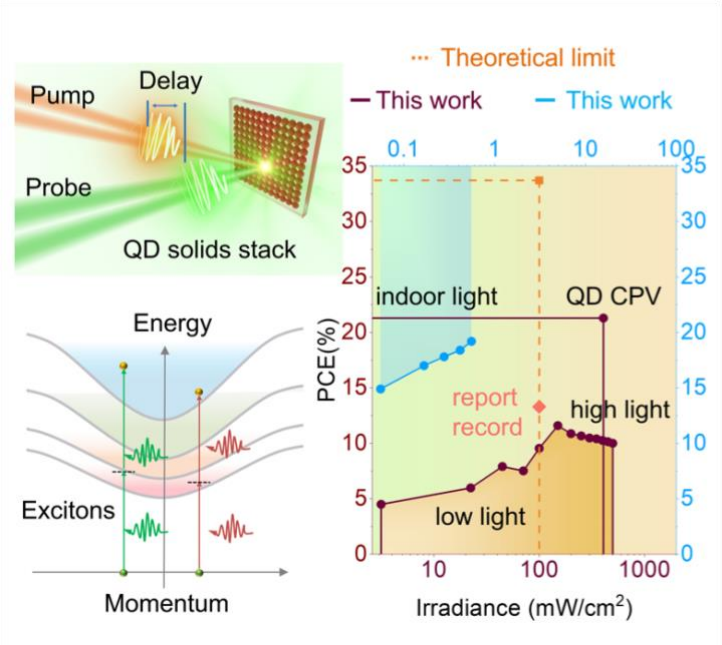

References:

1. Colloidal Quantum Dots: The Artificial Building Blocks for New-Generation Photo-Electronics and Photochemistry, Isr. J. Chem. 2019, 59, 637. https://doi.org/10.1002/ijch.201900069
2. Highly Monodispersed PbS Quantum Dots for Outstanding Cascaded-Junction Solar Cells, ACS Energy Lett. 2016, 1, 4, 834–839. https://doi.org/10.1021/acsenergylett.6b00294
3. Chemically encoded self-organized quantum chain supracrystals with exceptional charge and ion transport properties, Nano Energy 2019, 62, 764-771. https://doi.org/10.1016/j.nanoen.2019.05.088
4. Colloidal quantum dot hybrids: an emerging class of materials for ambient lighting, J. Mater. Chem. C, 2020,8, 10676-10695. https://doi.org/10.1039/D0TC01349H
5. Multiphoton Absorption Stimulated Metal Chalcogenide Quantum Dot Solar Cells under Ambient and Concentrated Irradiance, Adv. Funct. Mater. 2020, 30, 2004563. https://doi.org/10.1002/adfm.202004563

A21_14 Theory of radiative recombination in broken-gap InAs/GaSb superlattices

Co´nal Murphy[1,2], Eoin P. O'Reilly[1,2], and Christopher A. Broderick1[,2,*]

[1]Tyndall National Institute, University College Cork, Lee Maltings, Dyke Parade, Cork T12 R5CP, Ireland [2]Department of Physics, University College Cork, Cork T12 YN60, Ireland 524 ∗Email: c.broderick@umail.ucc.ie, Web: https://twitter.com/TyndallPTG

Many environmentally, medically and industrially important molecules possess strong absorption features in the 3 – 5 µm mid-infrared wavelength range, including the greenhouse gases CO2 and CH4, as well as NOx pollutants. As such, there exists significant demand for robust and efficient optical emitters and detectors operating in this spectral range, to enable applications in gas sensing for environmental monitoring, medical diagnostics and industrial process control.

InAs/GaSb superlattices (SLs) have attracted significant attention as mid-infrared emitters [1] and detectors [2]. InAs/GaSb interfaces possess type-III ("broken-gap") band offsets, with the valence band edge of GaSb lying higher in energy than the conduction band edge of InAs (cf. Fig. 1(a)). When grown in thin repeating layers to form a SL, quantum confinement effects open up a band gap, leading to type-II-like carrier confinement with electrons (holes) primarily confined in InAs (GaSb) layers. Recent advances in materials growth have enabled high structural quality InAs/GaSb SLs to be achieved. In particular, inter-band cascade light-emitting diodes (IC-LEDs) based on [001]-oriented InAs/GaSb SLs have demonstrated high output power and wallplug efficiency relative to competing technologies at wavelengths close to 4 µm [1]. Here, we present a quantitative theoretical analysis of the electronic and optical properties of these structures, with the aim of elucidating the origin of the observed high output power of prototype IC-LEDs.

To analyse InAs/GaSb SLs we employ an 8-band k·p Hamiltonian in conjunction with a reciprocal space plane wave expansion method [3] to compute the electronic properties: the band dispersion in the plane perpendicular to [001], and the miniband dispersion along [001]. The built-in periodicity of the plane wave basis states provides a natural framework to efficiently compute SL properties, allowing to compute the SL miniband structure and density of states (DOS) using a calculational supercell consisting only of a single superlattice period. Using the calculated SL band structure and eigenstates, we compute spontaneous emission spectra and estimate the radiative recombination coefficient B.

Our calculations reveal significant delocalisation of the lowest bound electron state (e1) in the SL, leading to large electron-hole overlap in the hole-confining GaSb layers (cf. Fig. 1(a)). The leakage of electron probability density into GaSb layers is driven by a combination of low InAs electron effective mass and narrow layer thicknesses (t ⍰ 2.5 nm), and leads to strong coupling of bound electron states in neighbouring periods evidenced by significant electron miniband dispersion (cf. Fig. 1(b)). The large electron-hole overlap in these structures results in increased inter-band optical matrix elements compared to conventional type-II structures, leading to values of B in InAs/GaSb SL IC-LEDs which are comparable with those in several classes of pseudomorphic and metamorphic type-I quantum well structures.

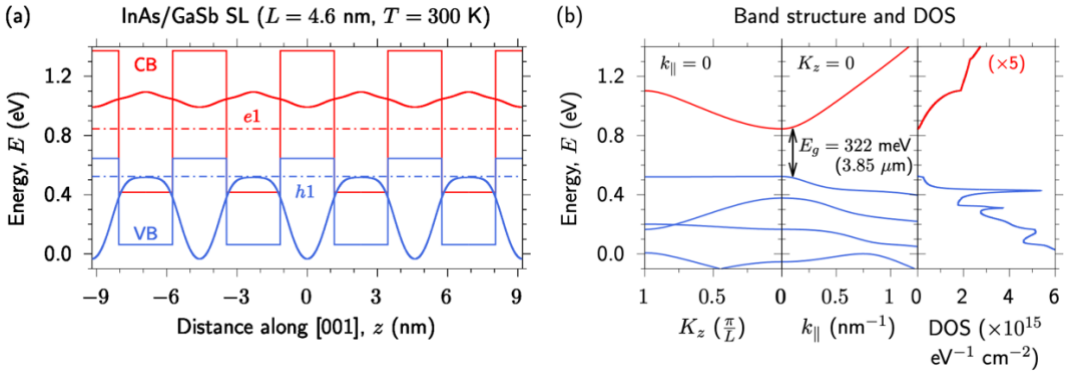

Figure 1: (a) Calculated conduction band and valence band offsets (CB and VB; solid red and blue lines, respectively), and electron and hole ground state probability densities (e1 and h1; solid red and blue lines, respectively), for several periods of an InAs/GaSb SL having equal InAs and GaSb layer thickness t = 2.3 nm (SL period L = 4.6 nm). Dash-dotted red and blue lines respectively show the calculated electron and hole ground state energies. (b) Calculated SL miniband structure (left-hand panel), in-plane band dispersion (centre panel), and density of states (DOS; right-hand panel) for the InAs/GaSb SL of

This work was supported by the Irish Research Council (IRC; via Government of Ireland Postgraduate Scholarship GOIPG/2020/1252 to C.M.), by Science Foundation Ireland (SFI; project no. 15/IA/3082), and by the National University of Ireland (NUI; via the Post-Doctoral Fellowship in the Sciences to C.A.B.). The authors thank Dr. Qi Lu and Prof. Anthony Krier (Lancaster University, U.K.) for useful discussions.

[1] Y. Zhou, Q. Lu, X. Chai, Z. Xu, J. Chen, A. Krier and L. He, Appl. Phys. Lett. 114, 253507 (2019)
[2] S. Abdollahi Pour, E. K. Huang, G. Chen, A. Haddadi, B.-M. Nguyen and M. Razeghi, Appl. Phys. Lett. 98, 143501 (2011)
[3] E. P. O'Reilly, O. Marquardt, S. Schulz and A. D. Andreev, Chapter 5, Multi-Band Effective Mass Approximations, Springer (2014)

A21_52 Mid-wavelength infrared (MWIR) type-II InAs/GaSb superlattice for NOx sensing

D.O. Alshahrani[1*], D.C.M. Kwan[1], D.L. Huffaker[1,2,3], E. Anyebe[2], and M. Kesaria[1*]

*[1]School of Physics and Astronomy, Cardiff University, UK [2]School of Engineering, Cardiff University, UK, Present address: 3Electrical Engineering Department, The University of Texas at Arlington, USA *Corresponding email contact: alshahranid@cardiff.ac.uk and kesariam@cardiff.ac.uk*

Environmental pollution is one of the greatest challenges confronting humanity globally. Nitric oxide (NO) and nitrogen dioxide (NO2), which are collectively referred to as NOx, are highly poisonous and detrimental to air quality and a primary source of air pollution, contributing to the formation of smog and acid rain [1]. NOx is a toxic gas produced during combustion of fossil fuels in power plants and automobile engines as well as during lightning in thunderstorms and contributes to numerous functions in the human body where it is produced in inflammatory processes [2]. There is an urgent need for highly sensitive photodetectors operating in the 5.1 - 5.6 µm wavelength range at high temperature, for low-cost detection of NOx gas. Although Mercury Cadmium Telluride (MCT) and Quantum Well Infrared Photodetectors (QWIPs) are well-established technologies in mid-wavelength infrared (MWIR) photodetection, they require cryogenic cooling for optimal performance at high temperatures. Type-II superlattices (T2SL) have emerged as a promising alternative due to their flexible and more controllable bandgap engineering through the design of the SL layer thickness/composition and coherency strain. The InAs/GaSb T2SL infrared material is particularly attractive owing to its enormous potential for high device performance at high temperature with significantly reduced dark current [3] and high responsivity [4]. There are very limited reports [5] on near room temperature photodetection using InAs/GaSb SL within the spectra window for NOx detection. More so, given the limited investigation [6] of the temperature-dependent Photoluminescence (PL) studies of InAs/GaSb SL, it is crucial to undertake a detailed investigation of the temperature- dependent PL characteristic of InAs/GaSb SL to enable a better understanding of their optical property at high temperature.

Here, we present the optical and electrical performance of Ga-based, InAs/GaSb T2SL layers and photodiodes operating in the 5.1–5.5 µm range which is desirable for NOx detection. A dominant PL peak at around 5.3 µm at 77 K was obtained for the Ga-based samples with an intensity which is less sensitive to changes in temperature compared to a reference Ga-free SL sample **(Figure 1a)**. The PL peak intensity of the Ga-based T2SL with an intentional InSb layer was found to be less responsive to changes in temperature and tuned to longer wavelength suitable for NOx sensing. The dark current density of the fabricated photodiode was also compared with the current state-of-the-art photodetectors and the ''MCT-Rule 07'' as shown in **Figure 1b**. Current-Voltage modelling of the fabricated photodiode demonstrates that at a temperature of 110 K, generation recombination (G-R) and trap assisted tunnelling (TAT) currents dominate below and above an applied bias of ~0.2 V. However, at higher operating temperature (200-300 K), diffusion current is prevalent at low applied bias while G-R and TAT are dominant at high applied bias.

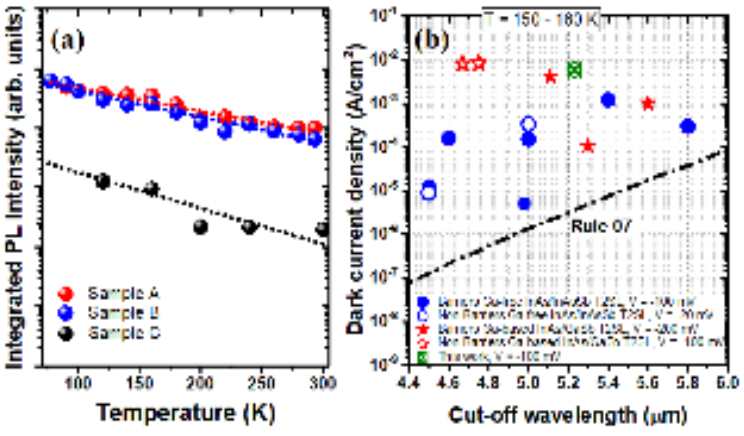

***Figure 1. (a)** Integrated PL intensity as a function of temperatures for both Ga-based samples (A and B) and Ga-free (sample C). **(b)** Dark current density versus the cut-off wavelength for barriers and non-barriers photodetectors.*

References

[1] R.J. Hargreaves et al., J. Quant. Spectrosc. Radiat. Transf. 232, 35, 2019. [2] J. Wojtas et al., Sensors, 17, 513, 2017. [3] A. Rogalski, Infrared Phys Technol. 54, 136, 2011.[4] M. J. Hobbs et al., Proc. SPIE 8899, 2013. [5] P. Martyniuk et al., Solid-State Electron. 119, 1, 2016. [6] C. Cervera et al., J. Appl. Phys. 106, 033709, 2009.

A21_54 Long-wavelength infrared (LWIR) type-II InAs/GaSb superlattice on GaAs

D.C.M. Kwan[1*], D. Alshahrani, D.L. Huffaker[1,2,3], E Anyebe[2], and M. Kesaria[1*]

*[1]School of Physics and Astronomy, Cardiff University, UK. [1]School of Engineering, Cardiff University, UK. Present address: [3]Electrical Engineering Department, The University of Texas at Arlington, USA.*Corresponding email contact: kwandc@cardiff.ac.uk and kesariam@cardiff.ac.uk*

Infrared (IR) radiation contains vital information about our environment invisible to both conventional cameras and the human eye. The long-wavelength infrared (LWIR) spectral range is the most interesting due to its coincidence blackbody with blackbody radiation at room temperature and insusceptibility to atmospheric absorption. As such, LWIR detectors are becoming increasingly important for defence, space and human body imaging applications. HgCdTe (MCT) is the state-of-the-art material system for most LWIR detector applications but drawbacks such as high production costs and fabrication difficulties have motivated the search for an alternative. The InAs/GaSb Type-II superlattice (T2SL) has emerged as the most promising competitor to MCT (Fig. 1) due to suppression of Auger recombination, fabrication advantages and good bandgap tunability [1]. In recent years, for the development of larger, cheaper LWIR T2SL focal plane arrays (FPA), semi-insulating GaAs substrates are becoming preferred to conventional GaSb substrates due to mature GaAs technology. To enable the transition from GaSb to GaAs, Huffaker et. al. [2] proposed dislocation filtering enabled by the interfacial misfit (IMF) array. There is therefore a desire to test the efficacy of the IMF array in preserving the material quality of T2SLs grown on GaAs substrates.

To investigate the effect of the IMF array as a dislocation filter on the LWIR InAs/GaSb T2SL the optical, structural and dark current of a "Ga based" LWIR T2SL on a GaSb substrate is compared with that of a GaSb/IMF array/GaAs substrate. X-ray diffraction (XRD), photoluminescence (PL) and current-voltage (I-V) characterisations were performed. Ga based T2SL show strong LWIR emission from 77 – 240 K (Fig. 2). However, a significant reduction in the material quality and degradation of device performance of the InAs/GaSb T2SL on GaAs substrate is observed compared to GaSb substrates. These results suggest that a strain balanced metamorphic buffer layer (MBL) is required, in combination with the IMF, to maintain high material quality.

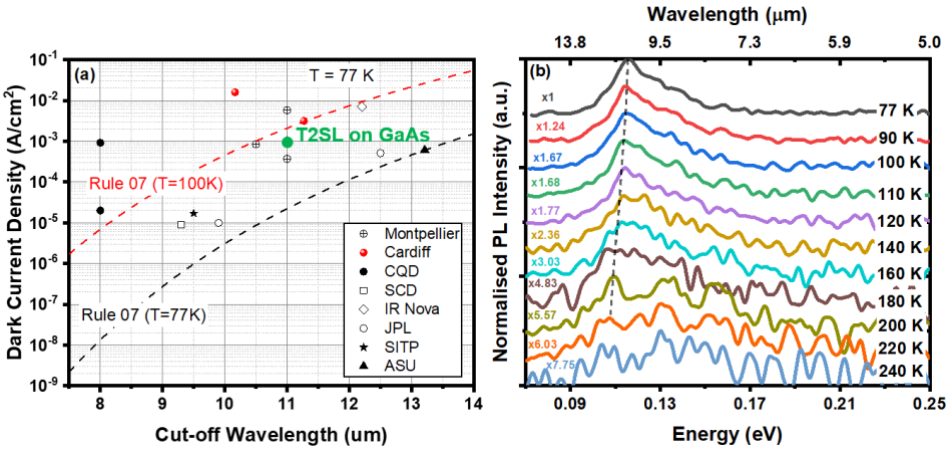

Fig 1. (a) Survey of T2SL dark current, green shows T2SL on GaAs from Ref. [3]. (b) PL from the T2SL on GaAs.

References

[1] Rogalski, A. et al. (2017). Appl. Phys. Rev. 4(3), p. 031304
[2] Huang, S. et al. (2009) J. Appl. Phys. 105, p. 103104.
[3] Pour, S.A. et al. (2009). Appl. Phys. Lett. 95(17), p. 173505

Abstracts

Session 10: Modulators and Modulation

A21_48 Novel Design for Electroabsorption Modulator Based on Microstrip Transmission Line Technology

Ali Al-Moathin[1*], Chong Li[1], Lianping Hou[1], and John H. Marsh[1]

[1] *James Watt School of Engineering, University of Glasgow, Glasgow G12 8QQ, U.K. * Corresponding author: a.al-moathin.1@research.gla.ac.uk*

Electroabsorption modulators (EAMs) integrated with distributed feedback (DFB) lasers (EMLs) are commonly used in the backbone of high bit-rate optical communication systems and are now migrating into access networks such as passive optical networks (PONs). They combine high-speed modulation, a high extinction ratio and low chirp with a low drive voltage and are compact and easy to use [1], [2]. The modulation speed of the EAM is limited by the electrical optical interface (EOI) which is conventionally configured with either a lumped or a travelling-wave (TW) electrode. The TW configuration overcomes the *RC*-time limit associated with the lumped configuration by matching the circuit impedance to that of the source, however the material structure, device size and/or the complexity of monolithic integration frequently make it difficult to implement.

In this work, a new approach for EML fabrication is presented based on monolithic microwave photonic integrated circuit technology. The structure of the material is a *p-i-n* separate confinement heterostructure grown in the AlGaInAs/InP system with an epitaxial layer described in [3]. The EAM design is illustrated in Fig. 1(a) where the width of the EAM ridge is 2.5 µm with an intrinsic capacitance calculated to be 1.4 fF µm-1. The surface of the EAM was deep-etched down to the heavily doped substrate then planarized with 5-µm-thick Hydrogen Silsesquioxane (HSQ), as shown in Fig 1(b), which was used as a low-*k* substrate for integrating the electrode [4], [5]. The equivalent circuit of the EAM was simulated, using AWR Microwave Office [6], to optimize the impedance matching and bandwidth. Accordingly, the electrode was designed as a microstrip microwave circuit feeding a 170-µm-long EAM. The circuit comprises a shunt open-stub of 0.16 λg length located 0.1 λg away from the load (Fig. 1(a)), where λg is the guided wavelength of the centre RF modulation frequency of 50 GHz. Fig. 1(c) shows the simulated S11 parameter at the input port of the electrode, which indicates a −10 dB bandwidth of 20 GHz can be achieved over the frequency band from 40 GHz to 60 GHz.

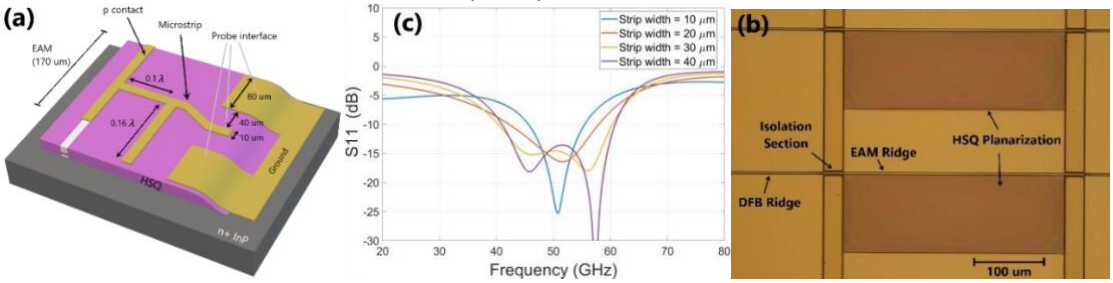

Fig. 1. (a) Schematic of the EAM designed with microstrip matching circuit, (b) sample surface after HSQ planarization, and (c) simulated S11 parameter.

In summary, we have designed a circuit using a new thin-film planarization process that can deliver high modulation speeds for EMLs. The manufacturing process is simple, cost-effective, and suitable for monolithic integration of advanced photonic circuits. The design of the electrical interface ensures S11 < –10 dB for frequencies from 40 GHz to 60 GHz for a 50 Ω source, with dimensions designed for direct probing with microwave on-wafer probes. The design ensures maximum RF power is delivered to the modulator with minimum reflections over the frequency range. The matching circuit has the advantages of impedance matching the parasitic capacitance of the device, reducing signal loss because of its compact design, and avoiding the need for bond wires.

This work was supported by the EPSRC Centre for Doctoral Training in Photonic Integration and Advanced Data Storage (EP/L015323/1).

References

[1] M. Theurer, G. Przyrembel, A. Sigmund, W. D. Molzow, U. Troppenz, and M. Möhrle, “56 Gb/s L-band InGaAlAs ridge waveguide electroabsorption modulated laser with integrated SOA,” Phys. status solidi, vol. 213, no. 4, pp. 970–974, 2016. [2] T. Y. and F. K. W. Kobayashi, M. Arai, N. Fujiwara, T. Fujisawa, T. Tadokoro, K. Tsuzuki, “Wide temperature range operation of 10- /40-Gbps 1.55-µm electroabsorption modulator integrated DFB laser,” OECC2010 15th, vol. 1, no. July, pp. 9–10, 2010. [3] A. Al-Moathin, L. Hou, E. D. Gaetano, and J. H. Marsh, “EML Based on Lumped Configuration, Identical Epitaxial Layer and HSQ Planarization,” in 2020 International Conference on UK-China Emerging Technologies (UCET), 2020, pp. 1–4. [4] A. Al-Moathin, L. Hou, S. Thoms, and J. H. Marsh, “Novel Hydrogen Silsesquioxane Planarization for Electronic-Photonic Integrated Circuit Applications,” in Semiconductor and Integrated Optoelectronics Conference (SIOE), 2019. [5] A. Al-Moathin et al., “Thick film hydrogen silsesquioxane planarization for passive component technology associated with electronic- photonic integrated circuits,” J. Vac. Sci. Technol. B, Nanotechnol. Microelectron., vol. 37, no. 6, p. 61210, 2019. [6] “AWR | Microwave Office Design Environment.” [Online]. Available: https://www.awr.com/. [Accessed: 15-Jun-2020].

A21_46 Low-Power Photonic Modulators for Neuromorphic Computing

Joshua S. Male, George Duffett, Christopher P. Reardon, and Thomas F. Krauss*

Department of Physics, University of York, York, UK

The number of transistors on a chip doubles every two years in accordance with Moore's Law[1], which has guided the development of semiconductor electronics for over 50 years. Computer performance is currently limited by data transfer between the central processing unit (CPU) and random-access memory (RAM) unit, known as the von Neumann bottleneck[2]. Consequently, conventional computing systems are approaching an asymptote of efficiency known as the digital efficiency wall[3]. Overcoming the digital efficiency wall requires a new computing architecture. Introducing concepts from neural networks and optical signal processing has been recognised as a possible solution to overcoming these bottlenecks[4]. Given that an optical lens produces a Fourier transform in a single step, and that multiplications in Fourier space are equivalent to convolutions in real space, optical systems pose an attractive solution. Accordingly, we are developing an optical system based on Fourier optics to perform the convolution operation, common in neural networks, in Fourier space.

Such a system requires the efficient transfer of data from the electrical domain to the optical domain. We have identified the silicon nitride waveguide system as a suitable optical domain platform because it offers low-loss operation and can carry relatively high-power optical signals, which are required at the input of a large scale coherent optical system. To achieve efficient modulation in this system, we propose to utilise the plasma dispersion effect[5] in a transparent conductive oxide (TCO). We propose indium tin oxide (ITO), which is a promising TCO material for electro-optic modulation due to its low resistivity and high carrier concentration. Applying a bias voltage alters the carrier concentration in an accumulation layer at the surface of the ITO which, according to the Drude model, changes the local permittivity and the effective index of the waveguide. The bias voltage can be applied in a metal-oxide-semicondcutor (MOS) configuration and the effective index shift in the modulator can be increased by increasing the mode overlap with the accumulation layer.

We have studied an optical phase modulator based on these concepts consisting of a silicon nitride waveguide and a gold-silica-ITO MOS capacitor for modulation, as shown in Figure 1(a), that features a π-phase length, L_π, of 70µm. Our simulations [Figure 1(b)] show that, if fabrication can be optimised, it is

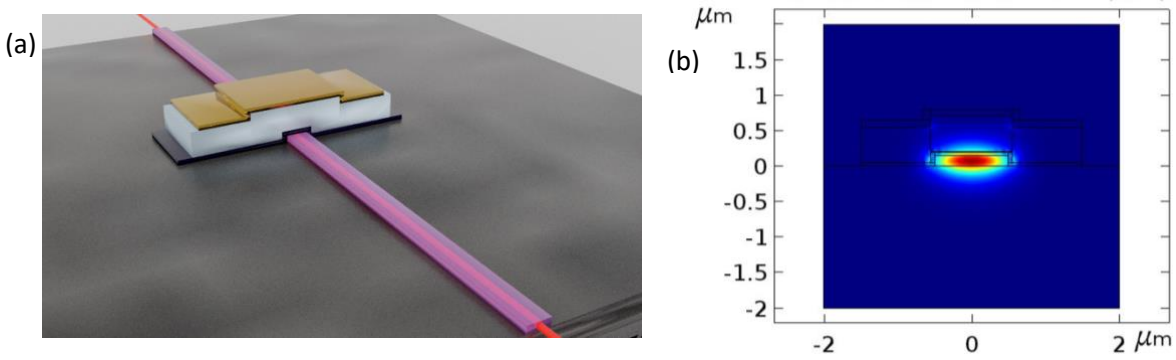

Figure 3: (a) Concept model of proposed MOS capacitor waveguide modulator. (b) Simulated cross-section of waveguide

possible to develop a modulator with a π-phase length below 50µm. A key requirement of such a modulator is to control the carrier concentration of the ITO material via the deposition method, and we discuss how this can be controlled.

1.Moore, G. E. Cramming More Components Onto Integrated Circuits. *Proc. IEEE* **86**, 82–85 (1998). 2. Edwards, J. & O'Keefe, S. Eager recirculating memory to alleviate the von Neumann Bottleneck. in *2016 IEEE Symposium Series on Computational Intelligence (SSCI)* 1–5 (2016). doi:10.1109/SSCI.2016.7850155. 3. Denning, P. J. & Lewis, T. G. Exponential laws of computing growth. *Commun. ACM* **60**, 54–65 (2016). 4. B. Rajendran, A. Sebastian, M. Schmuker, N. Srinivasa, & E. Eleftheriou. Low-Power Neuromorphic Hardware for Signal Processing Applications: A Review of Architectural and System-Level Design Approaches. *IEEE Signal Processing Magazine* **36**, 97–110 (2019). 5. Mendoza Herrera, L. J., Arboleda, D. M., Schinca, D. C. & Scaffardi, L. B. Determination of plasma frequency, damping constant, and size distribution from the complex dielectric function of noble metal nanoparticles. *Journal of Applied Physics* **116**, 233105 (2014). 6. Reed, G. T., Mashanovich, G., Gardes, F. Y. & Thomson, D. J. Silicon optical modulators. *Nature Photonics* **4**, 518–526 (2010). 7. Liu, K., Ye, C. R., Khan, S. & Sorger, V. J. Review and perspective on ultrafast wavelength-size electro-optic modulators. *Laser & Photonics Reviews* **9**, 172–194 (2015).

A21_23 A direct epitaxial approach to achieve a monolithic on-chip integration of a HEMT and a single micro-LED with a high modulation bandwidth

Yuefei Cai, Jack I.H. Haggar, Chenqi Zhu, Peng Feng, Jie Bai and Tao Wang*

Department of Electronic and Electrical Engineering, University of Sheffield, Sheffield, S1 3JD E-mail: t.wang@sheffield.ac.uk*

There is an increasing demand of developing visible light communications (VLCs) as a complementary technology to radio frequency (RF) based Wi-Fi and 5G, where III-nitride visible light emitting diodes (LEDs) used as transmitters are the key components. VLCs require III-nitride visible micro-LEDs (µLEDs) with a high modulation bandwidth. Thus, µLEDs always need to be driven at a high injection current density on a kA/cm^2 scale that is about two orders of magnitude higher than those for normal visible LED operation are. For µLEDs which are traditionally fabricated by dry-etching techniques, dry-etching induced damages are unavoidable, leading to both a substantial reduction in performance and a great challenge to viability at a high injection current density. Furthermore, conventional biasing (which is simply applied across a p-n junction) is good enough for normal LED operation, but generates a great challenge for a single µLED, which needs to be modulated at a high injection current density and at a high frequency.

In this work, we have proposed a new concept for an epitaxial integration and then demonstrated a completely different method which allows us to achieve an epitaxial integration of a single µLED with a diameter of 20 µm and an AlGaN/GaN high electron mobility transistor (HEMT), where the emission from a single µLED is modulated by tuning the gate-voltage of its HEMT. Furthermore, such a direct epitaxial approach has eliminated any dry-etching induced damages. As a result, we have demonstrated an epitaxial integration of monolithic on-chip µLED-HEMT with a record modulation bandwidth of 1.2 GHz on industry-compatible c-plane substrates. **Figure 1a** shows the optical microscope image of our monolithic on-chip integrated µLED-HEMT with a zoom-in scanning electron microscope (SEM) image, demonstrating that the circular gate of a HEMT surrounds a single µLED with 20 µm in diameter. The regions outside each µLED are the HEMT areas. A circular gate is fabricated around each single µLED, and its length, gate-to-source distance and gate width are 2 µm, 2 µm and 88 µm, respectively. The spacing between the gate and the n-GaN of each single µLED is 3 µm. Outside the circular gate regions, two semi-circular pads are fabricated as source pads for the HEMT. **Figure 1b** shows the frequency response of our single µLED controlled by its HEMT, namely, the normalized output power as a function of frequency measured under different gate bias of the HEMT. The frequency response measurements have been carried out as a function of injection current density, exhibiting a 3dB modulation bandwidth of 1.2 GHz at 13.3 kA/cm^2 which can be obtained under zero gate bias and 10V anode with respect to the source of the HEMT. This demonstrates the highest modulation bandwidth reported so far. **Figure 1c** presents the electro-luminescence (EL) spectra from the single µLED as a function of gate bias which controls injection current into the µLED, further confirming that our single µLED can be stably controlled by simply tuning the gate bias of its HEMT, which greatly simplifies the µLED driving circuitry.

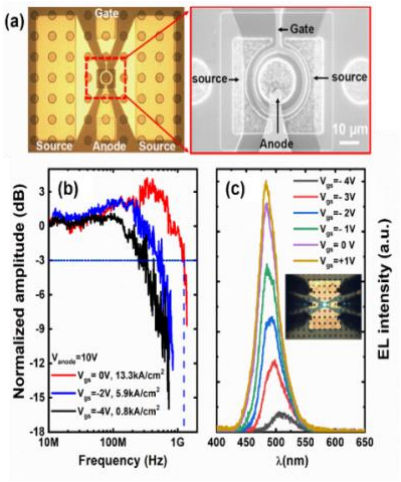

Fig. 1: (a) Microscope image of the whole device and SEM image of the active region; (b) Three-decibel bandwidth under different gate biases; (c) Spectra under different gate biases. The inset shows a typical EL emission image taken under V_{gs}= −4 V and V_{anode}=8V.

A21_44 High Modulation Bandwidth of Semipolar (11−22) InGaN/GaN LEDs with Long Wavelength Emission

Jack IH. Haggar, Yuefei Cai, Suneal S. Ghataora, Richard M. Smith, Jie Bai and Tao Wang*

Department of Electronic and Electrical Engineering, The University of Sheffield, Sheffield S1 3JD, United Kingdom
**E-mail: t.wang@sheffield.ac.uk*

A fundamental problem with the traditional "blue LED + yellow phosphor" fabrication technique for visible light communications (VLC) is the slow response time characteristic of yellow phosphors, consequently limiting the modulation frequency to no more than a few MHz.[1-3] In addition, the blue LEDs that are commercially available are grown on c- plane sapphire substrates intrinsically produce piezoelectric fields as a result of the strain generated by the large lattice mismatch between InGaN and GaN. As a result, the LEDs exhibit a reduction in the overlap of the electron and hole wave functions leading to an increased radiative recombination lifetime of 10−100 ns, reduced quantum efficiency and efficiency droop.[4,5] One of the most promising approaches to overcoming the intrinsic polarization is to grow LEDs along a nonpolar or semipolar orientation thereby increasing the electron-hole wave function overlap and decreasing the radiative recombination lifetime. In this work, frequency response measurements have been performed on semipolar (11−22) LEDs with long emission wavelengths from green to amber demonstrating a modulation bandwidth of up to 540 MHz for green LEDs with a typical size of 330 × 330 μm^2, a record modulation bandwidth for III- nitride macro-LEDs (not micro-LEDs) reported so far. This paper also presents the first report on the modulation bandwidth of III-nitride based yellow and amber LEDs and is also the record for the longest wavelength III-nitride LED achieved. These results agree with differential carrier lifetime measurements.

References [1] Wang, S.W.; Chen, F.; Liang, L.; He, S.; Wang, Y.; Chen, X.; Lu, W. *IEEE Wirel. Commun.* **2015**, *22*, 61. [2] Chow, C.W.; Yeh, C.H.; Liu, Y. F.; Huang, P. Y.; Liu, Y.. *Opt. Commun.* **2013**, *292*, 49. [3] Le Minh, H.; O'Brien, D.; Faulkner, G.; Zeng, L.; Lee, K.; Jung, D.; Oh, Y.; Won. *IEEE Photon. Technol. Lett.* **2009**, *21*, 1063. [4] Bernardini, F.; Fiorentini, V.; Vanderbilt, D. *Phys. Rev. B*, **1997**. *56*, R10024. [5] Takeuchi, T.; Amano, H.; Akasaki, I. Jpn. J. Appl. Phys. **2000**. 39, 413. [6] Haggar, J.I.H.; Cai, Y.; Ghataora, S.S.; Smith, R.M.; Bai, J.; Wang, T. ACS Appl. Electron. Mater. **2020**,2 2363–2368.

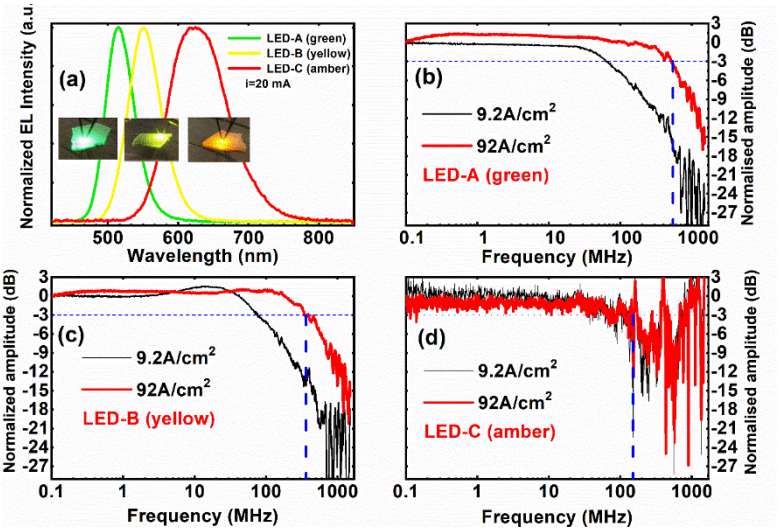

Fig.1 (a) Typical EL spectra of the three LEDs measured at 20 mA injection current in a CW mode at room temperature. Insets show their respective EL emission images taken at 20 mA, respectively; and frequency response of LED-A **(b)**, and LED-B **(c)** and LED-C **(d)**.

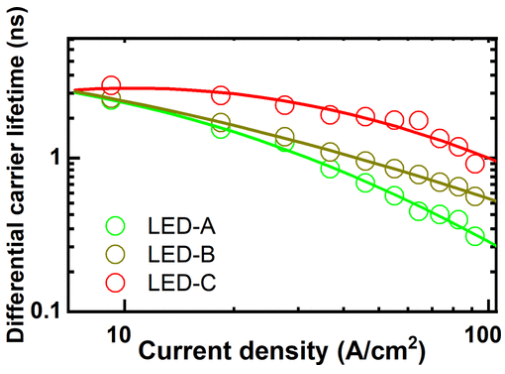

Fig.3 Differential carrier lifetimes of the three LEDs as a function of injection current density, which are extracted from the frequency response measurements. Solid lines are guides to the eye.

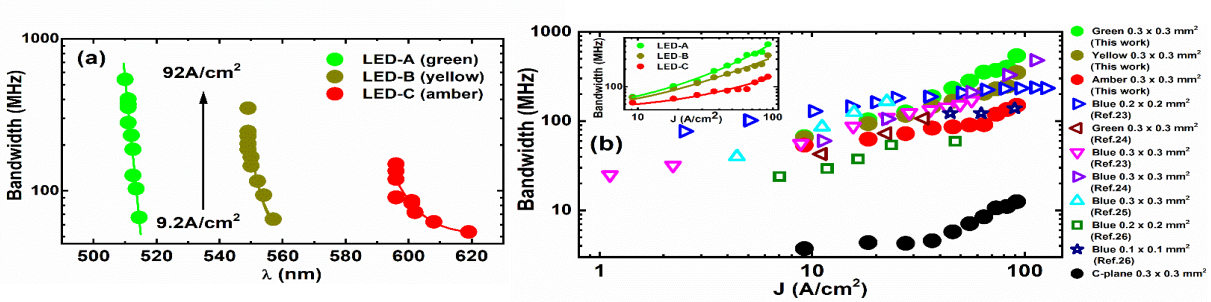

Fig. 2 (a) 3 dB modulation bandwidth as a function of injection current density from 9.2 A/cm^2 to 92 A/cm^2 and their corresponding emission wavelength for each injection current density for the three LEDs; **(b)** Benchmarking our device performance against current state-of-the-art data from semi-polar macro- LEDs (> 100 × 100 µm^2) in terms of 3 dB modulation bandwidth. Our data obtained in this work are exhibited by solid symbols, while the data collected from literature are presented as open symbols with different colours. Inset only includes our data from LED-A, LED-B ad LED-C. Information about benchmarked references can be found in [6]

Abstracts

Session 11: Posters II

A21_08 Time/Frequency Division Multiplexing for magnetic imaging arrays using Quantum Well Hall Effect Sensors

R. Murshudov, C.W. Liang, J. Sexton, J.W. Watson, M. Missous

Ruslan.Murshudov@manchester.ac.uk

Quantum Well Hall Effect (QWHE) sensors are highly sensitive magnetic flux sensors, which have been demonstrated to be suitable for imaging in the field of electromagnetic Non-Destructive Testing and Evaluation (NDT&E) [1]. This imaging can be performed by either individual scanned sensors, or with arrays [2]. The work here proposes a new method for configuring such sensors in imaging arrays to optimise scan times through a combination of Frequency Division Multiplexing (FDM) and Time Division Multiplexing (TDM). While this work is presently in an early stage, the considerations involved in designing such an imaging array will be discussed here.

QWHE sensors take advantage of the Hall effect to measure magnetic fields. A commonly used method for noise reduction in such sensors is superheterodyne mixing, or using an AC biasing frequency to shift the measured signal above 1/f noise [3]. This method is analogous to amplitude modulation being used to shift audio frequency signals into the kHz-MHz range for transmission in communications systems [4]. In this analogy, the biasing signal acts as a carrier frequency and the measured magnetic field used for imaging corresponds the message signal. By continuing this analogy, the signal path from sensor output to Analogue Digital Converter (ADC) input can be considered a transmission channel. For such a channel, the upper limit of the bandwidth is limited more by the supporting electronics (e.g. post sensor amplifiers) rather than the sensors themselves, which have a linear response up to MHz-GHz range (depending on the size of the sensor from 5-70 µm).

When using a single sensor, the utilised channel bandwidth is centred around the biasing frequency and limited to the highest imaging frequency used. With a single sensor, this results in most of the available channel bandwidth going unused. With FDM, for an array of N sensors, each sensor should be biased to a unique frequency, where the biasing frequencies are separated by at least 1 imaging frequency bandwidth to prevent overlap. The outputs of the sensors can then be summed into a single channel, allowing multiple sensors to be simultaneously measured through FFT peak extraction by a single ADC. Similar approaches to using FDM in other sensor arrays have been used by various groups [5], [6]. The work here however considers how FDM can be adapted for QWHE imaging arrays and combined with other methods to maximise the number of available sensors for imaging systems.

This proposed method suggests using TDM is conjunction with FDM, such that for a 2D NxM array, each column of N would share a biasing frequency and each row of M would then contain a full set of the frequencies used. These rows would then be multiplexed in the time domain (i.e sequentially measured individually), allowing a single ADC channel to measure NxM sensors where N is limited by channel bandwidth, and M is limited by desired scan times. This could further be expanded by using multiple ADC channels, allowing for a total of AxNxM sensors in an array, where A is the number of ADC channels available.

With all this considered, ADC channels, available channel bandwidth, and acceptable scan times are all still limited factors and the area covered by an array will be inversely proportional to the desired sensor pitch. For this reason, the minimum detectable features size should be considered first, in order to determine the maximum acceptable sensor pitch (and as a result the maximum available scan area).

1.J. M. Watson, C. W. Liang, J. Sexton, and M. Missous, “Magnetic field frequency optimisation for MFL imaging using QWHE sensors,” *Insight: Non-Destructive Testing and Condition Monitoring*, vol. 62, no. 7, pp. 396–401, Jul. 2020, doi: 10.1784/insi.2020.62.7.396. 2. C. W. Liang, E. Balaban, E. Ahmad, Z. Zhang, J. Sexton, and M. Missous, “A real time high sensitivity high spatial resolution quantum well hall effect magnetovision camera,” *Sensors and Actuators, A: Physical*, vol. 265, pp. 127–137, Oct. 2017, doi: 10.1016/j.sna.2017.08.035. 3. C. W. Liang, “A High Spatial Resolution Magnetovision Camera Using High-Sensitivity Quantum Well Hall Effect Sensors,” Manchester, 2017. 4. Steven A. Tretter, *Communication System Design Using DSP Algorithms*. Boston MA: Springer US, 2008. 5. A. Dandridge, A. B. Tveten, A. M. Yurek, A. D. Kersey, and E. C. Mcgarry, “Frequency Division Multiplexing of Interferometric Sensor Arrays 00,” 1989. Accessed: Jan. 19, 2021. [Online]. 6. M. Jouda, O. G. Gruschke, and J. G. Korvink, “Implementation of an in-field CMOS frequency division multiplexer for 9.4 T magnetic resonance applications,” *International Journal of Circuit Theory and Applications*, vol. 43, no. 12, pp. 1861–1878, Dec. 2015, doi: 10.1002/cta.2043.

A21_06 Noise reduction using Parallel Arrays of Quantum Well Hall Effect Sensors for picoTesla magnetic fields detection.

A. Lindley

Quantum Well Hall Effect (QWHE) sensors are currently limited to measuring magnetic fields around the low nanoTesla range with power dissipation of a few mW. This research seeks to improve upon this limitation by taking advantage of the resistive nature of the QWHE sensor and the resistance reducing effect of parallel connections. It is expected that the total electrical noise (thermal, shot, and flicker noises) in QWHE sensors, when connected in parallel, will reduce by a factor of $1/\sqrt{N}$, where N is the number of sensors. As such a Parallel Array of 100 sensors would see a 10-fold reduction in noise, and a 10,000-element array would produce a 100-fold reduction in noise. This makes use of the inherent advantages of the QWHE sensor over other similar magnetometers. QWHE sensors, are small, mass producible, have low power dissipation, and are amenable to integration with on-chip electronics. This combination of factors makes it feasible to manufacture large parallel arrays of QWHE sensors directly on a wafer.

The work described in this paper looks at demonstrating this $1/\sqrt{N}$ reduction in noise. PCBs were designed and fabricated initially for a 4, and 9, elements array. The noise spectrum of DC biased sensors in the absence of applied magnetic field was measured from DC to 52 kHz. This was repeated for combinations of 1-9 parallel sensors, whilst keeping the applied current per sensor constant. The PCB is configured such, that through the use of switch banks, the 4 pin QWHE sensors can be completely isolated when not part of the parallel array.

This noise reduction effect has been confirmed in both cases, with the two PCB based parallel arrays showing a reduction in thermal, shot, and flicker noise. The noise reduction followed the trend of $1/\sqrt{N}$ exactly. This provides a tentative first proof that simply placing QWHE sensors in parallel could provide a noise reductive effect for the system, potentially enabling QWHE sensors to measure magnetic fields as small as single digit picotesla in magnitude. There are further concerns, however, for this approach to be successful, it must not interfere too heavily with the magnetic field reading itself. This is the next crucial piece of data to acquire and will be the next focus of this research. Furthermore, the noise reduction effect must be confirmed for larger parallel arrays with a 100- element array already in production. As the number of sensors is increased, however, the physical size of the PCB will become preventative with this 100-element discrete sensor array already having an area of ~$10cm2$. As such the designs will have to move onto integration at the wafer level. Due to the small size of the QWHE sensor on the wafer it is expected that a 10,000-element array would occupy no more than $1cm2$.

This research provides a simple method that could potentially improve the QWHE sensors magnetic field detectability by an order of magnitude. This will allow the QWHE sensor to perform magnetometry on effects it would not have been able to before, such as Magnetocardiography and Magnetoencephalography. Both of these usages rely on bulky and expensive equipment that could be wholly replaced if this research proves feasible.

A21_37 Hybrid Plasmonic-Grating TE-Pass Polarizer Based on SOI

Ola Youssef. M. Hiza1, B. M. Younis2,3, Nihal Fayez Fahmy Areed1, S. S. A. Obayya2* and Mohamed Farhat O. Hameed 2,4,5*

[1]*Faculty of Engineering, Electronics and Communications Department, Mansoura University, Mansoura 35516, Egypt.*
[2]*Centre for Photonics and Smart Materials, Zewail City of Science and Technology, October Gardens, 6th of October City, Giza 12578, Egypt.*
[3]*Electronics and Communications Department, Misr Higher Institute for Engineering and Technology (MET), Mansoura 35516, Egypt.*
[4]*Nanotechnology and Nanoelectronics Engineering Program, Zewail City of Science and Technology, October Gardens, 6th of October City, Giza 12578, Egypt.*
[5]Mathematics and Engineering Physics Department, Faculty of Engineering, Mansoura University, Mansoura 35516, Egypt.
*Corresponding author: sobayya@zewailcity.edu.eg, mfarahat@zewailcity.edu.eg

In this paper, hybrid plasmonic grating (HPG) transverse electric (TE) pass polarizer based on silicon-on-insulator platform is proposed and analyzed. The corrosion free noble metal Rhodium (Rh) [1] is used as an alternative plasmonic material instead of the conventional silver and gold plasmonic materials. Figure 1 shows a 2D schematic diagram of the proposed polarizer. Further, 1D grating of Rh/air is used in z-direction over the Si3N4 layer in order to increase the losses of the quasi TM mode. Therefore, the suggested design can confine the quasi-TE mode in the Si core with low loss while the quasi-TM mode suffers from high power leakage towards the plasmonic material. The modal analysis of the proposed design is calculated using full-vectorial finite difference method (FVFDM). The influence of the structure geometrical parameters is studied to maximize the extinction ratio (ER) and minimize the insertion loss (IL). The suggested design offers high ER of about 35 dB with a compact device length of 4.4 µm at the operating wavelength of 1.55 µm.

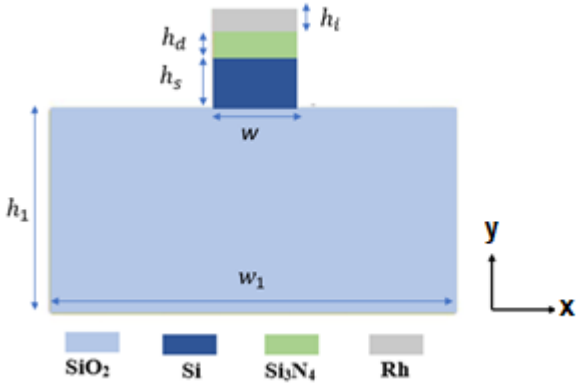

/

References

[1] A. K. Mishra, S. K. Mishra, “Gas sensing in Kretschmann configuration utilizing bi-metallic layer of rhodium-silver in visible region”, Sensors Actuators B: Chem, pp. 969-973, 2016

A21_38 Highly Efficient Dual D-shaped PCF Biosensor

Yusuf Gamal[1,2], B. M. Younis[2,3], S.F. Hegazy[1,2], Y. Badra[1], Mohamed Farhat O. Hameed[2,4,5], and S.S. A. Obayya[2]

[1] *Engineering Application of Laser Department, National Institute of Laser Enhanced Science (NILES), Cairo University, Egypt.*
[2] *Center for Photonics and Smart Materials, Zewail City of Science and Technology, October Gardens, 6th of October City, Giza 12578, Egypt*
[3] *Electronics and Communications Engineering Department, Misr Higher Institute for Engineering and Technology (MET), Mansoura, Egypt*
[4] *Nanotechnology and Nanoelectronics Department, Zewail City of Science and Technology, October Gardens, 6th of October City, Giza 12578, Egypt*
[5] *Mathematical and Engineering Physics Department, Faculty of Engineering, Mansura University, Egypt.*
**Corresponding authors: sobayya@zewailcity.edu.eg , mfarahat@zewailcity.edu.eg*

In this work, highly efficient dual D-shaped photonic crystal fiber (PCF) biosensor is reported and studied using full vectorial finite element method. The analyzed structure as shown in Fig. 1 has three successive rings of air holes arranged in a triangular lattice to form the cladding region in a silica background. The first ring diameter (d_s) is smaller than those of the second and third rings. Additionally, two gold rods [1] are attached on the dual etched surfaces by using capillary force and air pressure technique [2]. The simulation results show that a very strong coupling occurs between the fundamental y-polarized mode supported by the PCF core and the surface plasmon (SP) mode on the gold surfaces at a specific wavelength. The resonance wavelength is a function of the analyte refractive index. The proposed sensor achieves high sensitivity of 12800 nm/RIU through analyte refractive index range 1.31-1.32. The proposed D-shaped PCF biosensor can be fabricated by polishing the PCF as reported in [3].

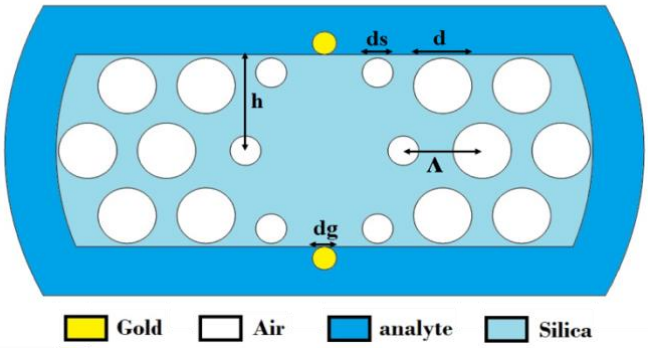

Figure 1. Cross-section of the suggested dual D-shaped PCF biosensor.

References

[1] M. Y. Azab, M. F. O. Hameed, A. M. Nasr, and S. S. A. Obayya, "Multi-functional plasmonic biosensor based on alcohol-filled PCF," in *Physics and Simulation of Optoelectronic Devices XXVII*, 2019, vol. 10912, p. 109121H.

[2] N. Luan, R. Wang, W. Lv, Y. Lu, and J. Yao, "Surface plasmon resonance temperature sensor based on photonic crystal fibers randomly filled with silver nanowires," *Sensors*, vol. 14, no. 9, pp. 16035–16045, 2014.

[3] T. Wu *et al.*, "Surface plasmon resonance biosensor based on gold-coated side-polished hexagonal structure photonic crystal fiber," *Opt. Express*, vol. 25, no. 17, pp. 20313–20322, 2017.

A21_34 Tunable Mode Converter Based on Dual Core Photonic Crystal Fiber

Mohamed Mohsen H. Mahmoud[1,2,] B. M. Younis[3,4], Nihal F. F. Areed[2], Mohamed Farhat O. Hameed [3,5,6*,] and S. S. A. Obayya[2*]

[1]Telecom Egypt, voice core planning team, Smart Village, 6th of October City, Giza, Egypt.
[2] Electronics and Communications Department, Faculty of Engineering, Mansoura University, Mansoura 35516, Egypt.
[3]Centre for Photonics and Smart Materials, Zewail City of Science and Technology, October Gardens, 6th of October City, Giza 12578, Egypt.
[4]Electronics and Communications Department, Misr Higher Institute for Engineering and Technology (MET), Mansoura 35516, Egypt.
[5]Nanotechnology Engineering Program, Zewail City of Science and Technology, October Gardens, 6th of October City, Giza 12578, Egypt.
[6]Mathematics and Engineering Physics Department, Faculty of Engineering, Mansoura University, Mansoura 35516, Egypt.
[*]Corresponding author: sobayya@zewailcity.edu.eg , mfarahat@zewailcity.edu.eg

In this paper, compact tunable mode converter is reported based on asymmetric liquid crystal (LC) dual-core PCF (ADC-PCF). The right core of the suggested PCF has a large hole infiltrated by nematic LC material as shown in Fig.1. However, the left core has the same refractive index of the background material of FK51A. The conversion characteristics of the proposed converter are evaluated by using the full vectorial finite difference method (FVFDM) [1]. In this context, the conversion wavelength is controlled through the thermo-optically tunable characteristics of the LC material. The numerical results reveal that high mode conversion occurs between the fundamental LP01 and LP11 modes at a device length of 403.6 µm and wavelength of 1.3 µm. Additionally, the fabrication tolerance of the proposed design is studied showing high immunity to fabrication errors through wavelength range from 1285 nm to 1363 nm. The suggested ADC-PCF can be fabricated by stack and draw method [2] and the selective filling of the PCF can realized as described by Xiao et al. [3].

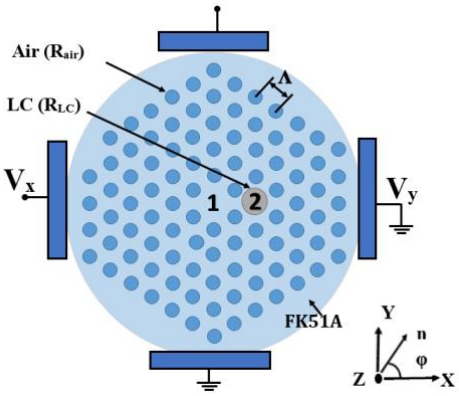

/

References

[1] A. B. Fallahkhair, K. S. Li, and T. E. Murphy, "Vector finite difference modesolver for anisotropic dielectric waveguides," J. Light. Technol., vol. 26, no. 11, pp. 1423–1431, 2008.
[2] J. C. Knight, T. A. Birks, P. S. J. Russell, and D. M. Atkin, "All-silica single-mode optical fiber with photonic crystal cladding," Opt. Lett., vol. 21, no. 19, pp. 1547–1549, 1996.
[3] L. Xiao, W. Jin, M. S. Demokan, H. L. Ho, Y. L. Hoo, and C. Zhao, "Fabrication of selective injection microstructured optical fibers with a conventional fusion splicer," Opt. Express, vol. 13, no. 22, pp. 9014–9022, 2005.

A21_62 An Extension of the Inverse Fourier Method for Index-Patterned Laser Design.

Niall Boohan[1,2,*] and Eoin P. O'Reilly[1,2,]

[1]*Tyndall National Institute, Lee Maltings, Dyke Parade, Cork T12 R5CP, Ireland*
[2]*Department of Physics, University College Cork, Cork T12 YN60, Ireland*

The use of index-patterned Fabry-Pérot lasers, where a small number of slot-like features are introduced along the laser cavity, is well established as a route to low cost, reliable single-frequency devices [1]. We use a Fourier-transform based inverse scattering method here to show how a modified choice of inverse function can deliver a 25% improvement in modal threshold gain selectivity compared to the originally proposed use of a constant inverse function for slot selection [2]. To preferentially select a given mode, the perturbation introduced by an ideal slot should introduce a quarter-wavelength sub-cavity which is an integer number of half-wavelengths from the more distant mirror, and therefore an odd number of quarter wavelengths from the closer mirror. Light scattered to the further mirror then adds to the modal gain, while light scattered to the closer mirror reduces the overall modal gain. Hence, features introduced near the facets have a much larger impact than features introduced in the centre of the cavity. The use of a constant inverse scattering function ($f(\epsilon L)$ = 1; − 1 ≤ ϵ ≤ 1) 22 preferentially selects a single mode, while leaving neighbouring modes unperturbed (red curves, Figs. 1 and 2). Implementation of this function however requires many slots near the centre of the cavity, reducing the overall gain selectivity that can be achieved. The Fourier transform of the inverse function $f(\epsilon L)$ = $|\epsilon|$ partially selects the two modes neighbouring the primary mode (green curves), but gives greater overall mode selectivity, due to a higher proportion of slots being near the laser facet. Investigating more complex inverse scattering functions, we find that $f(\epsilon L)$ = ϵ2 − 2ϵ3 leads to a further improvement in selectivity in the first order model (blue curve).
We confirm our results using a transfer matrix method (TMM) [3] to investigate the effects of higher order scattering omitted in the 1st order design model. Because the TMM method becomes unstable at gain levels at or just above threshold, we estimate how threshold gain varies with mode number in the TMM case by calculating the gain required for each mode to reach a fixed high output power, close to but just below threshold. The TMM results confirm (i) that the first-order inverse scattering approach provides an excellent estimate of mode selectivity for each inverse function used, and (ii) that, of the functions investigated, the $f(\epsilon L)$ = ϵ2 − 2ϵ3function shows the greatest selectivity and improvement in modal suppression across the wavelength range considered.

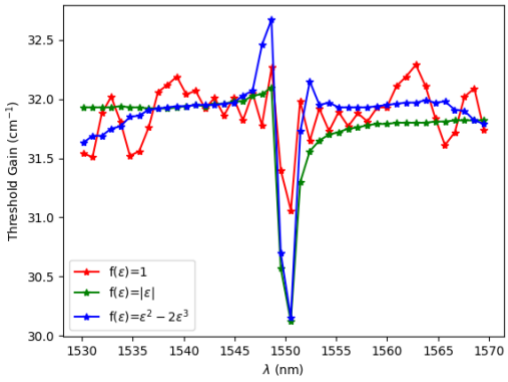

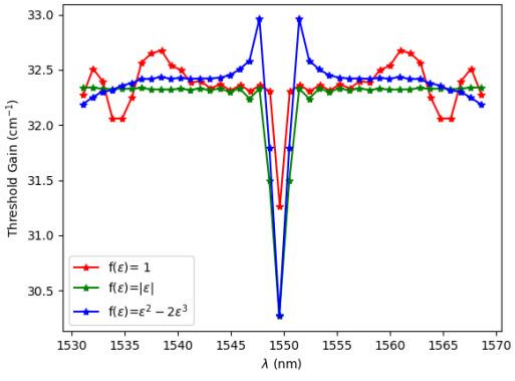

References

[1] Patchell, John, et al. "Specifying the wavelength and temperature tuning range of a Fabry-Perot laser containing refractive index perturbations." Opto-Ireland 2005: Optoelectronics, Photonic Devices, and Optical Networks. Vol. 5825. International Society for Optics and Photonics, 2005.[2] O'Brien, S., and O'Reilly, E.P. "Theory of improved spectral purity in index patterned Fabry-Perot lasers." Applied Physics Letters 86, no. 20 (2005): 201101.[3] Rumpf, Raymond C. "Improved formulation of scattering matrices for semi-analytical methods that is consistent with convention." Progress in Electromagnetics Research 35 (2011): 241

A21_67 Effect of external cavity length on speckle generated by a laser diode under optical feedback

Christopher Evered, Yuanlong Fan, Kang Li, Ali Roula and Nigel Copner

Wireless & Optoelectronics Research & Innovation Centre, Faculty of Computing, Engineering and Science, University of South Wales, Pontypridd, CF37 1DL, United Kingdom

Laser diode chaos gives rise to "coherence collapse", a phenomenon characterised by drastic spectral linewidth broadening of 1.5 – 6 nm resulting from external optical feedback (EOF) [1, 2]. In addition to chaos-based secure communications and random number generation [3, 4], laser diode chaos is used for speckle reduction in full-field imaging applications [1, 2, 5]. Laser speckle degrades image fidelity by obscuring surface features with bright and dark spots attributed to coherent interference. The effect of feedback strength and injection current on laser speckle was investigated in [1] and [2], respectively. However, the literature around the effect of external cavity length (ECL), which is known to have significant influences on the dynamical behaviour of laser diodes, is scarce. Therefore, in this paper, the dynamics in a laser diode was investigated both numerically and experimentally by varying the ECL to find out the effect of ECL on laser speckle.

Laser speckle is characterised by the speckle contrast C, $C = \sigma_I / \langle I \rangle$ [6], where σ_I is the standard deviation of pixel intensity (corrected for photon shot noise) and <I> is the average pixel intensity. A value of C=1 is obtained for fully developed speckle patterns where the light is fully coherent. Conversely, C~0 means that speckle is negligible and the light is fully incoherent [2].

In this experiment, the injection current to the laser diode was fixed at 1.5 times the threshold current, and it was found that the speckle contrast generated by a laser diode without EOF was 0.45. Having established this baseline, we reflected approximately 20% of its output light back into the laser cavity using a mirror, and C was reduced to 0.33, 0.34, 0.35, and 0.39 at four discrete external cavity lengths measuring 10.5, 12, 20, and 30 cm, respectively. The measured pixel intensity distributions used to calculate C are shown in Figure 1.

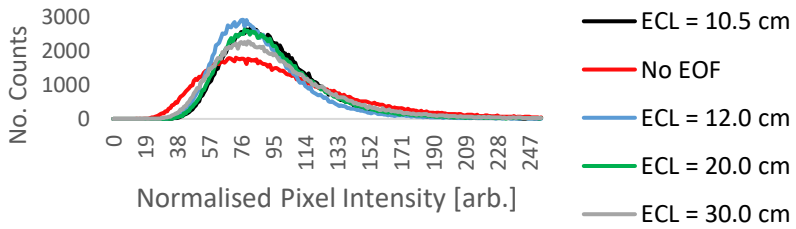

Figure 1. Pixel intensity distributions in a 400x400 pixel region illuminated by a laser diode with and without external optical feedback (EOF). ECL: External cavity length.

Simulation of the modified Lang-Kobayashi equations [4, 7] at these discrete parameter sets shows that the laser was stable without EOF and chaotic with EOF at each external cavity length. A reduction in C can be attributed to the spectral broadening and associated low-coherence emission characterised by laser diode chaos.

Acknowledgement: The authors gratefully acknowledge financial support provided by the Welsh European Funding Office (WEFO) and the Knowledge Economy Skills Scholarships (KESS).

1.Qiannan, Z., Z. Ruifeng, and L. Qiang, Analysis of speckle suppression by laser spectral broadening. Opto-Electronic Engineering, 2016. **43**(12): p. 206-211. 2.Halpaap, D., et al., Experimental study of speckle patterns generated by low-coherence semiconductor laser light. arXiv.org, 2020. **30**(6). 3.Sciamanna, M. and K.A. Shore, Physics and applications of laser diode chaos. Nature photonics, 2015. **9**(3): p. 151-162. 4.Uchida, A., Optical communication with chaotic lasers: applications of nonlinear dynamics and synchronization. 2012: John Wiley & Sons. 5.Dingel, B. and S. Kawata, Speckle-free image in a laser-diode microscope by using the optical feedback effect. Optics letters, 1993. **18**(7): p. 549-551. 6.Goodman, J.W., Speckle phenomena in optics: theory and applications. 2007: Roberts and Company Publishers. 7.Lang, R. and K. Kobayashi, External optical feedback effects on semiconductor injection laser properties. IEEE Journal of Quantum Electronics, 1980. **16**(3): p. 347-355.

A21_25 Preferred growth direction of III-V nanowires on differently oriented Si substrates

Haotian Zeng,[†,‖] Xuezhe Yu,[*,†,‖] H. Aruni Fonseka,[‡] Giorgos Boras,[†] Pamela Jurczak,[†] Tao Wang,[§] Ana M. Sanchez, [‡] and Huiyun Liu[†]

[†]*Department of Electronic and Electrical Engineering, University College London, London WC1E 7JE, United Kingdom*
[‡]*Department of Physics, University of Warwick, Coventry CV4 7AL, United Kingdom*
[§]*Department of Electronic and Electrical Engineering, University of Sheffield, Sheffield, S1 3JD, United Kingdom.*

Abstract

One of the nanowire characteristics is its preferred elongation direction. Here, we investigated the impact of Si substrate crystal orientation on the growth direction of GaAs nanowires. We first studied the self-catalyzed GaAs nanowire growth on Si (111) and Si (001) substrates. SEM observations show GaAs nanowires on Si (001) are grown along four <111> directions without preference on one or some of them. This non-preferential nanowire growth on Si (001) is morphologically in contrast to the extensively reported vertical <111> preferred GaAs nanowire growth on Si (111) substrates. We propose a model based on the initial condition of an ideal Ga droplet formation on Si substrates and the surface free energy calculation which takes into account the dangling bond surface density for different facets. This model provides further understanding of the different preferences in the growth of GaAs nanowires along selected <111> directions depending on the Si substrate orientation. To verify the prevalence of the model, nanowires were grown on Si (311) substrates. The results are in good agreement with the three-dimensional mapping of surface free energy by our model. This general model can also be applied to predictions of nanowire preferred growth directions by the vapor-liquid-solid growth mode on other group IV and III-V substrates.

Keywords: III-V Nanowires, MBE, Surface free energy, Growth direction

A21_24 Monte Carlo simulation of the transport characteristics of Gallium Nitride and compound semiconductor materials.

Mengxun Bai[1], Judy Rorsion[1]

[1] *Department of Electrical and Electronic Engineering, University of Bristol, Bristol BS8 1UB, U.K.*

Gallium Nitride is a semiconductor material that has drawn wide interest for both electronic and optoelectronic applications due to its wide direct energy band gap. Therefore, considerable work had been done into understanding the electronic transport characteristics of Gallium Nitride based on the work and techniques applied for other semiconductor materials. The most stable crystal state of GaN is wurzite, which has an in-built electric field but work is ongoing to investigate the growth of cubic GaN which has no in-built electric field.

To understand the transport characteristics it is important to consider in detail the possible scattering mechanisms of the carriers, which depend upon the band structure of the semiconductor. The Monte Carlo simulation approach has become the dominant simulation tool for modelling the transport characteristics of semiconductors. A single electron Monte Carlo technique is presented and will be used to simulate the equilibrium electron transport characteristics of GaN in wurzite and cubic form. The scattering rates are presented and linked to the band structure parameters. In addition, the importance of the scattering rate process in affecting the post-scattering direction is tracked, useful in considering non-equilibrium ballistic or quasi- ballistic transport relevant to future proposed work.

Initially the Monte Carlo results for cubic GaAs derived using the Monte Carlo code are compared to published GaAs results to validate the code and to investigate the importance of the various scattering processes at different electric fields. The scattering processes for the Γ-valley considered are: the polar optical phonon (POP) emission and absorption and the acoustic deformation potential (ADP). Figure1 shows the scattering rates for the Γ-valley related mechanisms for the parabolic and non-parabolic case.

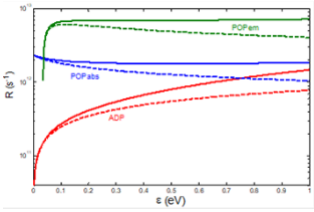

Fig.1: Scattering rates of the Γ valley processes. For these energies POP emission is the dominant one with the least important being ADP scattering. For higher energies ADP grows faster and overcomes the other two processes because it follows the trend of the density of states[2].

We have then considered intervalley scattering to the Λ-valley through non-equivalent inter-valley scattering. At this stage we have introduced equivalent intervalley scattering, polar optical phonon emission and absorption, and acoustic deformation potential scattering within the Λ-valleys. Figure2 shows the (non-parabolic) scattering rates of the Λ valley processes compared to those already discussed for the Γ valley.

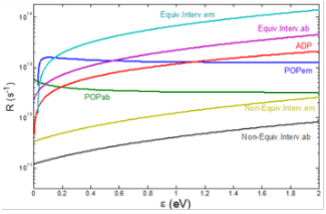

Fig.2: Scattering rates of the Λ valley processes. All of them are bigger than those of Γ valley due to the higher electron mass. Equivalent intervalley process is the dominant process here and what limits the mobility along with POP emission[2].

Finally, adding the non-equivalent intervalley scattering process only brings about small corrections to the high filed velocities leaving unchanged the maximum vd as well as the corresponding field. These results about field-velocity characteristics and mobility are shown in Figure 3.

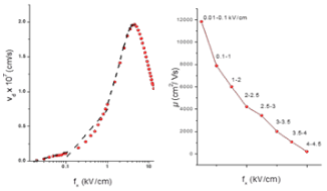

Fig.3: Velocity and mobility at various fields (all processes included)[2][3].

For cubic GaN the results will be similar in form to those for GaAs while for wurzite GaN piezoelectric scattering must also be included and the scattering results altered to the wurzite band structure[4]. Figure4 and Figure5 show the Monte Carlo results for GaN has been done in published work

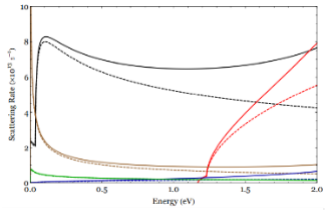

Fig4: Comparison of scattering rates derived using the parabolic (dashed) and cosine (solid) band-structure approximations assuming GaN parameters at a temperature of 300 K. POP (black), NPOP inter-valley (red) ADP (blue), PZ (green) and Impurity (brown) scattering rates are included in the comparison. [4].

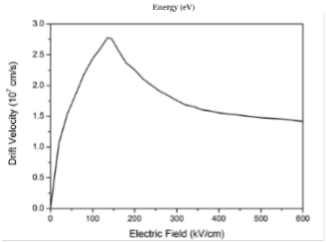

Fig5: the velocity-field characteristic of GaN at 300K. [4]

For investigating ballistic and quasi-ballistic non-equilibrium transport an ensemble Monte Carlo code will be developed from this single equilibrium Monte Carlo code which will be useful to GaN and GaN/AlGaN devices.

References:

1.Masia et.al., Phys. Rev. B, 73,073201,2006
2.Patane et.al., J. Phys.: Cond. Matter, 21, 174209, 2009 3.Fawcett et.al., J. Phys. Cehm Solids, 31, 1963, 1970 4.Fahy, et.al., Phys. Rev. B., 74, 035203,2006

A21_69 Performance-Mapping for Characterisation of 150mm VCSEL Wafers in Industry

J. Baker[1], D. G. Hayes[1], T. Peach[2], S. Shutts[1], P. M. Smowton[1,2], I. Davies[3]

[1]EPSRC funded Future Compound Semiconductor Manufacturing Hub, Cardiff University, UK
[2]Institute for Compound Semiconductors, Cardiff University, UK
[3]IQE plc

Vertical cavity surface emitting lasers (VCSELs) are utilised in a broad range of modern technologies and the VCSEL market is experiencing a rapid expansion in applications like 3D sensing and LiDAR. To address the increasing demand, manufacturers have scaled-up growth production to 150mm wafers with the aim of moving to even larger diameters in the future. As such, it has never been more important to maximise yield in the manufacturing process. This requires maximising uniformity across individual wafers, minimising variation in reactor conditions within growth chambers and ensuring consistency between separate growth runs. To achieve this, it is imperative that material quality can be rigorously tested to identify limitations of the growth and assess the suitability of the epitaxial structure design.

We report here on the use of performance-mapping for evaluation of epitaxial material quality. This involved the processing of many VCSELs across a full 150mm wafer and characterising the light-current-voltage and spectral behaviour of the devices. Wafer-maps were then compiled based on figures of merit from these measurements and used to assess the uniformity of the wafers with respect to the tolerances on features of device performance. Yield for devices under testing across the wafer was around 90%. We measure threshold currents between 0.15 and 4.1mA, and variation in the lasing wavelength between 936.0 and 945.8nm. The information extracted from these studies was contrasted with data from post-growth wafer characterisation to assess the validity and practicability of performance-mapping in providing insight into the quality of the crystal structure in a commercial setting.

A21_43 Checked Patterned Elemental Distribution in AlGaAs Nanowire Branches via Vapor-Liquid-Solid Growth

Xuezhe Yu,[†] Giorgos Boras,[†] H. Aruni Fonseka,[‡,∥] Dong Zhang,[§,∥] Haotian Zeng,[†] Ana M. Sanchez[‡] and Huiyun Liu[†]

[†]Department of Electronic and Electrical Engineering, University College London, London WC1E 7JE, United Kingdom
[‡]Department of Physics, University of Warwick, Coventry CV4 7AL, United Kingdom
[§]SKLSM, Institute of Semiconductors, Chinese Academy of Sciences, P.O. Box 912, Beijing 100083, China

Abstract

Morphological features, crystal defects and crystal phase can have a profound impact on the elemental distribution of ternary nanowires (NWs). Here, we report the synergic influence of the structure and crystal phase on the composition of branched, self-catalyzed $Al_xGa_{1-x}As$ NWs. Branching events were verified to increase with elevating Al incorporation, whilst twin defects and polytypism were observed to extend from the trunk to the branches, corroborating the epitaxial nature of the branch growth. The growth mechanism of the structures has been ascribed to accumulation of Ga adatoms at the concavities of the rough shell, in agreement with ab initio calculations which reveal that Ga tends to segregate at the trunk/branch interface. Interestingly, peculiar, intricate compositional variations are presented in the branched NWs, where Ga-rich stripes parallel to the growth direction of the branches intersect with sets of periodic arrangements of Ga-rich stripes which are perpendicular to them, leading to the realization of an element *checked pattern*. The periodic variations perpendicular to the growth direction of the branches are stemming from the constant rotation of the sample during growth, while Ga-rich stripes along the growth direction of the branches are understood to be driven by the different nucleation energies and polarities on facets of different crystallinity at the interface between the catalyst droplets and the branched NW tip. These results lead to further comprehension of phase segregation and could assist in the compositional engineering in ternary NWs via harnessing this intriguing phenomenon.

A21_20 PL modelling of GaAsBi layers to assist with improving material quality in optoelectronic devices.

N. J. Bailey[1], T. B. O. Rockett[1], J. P. R. David[1], R. D. Richards[1]

1. Department of Electronic and Electrical Engineering, University of Sheffield, UK

An adapted model used to simulate low-temperature photoluminescence spectra of gallium arsenide bismide is presented alongside data taken on several device structures. The usefulness of this model in relation to optimising device performance is discussed.

The formation of a localised distribution of states (LDOS) above the valence band in gallium arsenide bismide (GaAsBi) is well documented in the literature [1]. This effect can be seen as an s-shaped deviation from the Varshni relation at low temperatures [2]. As GaAsBi is of great interest for next generation lasers due to its potential to supress Auger recombination [3], it is important to understand how these localised states are affected by material growth conditions and if they can be supressed where required.

The model we present here is based on previous work by T. Wilson *et al.* [1], which has been modified to use a localised state distribution described by two Gaussians (see Fig.1). The methodology for constraining the model parameters is discussed, as are the final variables and how they relate to device performance.

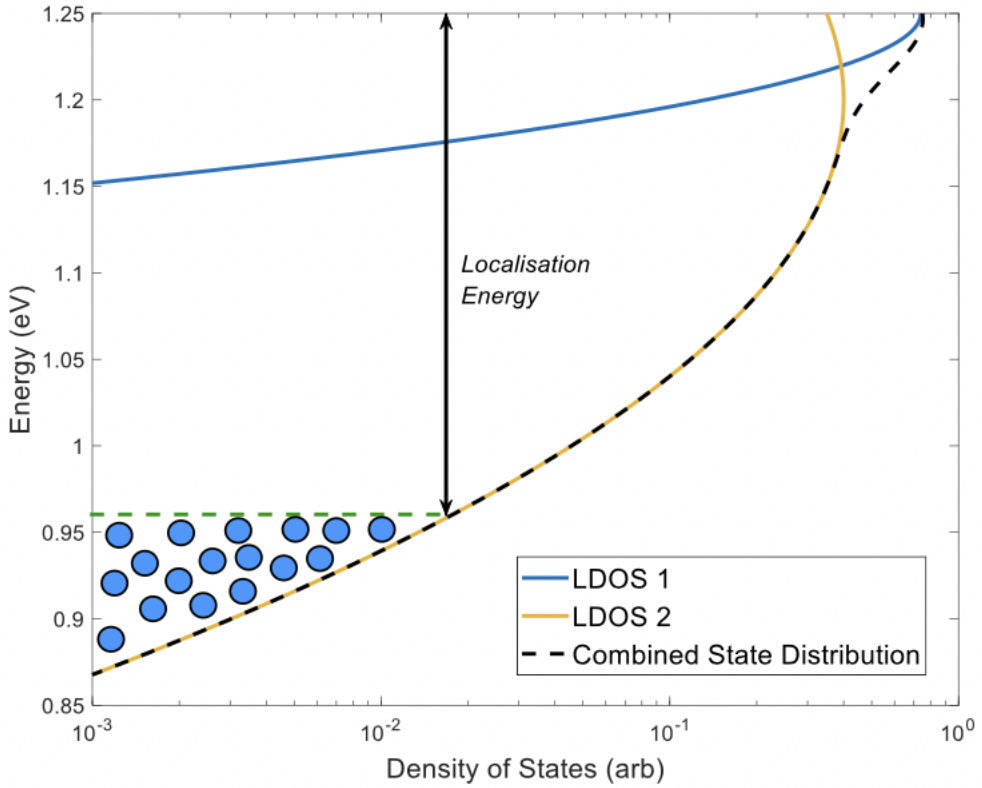

Figure 1 – Energy diagram depicting a distribution of localised states (dashed line) produced from two distinct Gaussian distributions (solid lines). Excited carrier filling (blue circles) starts at the lowest energies due to low temperature (~ 30 K).

1– Wilson, T., et al. "Assessing the nature of the distribution of localised states in bulk GaAsBi." Scientific reports 8.1 (2018): 1-10.

2– Mohmad, A. R., et al. "Localization effects and band gap of GaAsBi alloys." physica status solidi (b) 251.6 (2014): 1276-1281

3 – Hild, K., et al. "Auger recombination suppression and band alignment in GaAsBi/GaAs heterostructures." AIP Conference Proceedings. Vol. 1566. No. 1. American Institute of Physics, 2013.

A21_28 Highly Efficient Multi-Junctional Nanowires Solar Cell

Amr Hisham K. Mahmoud [1], Mohamed Hussein[1,2,3], Mohamed Farhat O. Hameed[1,4,5]*, Salah S. A. Obayya [1]*

[1]Centre for Photonics and Smart Materials, Zewail City of Science and Technology, October Gardens, Giza 12578, Egypt.
[2]Department of Physics, Faculty of Science, Ain Shams University, Abbassia 11566, Cairo, Egypt
[3]Light Technology Institute, Karlsruhe Institute of Technology, Engesserstrasse 13, 76131 Karlsruhe, Germany
[4]Nanotechnology and Nanoelectronics Engineering Program, University of Science and Technology, Zewail City of Science and Technology, Giza 12578, Egypt.
[5]Mathematics and Engineering Physics Department, Faculty of Engineering, Mansoura University, Mansoura 35516, Egypt,
**Corresponding authors: sobayya@zewailcity.edu.eg , mfarahat@zewailcity.edu.eg*

A novel design of multi-junction funnel-shaped nanowires solar cell (MJ-FSNWs) is introduced and numerically analyzed using 3D finite difference time domain (FDTD) method for efficient light trapping. The proposed design consists of 2 units: a cylindrical indium phosphate (InP) part which absorbs visible light, and conical silicon (Si) part to absorb the infrared wavelengths. The MJ-FSNWs enhance the absorption as compared to the previously reported funnel silicon nanowires (Si-FSNWs) [1]. The suggested MJ-FSNWs show a 37.1% in the ultimate efficiency (η) with photocurrent density (J_{sc}) of 30.4 mA/cm^2. This enhancement is due to the lower reflectivity of the InP than the silicon in the visible light region [2]. The suggested MJ-FSNWs unit cell is shown in Fig.1(a), while Fig.1 (b) reveals the absorption spectra of the reported MJ-FSNWs and the conventional Si-FSNWs solar cell (SC). The proposed MJ-FSNWs show higher absorption than the Si-FSNWs due to the combination of the two semiconductor materials with different bandgaps. Figure 1(c) shows the ultimate efficiency η and J_{sc} of the MJ-FSNWs and Si-FSNWs. The proposed SC shows η and J_{sc} of 37.1% and 30.4 mA/cm^2, respectively which are higher than that of the Si-FSNWs with η and J_{sc} of 32.9% and 26.9 mA/cm^2, respectively.

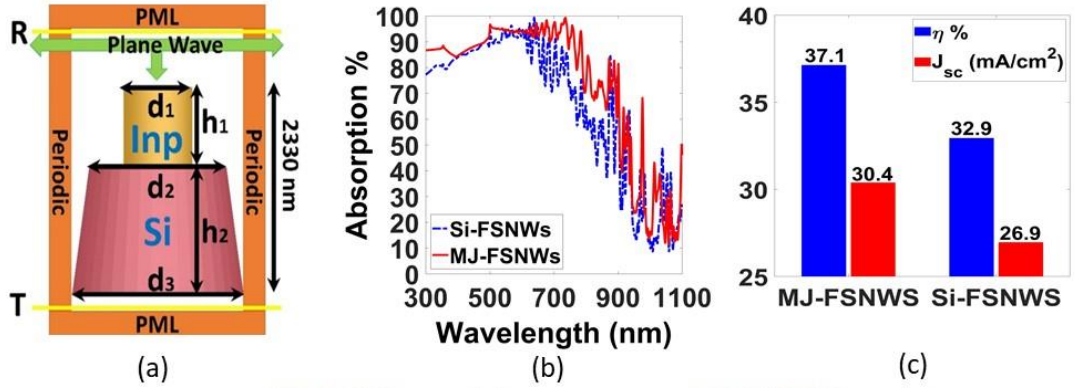

Fig.1: (a) Schematic diagram of the MJ-FSNWs, (b) Absorption spectra, and (c) η and J_{sc} of the reported MJ-FSNWs and conventional Si-FSNWs.

References

[1] M. Hussein, M. F. O. Hameed, N. F. F. Areed, A. Yahia, and S. S. A. Obayya, "Funnel-shaped silicon nanowire for highly efficient light trapping," Opt. Lett., vol. 41, no. 5, p. 1010, Mar. 2016.
[2] D. A. Goldman, J. Murray, and J. N. Munday, "Nanophotonic resonators for InP solar cells," Opt. Express, vol. 24, no. 10, p. A925, May 2016.

A21_31 Highly Efficient Perovskite Solar Cell

Awad Khaled[1], Mohamed Hussein[1,2,3], B. M. A. Rahman[4], K. T. V. Grattan[4], Mohamed Farhat. O. Hameed[1,5,6] and S. S. A. Obayya[1*]

[1] Centre for Photonics and Smart Materials, Zewail City of Science and Technology, October Gardens, 6th of October City, Giza, 12578, Egypt.
[2] Department of Physics, Faculty of Science, Ain Shams University, Abbassia 11566, Cairo Egypt.
[3]Light Technology Institute, Karlsruhe Institute of Technology, Engesserstrasse 13, 76131 Karlsruhe, Germany
[4]Department of Electrical and Electronic Engineering, City, University of London, London EC 1 V 0HB, United Kingdom
[5] Nanotechnology and Nanoelectronics Engineering Program, Zewail City of Science and Technology, October Gardens, 6th of October City, Giza, 12578, Egypt.
[6]Mathematics and Engineering Physics Department, Faculty of Engineering, Mansoura University, Mansoura 35516, Egypt
**Corresponding author: sobayya@zewailcity.edu.eg , mfarahat@zewailcity.edu.eg*

The light absorption through solar cells (SCs) can be highly improved using light trapping nanostructures [1]. In this study, NiO@GeSe core-shell nanostructures are used to improve the perovskite solar cell (PSC) efficiency. Figure 1 (a) shows the unit cell of a periodic PSC with and without the core-shell nanostructures. The geometrical parameters are studied using finite difference time domain (FDTD) via Lumerical software package [2] to maximize the light absorption. The absorption spectra of the studied structures are shown in Fig. 1 (b). It may be seen that the suggested designs have better absorption than the conventional PSC. The optimized core-shell nanostructures offer high photocurrent density (J_{ph}) of 23.86, and 25.34 mA/cm^2 using cylindrical and nanocone nanowires compared to 18.70 mA/cm^2 of the conventional PSC. This is due to the light trapping due to the embedded nanostructures in the active layer.

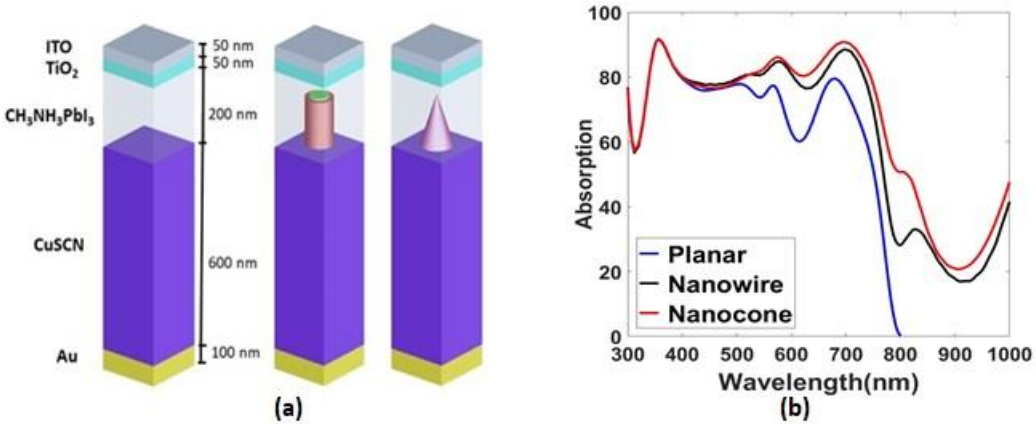

Fig. 1 (a) Unit cell and (b) the absorption spectra of the conventional planar PSCs and the reported PSC with cylindrical and conical nanowires.

References

[1] Abdelraouf, O.A., Allam, N.K., 2016. Towards nanostructured perovskite solar cells with enhanced efficiency: Coupled optical and electrical modeling. Sol. Energy 137, 364–370.
[2] https://www.lumerical.com/

Acknowledgement

The authors acknowledge the Science, Technology and Innovation Funding Authority (STIFA) at Egypt under the Institutional Links Grants. Egypt-UK Cooperation: Newton Mosharafa Program (30732). Grattan acknowledges support from the Royal Academy of Engineering.

A21_09 The Development of Novel Heterostructure Detector Diodes Through Physical Modelling.

Andrew Hadfield, Abdelmajid Salhi, James Sexton and Mo Missous

**School of Electrical & Electronic Engineering, The University of Manchester Manchester, M13 9PL, United Kingdom*

andrew.hadfield@manchester.ac.uk,

Abstract

Asymmetric Spacer Layer Tunnel (ASPAT) diodes, based on both GaAs and InP platforms, have for many years been proposed as zero bias detector diodes for both microwave and mm-wave purposes. Whilst these devices show some favourable characteristics over the currently near universal Schottky diodes, they do not match up in other key areas. One of these areas is the curvature coefficient (k_v) which is a key figure of merit for any detector diode. Schottky barrier diodes are inherently limited to a k_v of around $40V^{-1}$, whilst the ASPAT diodes highest reported figures are $28V^{-1}$ and $13V^{-1}$ for GaAs and InGaAs based devices respectively.

In this work new device structures are explored to increase the k_v of ASPAT diodes. Initial physical models of GaAs and $In_{0.53}Ga_{0.47}As$ based ASPAT diodes were produced and validated against experimental data from devices grown via Solid Source Molecular Beam Epitaxy. Following this, the validated physical models were used to simulate new tunnel diode structures, in which $In_xGa_{1-x}As$ quantum wells were added to the devices and $Al_xGa_{1-x}As$ introduced to the spacer. The results of these simulations showed marked improvements in the zero bias curvature coefficients of the devices with the highest device k_v exceeding the inherent Schottky barrier limit with a value of $42V^{-1}$.

This work will also cover how the addition of quantum wells and $Al_xGa_{1-x}As$ spacers effects other key device parameters such as junction capacitance and junction resistance, which must be kept to a minimum to maximise device cut-off frequency, allow for easier impedance matching and to ensure fast diode response. The addition of quantum wells to the devices reduced the zero-bias junction capacitances to 13fF and 11fF for $4\times4\mu m^2$ GaAs and $In_{0.53}Ga_{0.47}As$ based structures respectively compared with 23fF and 18fF for standard ASPAT devices without quantum wells, a reduction of ~ 50% and 40% respectively. The addition of an $Al_xGa_{1-x}As$ spacer to the GaAs based devices further reduced the zero bias junction capacitance to 9fF leading to an overall reduction of 60% from 23fF and increase in estimated cut frequency to 804GHz.

Device	**Cut off frequency GHz**	**k_v V^{-1}**
GaAs ASPAT	314	12
$In_{0.53}Ga_{0.47}As$ ASPAT	491	11
GaAs QW-ASPAT	532	33
$In_{0.53}Ga_{0.47}As$ QW-ASPAT	803	35
$Al_{0.2}Ga_{0.8}$ As QW-ASPAT	804	42

A21_45 Broadband Photon Harvesting in Organic Photovoltaic Devices Induced by Nanograting Templates

D. Chowdhury[1], S. Mohamed[2], G.Manzato[1], C.Mennucci[1], R.Chittofrati[1], Mohamed Hussein[2, 3,4]
Salah S. A. Obayya[2], Mohamed Farhat O. Hameed[2,5,6], F. Buatier de Mongeot[1]

[1]University of Genova, Department of Physics, Genova, 16146, Italy.
[2] Centre for Photonics and Smart Materials, Zewail City of Science and Technology, October Gardens, 6th of October City, Giza 12578, Egypt.
[3] Department of Physics, Faculty of Science, Ain Shams University, Abbassia 11566, Cairo, Egypt.
4Light Technology Institute, Karlsruhe Institute of Technology, Engesserstrasse 13, 76131 Karlsruhe, Germany
5Nanotechnology and Nanoelectronics Engineering Program, Zewail City of Science and Technology, October Gardens, 6th of October City, Giza, 12578 Egypt.
6Mathematics and Engineering Physics Department, Faculty of Engineering, Mansoura University, Mansoura, Egypt

Due to rising demand of clean-energy production, rapid development has been observed in the field of photovoltaics (PV) in the last few decades. Thin film organic photovoltaic (OPV) is an attractive alternative to conventional silicon solar cell due to its lightweight, flexible and low-cost. However, the optical absorption efficiency of the OPV should be increased and still represents an open issue which cannot be addressed adopting conventional light coupling strategies derived from thick PV absorbers. The light coupling to thin film solar cell can be obtained by nanostructuring at subwavelength scales with lower reflection losses and better light trapping [1]. Recently, by employing one-dimensional pseudo-periodic gratings fabricated in a self-organized fashion via de-focused ion beam sputtering (IBS), we demonstrated promising efficiency enhancement in thin film inorganic a:Si devices [2-3]. Here, adopting an alternative large area approach, we demonstrate that the use of a highly ordered one-dimensional (1D) nanograting leads to broadband photon harvesting in the supported thin film OPV devices. Laser interference lithography, in combination with reactive ion etching, provides the controlled tailoring of the height and pitch of the silica gratings, enabling controlled light trapping in the organic active layer (PTB7:PCBM). The optical properties of the textured interfaces are assessed experimentally. We have achieved the relative enhancement of the optical absorption as high as 19% over a broadband spectra from visible to near-infrared range for sub-wavelength structures of height 280 nm and period 300 nm respectively.

References:

[1] Yan-Gang Bi, Jing Feng, Jin-Hai Ji, Fang-Shun Yi, Yun-Fei Li, Yue-Feng Liu, Xu-Lin Zhangand Hong-Bo Sun, Nanophotonics, 7(2), 371, (2018).
[2] C. Mennucci, C. Martella, L.V. Mercaldo, I. Usatii, P. Delli Veneri and F. Buatier de Mongeot, Appl.Sci., 7(4), 355 (2017).
[3] C. Mennucci, MH Muhammad, M.F.O. Hameed, S.A. Mohamed, M.S. Abdelkhalik, S.S.A. Obayya, F. Buatier de Mongeot, Appl.Surf. Sci. 446.74-82 (2018).

Acknowledgements

We acknowledge financial support by Ministero degli Affari Esteri e della Cooperazione Internazionale (MAECI) in the framework of the Italy-Egypt bilateral program, and by ‘‘Science and Technology Development Fund” (STDF) at Egypt for the financial support under Italy/Egypt project number 25954. We also acknowledge support from Compagnia di San Paolo in the framework of project ID ROL 9361, from Ministero dell’Università e della Ricerca Scientifica (MIUR) through the PRIN 2015 Grant No. 2015WTW7J3, from ICTP, Trieste, Italy for a TRIL Fellowship (D.C.), and from Linz Institute for Organic Solar cell (LIOS), Johannes Kepler University, Linz, Austria for providing access to the research facility and hosting (S.M.).

A21_56_Modelling type-II superlattices for long-wavelength infrared detectors

P. E. O'Dowd Phanis[1], D. C. M. Kwan[1], D. O. Alshahrani[1], D. L. Huffaker[1,2]M. Kesaria[1]

[1]School of Physics and Astronomy, Cardiff University, UK
Present address: [2]Electrical Engineering Department, The University of Texas at Arlington, United States of America

Long-wavelength infrared (LWIR) detectors have many uses, ranging from military to astronomy. They are commonly made of HgCdTe due to its tunable bandgap. However, this material has many drawbacks including cost, issues with uniformity and high levels of dark current. Thus, the past few decades have seen a rise in alternatives to HgCdTe infrared detectors. One of the most promising alternative materials is type-II superlattice (T2SL) [1]. This new material boasts many advantages, such as easier and cheaper manufacturability as well as Auger recombination suppression. The most studied LWIR T2SL has been the InAs/GaSb T2SL, however, it has yet to live up to its full potential due to Ga-related defects which reduce the minority carrier lifetime. As such, Ga-free T2SLs are gaining increasing attention from the scientific community due to their longer minority carrier lifetimes whilst maintaining the advantages of a superlattice. However, they usually require thicker layers for strain balancing, which impacts the absorption coefficient, diminishing the quantum efficiency [2]. Therefore, there is a need to design strain balanced LWIR Ga-free T2SLs with short periods in order to achieve a quantum efficiency comparable to that of Ga-containing T2SLs.

This work model and compares the two types of T2SL through the use of Nextnano. The 8-band k.p method was applied in order to calculate the electronic band structure (E(k) dispersion curve) of the T2SLs and study their properties [3, 4]. The effect of Sb concentration and layer thickness on the energy bandgap of the Ga-free T2SL is investigated and compared to that of the Ga-containing T2SL. The strain balancing condition for the Ga-free T2SL was met through the use of virtual substrates. Using these virtual substrates leads to thinner layers as the average lattice constant of the T2SL can be matched to that of the virtual substrate, allowing for more flexibility in the layer thickness.

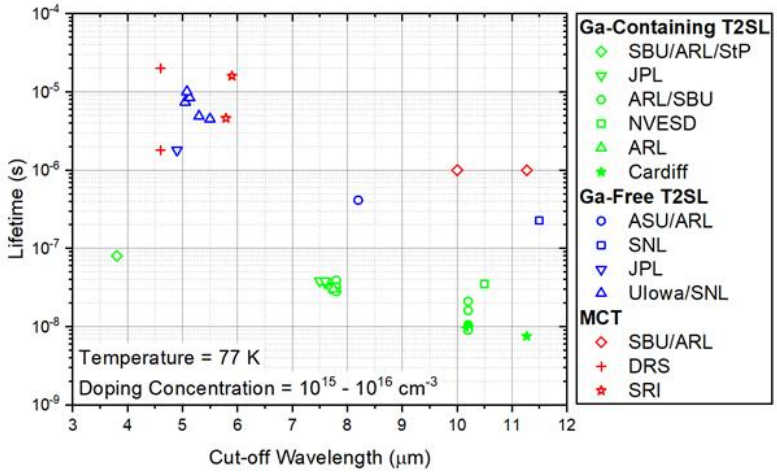

Figure 1: Depiction of the carrier lifetimes for various IR detectors in the mid-wave and long-wave regions

References

[1] Karim A. et al. (2013) *IOP Conf. Ser.: Mater. Sci. Eng.* 51, 012001
[2] Rogalski A. et al. (2017) *Appl. Phys. Rev.* 4, 031304
[3] Delmas M. et al. (2019) *Proc. SPIE* 10926, Quantum Sensing and Nano Electronics and Photonics XVI, 109260G
[4] Manyk T. et al. (2018) *Results in Physics* 11, 1119–1123

Abstracts

Session 12: Invited Speaker II

Invited **Membrane-based VCSELs and LEDs from the blue to the ultraviolet wavelength regime**

Åsa Haglund

Chalmers University of Technology, Department of Microtechnology and Nanoscience, Gothenburg, Sweden

In recent years, there has been tremendous improvement in the performance of blue-emitting vertical-cavity surface-emitting lasers (VCSELs) and in many aspects their performance characteristics are now on par with that of GaAs-based infrared-emitting VCSELs. The blue VCSELs are now on the brink of commercialization thanks to advances in thermal management, optical confinement, mirror reflectivity, and electrical injection.

In this talk, I will give an overview of the challenges to realize high-performing III-nitride VCSELs, summarize state-of-the-art results and discuss potential applications for these devices. In addition, I will outline the main challenges in extending the emission wavelength into the ultraviolet. In more detail, I will highlight our schemes for optically guided devices that are used in the best blue VCSELs today and our approach to simultaneously achieve high-reflectivity mirrors and good control over the cavity length enabled by membranes created by electrochemical etching. The latter resulted in the demonstration of the world's shortest emission wavelength from a VCSEL at around 310 nm. We have also used the same methodology to lift-off fully processed LEDs from their substrate and realize thin-film flip-chip UV LEDs with the hope to improve the poor light extraction efficiency in these devices and also allow for the reuse of precious substrates.

Spatial and Mural Guidance

Spatial

To Join Spatial:

1. Open the link https://spatial.chat/s/sioe2021 in your browser
2. When prompted, type in your full name and a short bio. Although the bio is optional. It is a good place to include information such as what institution or company you are from, or what your area of research is.
3. Click "Continue" to enter the space
4. You will be prompted to turn on your camera and microphone. Do this by clicking the red camera and microphone icons. These should turn green.
   Having difficulty connecting your audio and/or microphone? If you are not able to connect to video or audio, you might need to change the camera or microphone input by using the drop-down menus. Ensure that you have enabled your browser to access your camera and microphone in your security settings. In chrome, this is located by clicking on the padlock icon in the address bar.
5. Once you have connected your audio and microphone, click "Join Space" to enter Spatial.
6. In Spatial:
   - Navigate by clicking and dragging your icon around,
   - Zoom with your mouse scroll wheel, or using your laptop trackpad (alternatively you can also use the zoom options in the bottom right),
   - Change rooms by clicking on the room name on the right,
   - Turn off your microphone or camera by clicking on the options at the bottom,
   - Access help with the help button in the top right,
   - Leave the space with the "leave space" button in the top right.

These instructions are also available as a video: https://drive.google.com/file/d/1Ex_p-EkCAq0jptt3CPzfwIZokpuC9j19/view

If you are still having difficulties after following these instructions, email the events team, **conference@cardiff.ac.uk**

Spatial guidance (with images)

To join spatial:

1. Open the link https://spatial.chat/s/sioe2021 in your browser
2. When prompted, type in your name and a short bio.

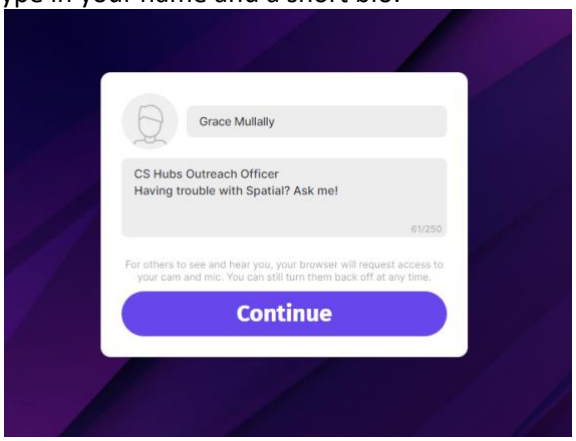

3. Click "Continue" to enter the space
4. You will be prompted to turn on your camera and microphone. Do this by clicking the red

camera and microphone icons. These should turn green.

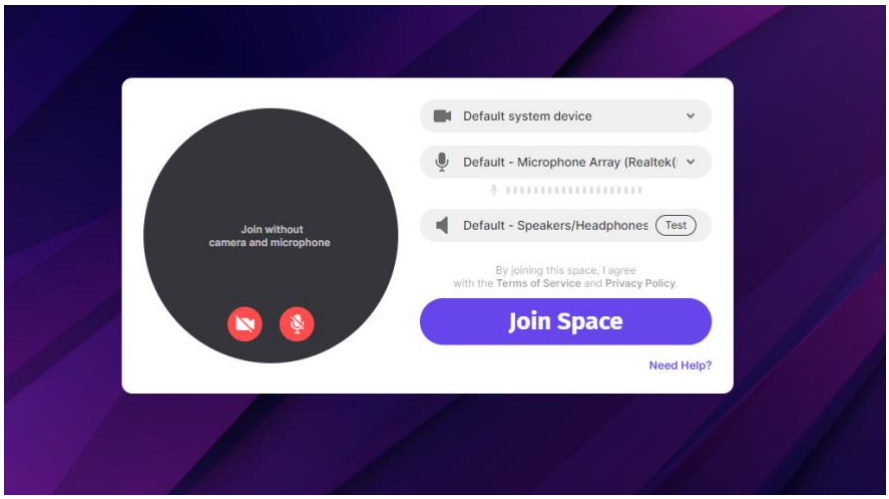

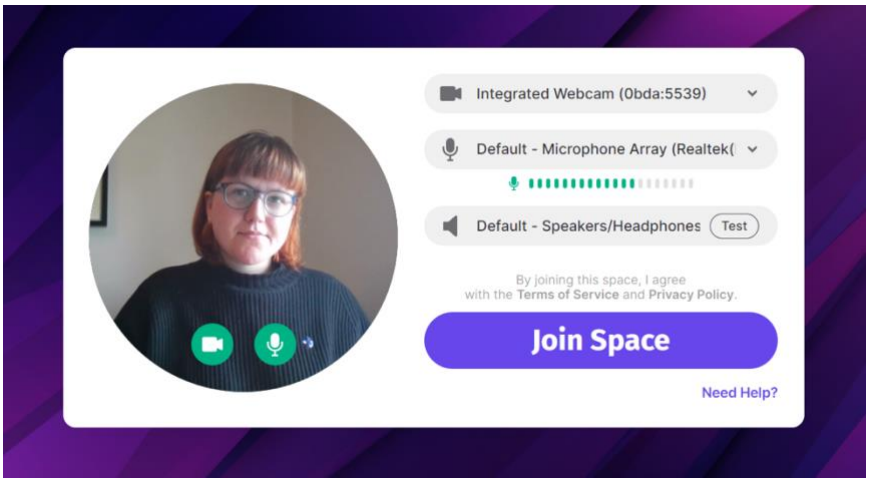

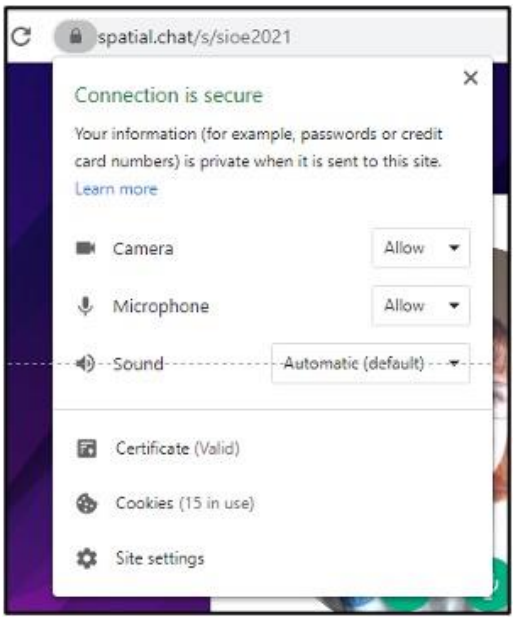

Having difficulty connecting your audio and/or microphone? If you are not able to connect to video or audio, you might need to change the camera or microphone input by using the drop down menu. Ensure that you have enabled your browser to access your camera and microphone in your security settings. In firefox and chrome, this is located by clicking on the padlock icon in the address bar.

5. Once you have connected your audio and microphone, click “Join Space” to enter Spatial.

6. In Spatial:
Navigate by clicking and dragging your icon around,
Zoom with your mouse scroll wheel,
Change rooms by clicking on the room name on the right,
Turn off your **microphone** or **camera** by clicking on the options at the bottom,
Access **help** with the help button in the top right,
Leave the space with the "leave space" button in the top right.

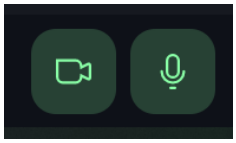

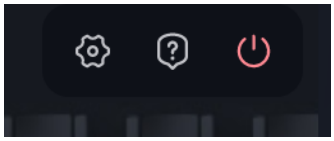

These instructions are also available as a video, watch here

Mural

During the panel session (session 8) you will be assigned a Zoom breakout room and your facilitator will share a link with you to your Mural room at the relevant time.

- When you click on the link for your Mural breakout room you will be asked to enter your name. Please add your name as it will make the session easier to facilitate and recognise your contributions. Your breakout room facilitator will provide you with an introduction to Mural and how to use the sticky note function to you can write answers to the discussion questions.
- If you double left click you mouse you will be able to add a sticky note anywhere on the Mural, or you can right click and select add sticky note.

This video provides more guidance on adding content to Mural:
https://www.youtube.com/watch?v=CmYaxcTzD6Y&list=PLDZa1OFNww6MPz6QwASaF8fFEQGeiJadL&index=3
At the end of the breakout session, you will leave your breakout room and return to the main Zoom meeting to take part in a wider discussion with all delegates during the summary session.